UNDERSTANDING THE EFFECTS OF RAPID ADAPTATION ON PREDATOR-PREY INTERACTIONS USING THE THEORY OF FAST-SLOW DYNAMICAL SYSTEMS

A Dissertation

Presented to the Faculty of the Graduate School

of Cornell University

in Partial Fulfillment of the Requirements for the Degree of

Doctor of Philosophy

by

Michael Henry Cortez

January 2011

UNDERSTANDING THE EFFECTS OF RAPID ADAPTATION ON PREDATOR-PREY INTERACTIONS USING THE THEORY OF FAST-SLOW DYNAMICAL SYSTEMS

Michael Henry Cortez, Ph.D.

Cornell University 2011

Interspecific interactions depend not only on the population densities of the interacting species, but on their phenotypes as well. Variation in ecologically important species traits can be heritable or plastic in nature and both yield phenotypic change that occurs at rates comparable to or faster than those of ecological dynamics. This thesis explores how the effects of heritable and plastic phenotypic variation on community dynamics can be captured under one unifying theory using the theory of fast-slow dynamical systems.

The analysis presented here focuses on the limit where phenotypic change occurs faster than changes in species' abundances in predator-prey systems. This approach reduces model dimension and yields analytical results and graphical methods with predictive power about when new and unique dynamics will arise in ecological systems with rapid phenotypic change. In addition, while explicitly assuming a separation of time scales, the analysis of the fast adaptation limit yields insight into the consequences of adaptive change when the rates of the adaptive and ecological processes are comparable.

The results presented here show that evolution and phenotypic plasticity have different effects on the community dynamics of predator-prey systems. Rapid evolution has the potential to stabilize or destabilize population oscillations while phenotypic plasticity only stabilizes population oscillations. Evo-

lution can also yield population oscillations where the predator and prey are completely out-of-phase or one species oscillates while the other remains essentially constant. These two behaviors are not possible in phenotypically plastic or phenotypically fixed predator-prey systems.

This thesis also presents an analysis of the dynamics that arise in the vicinity of a transversal intersection of the critical manifold in multiple time scale biological systems. Such intersections are generic in fast-slow eco-evolutionary models and the results presented here show that complex dynamics arise near the transversal intersections of the critical manifold. These dynamics arise in regions of parameter space where periodic orbits exist and in phase space where the fast-slow structure of the system is no longer present.

BIOGRAPHICAL SKETCH

Michael was born on September 21, 1983 in Cheyenne, Wyoming. Along with his older sister, Lisa, younger brother, Kristofer, and younger sister, Caryn, Michael grew up a military brat. As a consequence, his youth was spent in various parts the country: Detroit, Michigan for two years; Rome, New York for five years; Andrews Air Force Base (now Joint Base Andrews Naval Air Facility), Maryland for two years; Derby, Kansas for five years; and finally Cadillac, Michigan for three years.

After graduating from Cadillac Senior High School, Michael attended Hope College in Holland, Michigan. He chose Hope College over the University of Michigan (U of M), because Hope's acceptance rate was better than U of M's acceptance rate into the U of M medical program. Despite his interest in becoming a medical doctor since the fifth grade (which barely usurped a career in paleontology), Michael continued to take mathematics classes for fun and after five semesters, decided he may as well major in it. While medical school was still a viable option for the future, the final nail was hammered into the coffin after Michael participated in a summer research project on mathematical ecology with Dr. Janet Anderson. Looking back only once since that summer, Michael graduated from Hope College in 2005 with a dual major in Chemistry and Mathematics, focused on a career in mathematical biology.

In the fall of 2005, Michael began his graduate education at Cornell University. As a student in the Center for Applied Mathematics, Michael's first step in infiltrating the world of biological and ecological research as a mathematician involved enlisting an advisor experienced in the arts of camouflage, disguise, and subterfuge. Three years of training and mentoring later, phase one was complete and an A exam was scheduled in May of 2008. After convincing a

true biologist that he was indeed a kindred soul, Michael passed the exam and earned his masters degree in Applied Mathematics. Due to his impending B exam, phase two comes to a close and Michael now faces his greatest challenge in infiltration yet. While writing these lines, Michael nears the completion of his Ph.D. and the start of a postdoctoral position at Georgia Institute of Technology in the School of Biology.

ACKNOWLEDGEMENTS

First and foremost, I thank my advisor, Stephen Ellner, for his guidance and support of my academic endeavors throughout my time at Cornell. His continual encouragement of my academic independence and training has been invaluable. There are not enough words to describe how thankful I am for his tutelage.

I am also grateful to John Guckenheimer and Nelson Hairston, Jr. for sitting on my committee. Their instruction in the classroom and advice while doing research has been a great asset to my training. In addition, I thank John for his guidance on the material presented in the third chapter of this thesis. That chapter would not have been possible without it.

I have had the privilege of participating in three lab groups while at Cornell. The open criticism of mathematical biology papers, including my own, by Steve and his "Lunchbunch" group has been an educational and often entertaining experience. I thank the group's current and former members: Patrick Ayscue, Lauren Childs, Ben Dalziel, Matt Holden, Paul Hurtado, Diego Moreno, Katie Sullivan, Rebecca Tien, and Jacob Wynne. Steve and Nelson's Chemostat Group has been an eyeopening experience into how biologists and mathematicians interact in the real world. My thanks to Aldo Barreiro, Lutz Becks, Teppo Hiltunen, Giles Hooker, Laura Jones, Joe Simonis, and Yuefeng Wu for insight into the challenges and excitement of interdisciplinary discussions. Finally, the mathematical discussions with John and his group, Sarah Iams, Christian Kuehn, Philipp Meerkamp, and Christopher Scheper, have facilitated my intellectual growth as an applied mathematician and my interest in dynamical systems.

My graduate education was funded by a graduate student fellowship from the Alfred P. Sloan Foundation and research grants awarded to Stephen Ellner

and his colleagues from the National Science Foundation and the James S. McDonnell Foundation. Their financial support has allowed me to the make the most of my time at Cornell.

The CAMsters are one of best things about the Center for Applied Mathematics. They have been my friends and colleagues throughout my tenure at Cornell and their camaraderie has always been present. Of special mention is my friend and former house mate of five years, Paul Hurtado, whose companionship through all things academic and non-academic I will miss the most as I leave Cornell. I also thank Christian Kuehn and Matt Holden for discussions that have helped clarify and correct my thoughts and ideas on whatever combination of biology and mathematics I had come up with at the time.

Finally, I thank my family for their support through the last five years. I am especially grateful to my parents who have inspired me and encouraged me all along the way, even when I disappear for months at a time. I am ever thankful for their unbounded care and patience.

TABLE OF CONTENTS

LIST OF FIGURES

CHAPTER 1

UNDERSTANDING RAPID EVOLUTION IN PREDATOR-PREY INTERACTIONS USING THE THEORY OF FAST-SLOW DYNAMICAL SYSTEMS

1.1 Abstract

The accumulation of evidence demonstrating the evolution of ecologically important traits at the same time and rate as ecological dynamics (e.g. changes in species' abundances or spatial distributions) has outpaced theory explaining the interplay between ecological and evolutionary processes with comparable time scales. This disparity between experiment and theory is partially due to the high dimensionality of eco-evolutionary models. Here we show how fast-slow dynamical systems theory can reduce model dimension, and we use that body of theory to study a general predator-prey system exhibiting fast predator or prey evolution. Our approach yields graphical methods that predict what underlying biological mechanisms allow new and unique dynamics (e.g. anti-phase and cryptic oscillations) to arise in ecological systems exhibiting fast evolution. Our analysis shows that these new dynamics are more likely arise when the prey is evolving. The fast evolution approach also yields analytical expressions that relate individual level characteristics (e.g. decelerating benefits for defense) with population level phenomena (e.g. population phase lags and the destabilization of ecological dynamics). Finally, while the theory requires a separation of time scales between the ecological and evolutionary processes, our approach yields insight into systems where the rates of those processes are comparable and thus is a step towards creating a general eco-evolutionary theory.

1.2 Introduction

Over the last thirty years, the evolution of ecologically important species' traits at ecological rates [eco-evolutionary dynamics: Fussmann et al., 2007, Kinnison and Hairston, 2007] has been observed in species of algae [Yoshida et al., 2003], bacteria [Bohannan and Lenski, 2000, Palumbi, 2001], birds [Grant and Grant, 2002], crustaceans [Hairston and Walton, 1986, Hairston and Dillon, 1990, Hairston et al., 1999], fishes [Conover and Munch, 2002, Heath et al., 2003, Kinnison et al., 2008, Reznick et al., 2008, 1997, Swain et al., 2007], mammals [Pelletier et al., 2007], plants [Siemann and Rogers, 2001, Lavergne and Molofsky, 2007] and reptiles [Sinervo et al., 2000]. Predator-prey and other exploiter-victim systems are important examples where eco-evolutionary dynamics have been observed. Changes in prey phenotypes can help the prey avoid encounters with predators [Hairston and Walton, 1986, Hairston and Dillon, 1990, Heath et al., 2003, Reznick et al., 1997, 2008] or defend against attacks [Bohannan and Lenski, 2000, Yoshida et al., 2003, Jones et al., 2009], while consumer evolution can allow for increased resource capture and consumption [Grant and Grant, 2002] and the ability to overcome prey defenses [Hairston et al., 1999]. Furthermore, genetic variation among individuals can have strong effects on observed community-level dynamics [Tuda, 1998, Hanski and Saccheri, 2006, Saccheri and Hanski, 2006, Bailey et al., 2009, Ezard et al., 2009, Johnson et al., 2009, Palkovacs et al., 2009, Post and Palkovacs, 2009].

These studies yield two complementary results. First, one can no longer assume that ecologically important traits are fixed on the time-scale of ecological dynamics such as changes in the abundance, structure, or distribution of populations. Second, heritable changes in phenotype that occur on the same

rate as ecological processes can influence the ecological interactions that cause them. These two observations emphasize the need to understand heritable changes within a population that occur fast enough to affect interspecific interactions while they are still taking place, and how they can change observable community-level patterns.

Recent studies have begun to develop theory to account for the interplay between ecological and evolutionary processes with comparable time scales in predator-prey systems. By comparable time scales, we mean that change of organismal traits occurs at the same time and pace as ecological dynamics. Most studies have focused on the qualitative and quantitative changes in population dynamics resulting from rapid evolution, but largely with models tailored to specific systems [Abrams, 1992, Abrams and Matsuda, 1997a,b, Yoshida et al., 2003, 2004, Jones et al., 2009]. While these studies have yielded qualitatively new population dynamics, the studies may not exhibit all possible eco-evolutionary dynamics and consequently new or unique dynamics can be missed. Furthermore, with only a few specific examples it is often difficult to determine the general biological and mathematical mechanisms that cause the new dynamical behavior to arise. Hence, we believe a more general theory is needed in order to characterize the full spectrum of dynamics that eco-evolutionary systems can exhibit.

An inherent difficulty in studying systems with rapid evolution is the intractability of higher (three or more) dimensional systems. Even simple predator-prey eco-evolutionary systems are difficult to understand since they must be of at least three dimensions (predator density, prey density, and a predator or prey trait). To begin developing a generalized eco-evolutionary the-

ory and to reduce model dimension, we start with an analytically tractable case where the evolution of a species occurs much faster than changes in population size. This separation of time scales is the opposite of that assumed in traditional theory but is not biologically ill-founded. Such a case can arise if there is a rapid turnover of individuals in a population and the birth rate is nearly equal to the death rate (for example, if the population is space limited and close to its carrying capacity). In this case, the average trait value of the population changes quickly while the total population size changes slowly.

Another justification for considering the fast evolution limit is that increasing the rate of evolution often preserves some of the main qualitative properties of the dynamics observed in systems where the ecological and evolutionary processes have comparable rates. Figure 1.1 *A* presents data from an experimental algal-rotifer system [Fussmann et al., 2000] where prey evolution has been shown to affect qualitative properties of the predator-prey oscillations [Yoshida et al., 2003, Meyer et al., 2006, Yoshida et al., 2007].

Figures 1.1 *B*, *C*, and *D* contain time series from a model, fitted with data, that predicts the dynamics of the algal-rotifer system [Jones and Ellner, 2007]. In figure 1.1 *B* with parameters estimated from experimental data, the evolutionary changes and population changes of the model occur on the same time scale. As the evolutionary processes are sped up by a factor of 5 (figure 1.1 *C*) and by a factor of 10 (figure 1.1 *D*), the essential qualitative properties of the dynamics do not change. In particular, the completely out-of-phase predator-prey oscillations in the data are preserved as the speed of evolution is increased in the model.

Figure 1.1 emphasizes a key point underlying our fast evolution approach.

When we speed up the evolutionary processes we are not positing that evolution can occur at instantaneous rates. Rather, we study the dynamics that occur in the fast evolution limit because these dynamics yield insight into the behavior exhibited by systems where the ecological and evolutionary processes have comparable rates. In figure 1.1, when the speed of evolution is increased, the eco-evolutionary dynamics do not become increasingly complicated, nor do they become increasingly unrealistic. Thus, by considering this extreme in evolutionary rates we can begin to develop a general eco-evolutionary theory.

We note that the opposite limit, where evolutionary processes are much slower than ecological processes, has been studied elsewhere in the literature [e.g. Decole et al., 2006, Khibnik and Kondrashov, 1997]. While the slow evolution viewpoint yields insight into the effects ecological processes have on evolutionary dynamics, our approach yields insight into the effects evolutionary processes have on ecological dynamics. Furthermore, the slow evolution limit does not predict or capture all experimentally observed population dynamics (e.g. the completely out-of-phase oscillations in figure 1.1 *A*). Since the fast evolution limit does yield insight into this behavior, our approach complements the traditional viewpoint and together these extremes can be used to understand systems where ecological and evolutionary rates are comparable.

Figure 1.1 also demonstrates why it is not sufficient to study only systems with inducible defenses [e.g. see Vos et al., 2004a] to understand the dynamics in systems with fast evolution. As the speed of evolution increases in figure 1.1, a lag between the switch in the direction of selection (vertical black lines) and a corresponding measurable change in the trait arises. For example, in figure 1.1 *D*, the direction of selection switches from favoring larger values of

the trait to favoring smaller values of the trait near day 60. In contrast, the trait does not begin to move towards smaller values until a few days later. This lag in the trait is not observed in ecological models with induced defenses and due to its influence on population dynamics, distinguishes ecological models with fast evolution from ones with induced defenses.

Mathematically, an eco-evolutionary model exhibiting fast evolution is a fast-slow dynamical system, an area known as singular perturbation theory [Arnold et al., 1995]. This body of theory allows one to study dynamical systems where there is a separation of time scales and some variables change much faster than others. The theory focuses on the limit where the fast variables are instantaneously fast so as to reduce the complexity of the mathematics. In this study we use fast-slow systems theory to study the effects of fast evolution in a single species on the ecological dynamics of a general predator-prey system. In our model, predator and prey evolution are nearly mathematically equivalent by a reversal of time. Consequently, we will present our results for the predator evolution case and discuss the differences that arise between the two.

In the next section, we introduce the basic concepts of slow-fast systems theory with a familiar predator-prey model. We then present our general predator-prey model with rapid predator evolution. The results section explores two consequences of predator evolution: how fast evolution stabilizes or destabilizes population dynamics and how the trait's trade-off curve influences population and trait time series. We then present a simple graphical technique that predicts the full spectra of possible population dynamics in systems with particular types of evolutionary dynamics. Finally we present the differences between predator and prey evolution.

Figure 1.1: Comparison of experimental and theoretical results for a predator-prey system as evolution is sped up. (*A*) Algal (*Chlorella vulgaris*, green circles) and rotifer (*Brachionus calyciflorus*, magenta '+') density data from Fussmann et al. [2000]. Units are 10^6 cells ml^{-1} (algae) and number of females ml^{-1} (rotifers). (*B-D*) Predator (magenta '+'), prey (green circles), and trait (solid blue) time series for a predator-prey model with prey evolution [Jones and Ellner, 2007]. The speed of evolution is (*B*) as fast as the ecological dynamics, (*C*) five times as fast, and (*C*) 10 times as fast. The black dashed lines denote when the direction of selection switches in the model. The trait values are rescaled such that the minimum value corresponds to 0 and the maximum value corresponds to 1.

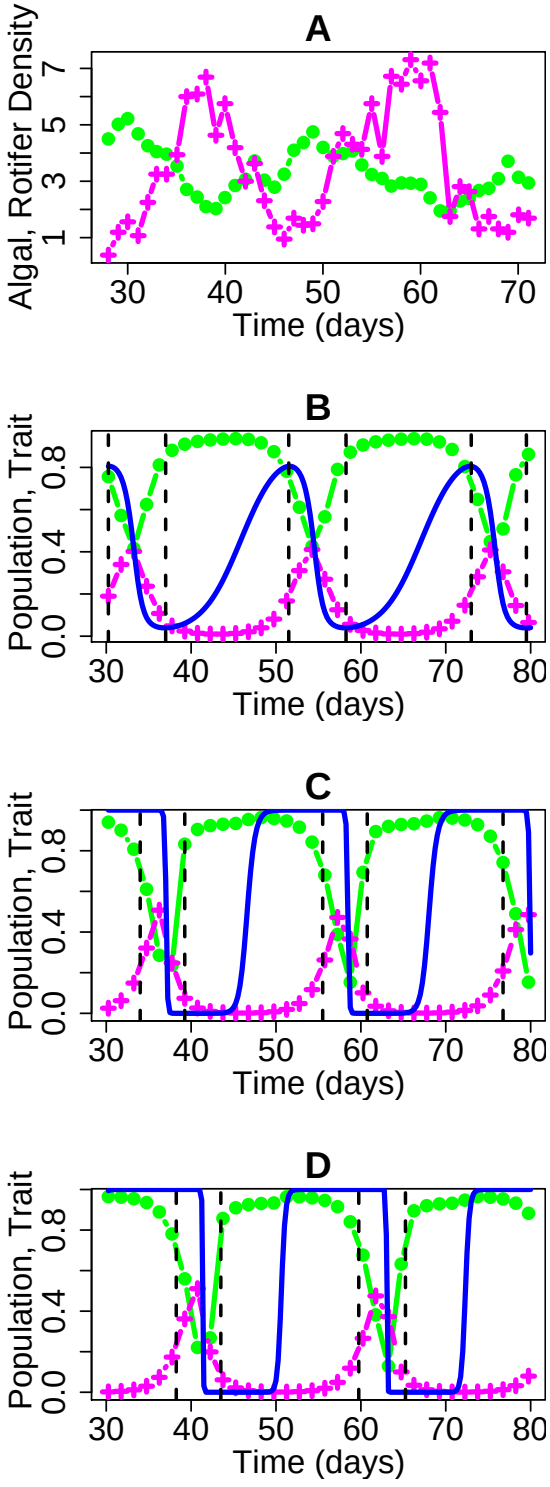
A
Algal, Rotifer Density
1
3
5
7
30
40
50
60
70
Time (days)
B
Population, Trait
0.0
0.4
0.8
30
40
50
60
70
80
Time (days)
C
Population, Trait
0.0
0.4
0.8
30
40
50
60
70
80
Time (days)
D
Population, Trait
0.0
0.4
0.8
30
40
50
60
70
80
Time (days)

1.3 Fast-Slow Systems and Models

To introduce some basic concepts of fast-slow dynamical systems we consider a modified Rosenzweig-MacArthur model [Rosenzweig and MacArthur, 1963]. We assume that the prey responds to ecological conditions faster than the predator. Such a case would be analogous to thinking about birds (long lifetimes) and their insect prey (shorter lifetimes). Our model is

$$\begin{aligned} \epsilon \frac{dx}{dt} &= x\left[r - \frac{x}{K} - \frac{ay}{1+hx}\right] \\ \frac{dy}{dt} &= y\left[\frac{bay}{1+hx} - d\right]. \end{aligned} \tag{1.1}$$

where x is prey density, y is predator density, r is the exponential growth rate of the prey without density limitation, K is the prey carrying capacity, a is the encounter rate, h is the handling time, b is the conversion of prey to predator density, and d is the per capita death rate of the predator. In this model, ϵ is a small positive number that represents the difference in time scales between the prey and predator species. It is meant to explicitly flag that the prey population processes are occurring on a faster time scale than the predator processes.

Solutions to a fast-slow system, like those in figure 1.2 *B*, behave in a way that is qualitatively different from models without a separation of time scales (figure 1.2 *A*). In particular, solutions of such a system spend nearly all of their time near an object called the critical manifold and the rest jumping between different pieces of the critical manifold. For a general fast-slow system, the critical manifold, C, is the set of equilibria of the fast variable when $\epsilon = 0$ and the slow variables are held constant. These points make up a collection of curves or planes in the full system. In system (1.1), C is the set of points satisfying

$dx/dt = 0$, or equivalently the predator axis and prey nullcline:

$$C = \left\{(x, y) : \; x\left[r - \frac{x}{K} - \frac{ay}{1 + hx}\right] = 0\right\}. \tag{1.2}$$

We divide C into three different curves: a left (C_L), a middle (C_M), and a right (C_R) branch. In figure 1.2 B, C_L is the predator axis (blue) and together C_M (green curve) and C_R (gray curve) make up the prey nullcline. When solutions to system (1.1) are near the critical manifold, they behave as if they were on it. Thus, to understand how solutions of a fast-slow system behave, we need to understand what solutions on the critical manifold do, where they jump away from it, and where they land near it.

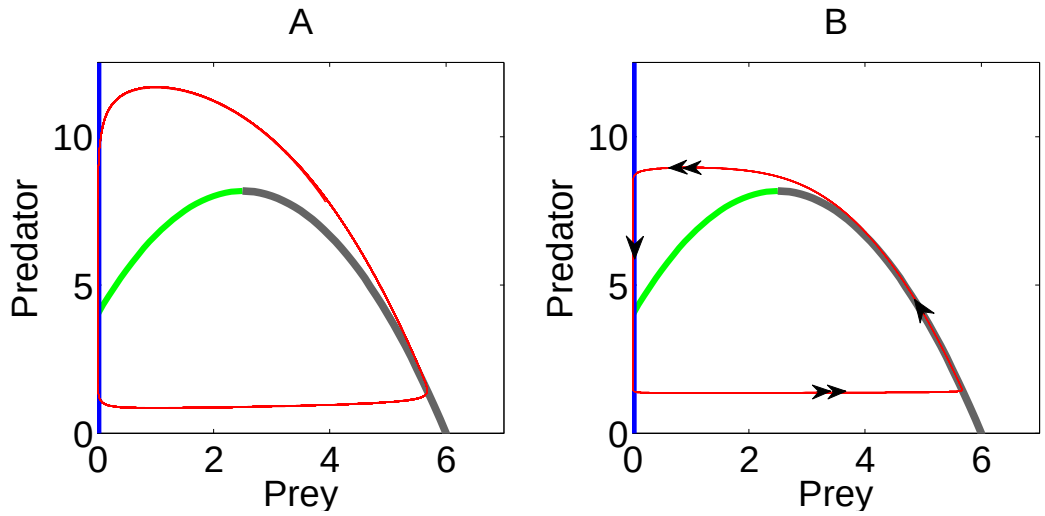

Figure 1.2: Example oscillatory dynamics (red) in a predator-prey system (1.1) with a fast prey species. The predator (vertical) axis and the green and gray curves define the left, middle, and right branches of the critical manifold, respectively. Double arrows in B indicate the direction of fast flow and the single arrows indicate the direction of the slow flow along the critical manifold. $\epsilon = 1$ in A and $\epsilon = 0.1$ in B. Other parameters are $a = 1$, $b = 1$, $d = .5$, $h = 1$, $K = 1.5$, and $r = 4$.

The single arrows in figure 1.2 B indicate how trajectories move on or near the critical manifold. When near C_L, solutions move down and when near C_R, solutions move up. Note that even though C is defined to be the equilibria

of the fast variable, solutions will still move near C because the fast and slow variables are coupled. The double arrows in figure 1.2 B indicate the stability of different parts of the branches. This stability dictates where solutions jump off of C (repelling behavior) and where they land on it (attracting behavior). In figure 1.2 B, the lower set of double arrows indicates that the piece of C_L below the green curve is repelling and that C_R is attracting. The upper set of double arrows indicates that the apex of C_R is repelling and the part of C_L above the green curve is attracting.

Solutions of a fast-slow system behave in the following manner. First, a solution quickly runs near to an attracting branch of the critical manifold. The solution then slowly moves as if constrained to that branch. If the solution encounters a stable equilibrium point on the branch, then the solution will go to that equilibrium. If it does not encounter one, then the solution will continue until it reaches a jumping point. After jumping, the solution will quickly run to a second stable branch of the critical manifold, land, and repeat the sequence.

As an example, consider the trajectory in figure 1.2 B and note that the equilibrium point for these parameter values is unstable and located on C_M. A solution starting near the lower set of double arrows quickly runs to C_R. Then the solution slowly moves up C_R until it nears the apex of the prey nullcline (where the C_M and C_R meet). Near the apex, the solution jumps off C_R and quickly runs to the upper part of C_L. Once near C_L, the solution moves down the predator axis until it jumps off somewhere below the intersection of C_L and C_M (where the green and blue curves intersect). The cycle then repeats.

There are two significant advantages to restricting our attention to the dynamics on the critical manifold instead of analyzing the full system. First, since

the critical manifold is of lower dimension than the full system, the restriction makes the mathematical analysis simpler. For system (1.1), we can understand a two-dimensional model by analyzing one-dimensional branches of the critical manifold. Second, the dynamics that occur when $\epsilon \approx 0$ can be used to understand and predict dynamics when $\epsilon \approx 1$. Consider the trajectory in figure 1.2 *A* that spends almost no time near C_R when $\epsilon = 1$ and the trajectory in figure 1.2 *B* that spends almost half of its time near C_R when $\epsilon = 0.1$. As ϵ decreases to zero, the position of C does not change and solutions stick closer to C for longer periods of time. In addition, the periodic orbit retains it's qualitative shape as ϵ becomes smaller. Thus, while we don't necessarily believe that the prey species dynamics will be infinitely faster than those of the predator ($\epsilon \approx 0$), that limit yields insight into the dynamics that occur when prey is moderately faster than the predator ($\epsilon \approx 1$).

1.3.1 Predator-Prey Model with Predator Evolution

Here we present a general predator-prey model with predator evolution that will be the focus of the chapter. Due to our model's level of generality, a system with predator evolution can be transformed into a system with prey evolution mathematically by reversing time (see appendix A.1). Most results carry over between the two cases (see appendix A.6). Differences that arise between the two types of evolution will be presented in section 1.4.4.

Our general model for a predator-prey system (y, x respectively) with fast

evolution of the mean predator trait value, β, is given by

$$\begin{aligned} \frac{dx}{dt} &= F(x) - G(x, y, \beta) \\ \frac{dy}{dt} &= H(x, y, \beta) - D(y, \beta) \\ \epsilon \frac{d\beta}{dt} &= B(\beta) V \frac{\partial}{\partial \beta} \left[\frac{1}{y} \frac{dy}{dt} \right]. \end{aligned} \tag{1.3}$$

F is the growth rate of the prey population in the absence of predation, G is the predation rate of the prey, H is the composition of the prey to predator conversion and predation rate of the prey, and D is the death rate of the predator population. The product $B(\beta)V$ defines the additive genetic variance of the trait, where $B(\beta)$ is a bounding function for the trait β. A typical functional form we will use is $B(\beta) = (\beta - \beta_{min})(\beta_{max} - \beta)$, where β_{min} and β_{max} are the minimal and maximal values the trait can attain. ϵ is a small positive value that flags the separation of time scales between the ecological and evolutionary processes. By decreasing the value of epsilon, we speed up the rate of evolution (e.g. see figure 1.1). Throughout the text, any variable subscripts denote partial derivatives, e.g. H_β is short for $\partial H/\partial \beta$ and $G_{x\alpha}$ is short for $\partial^2 G/\partial x \partial \alpha$.

Typically the functions F, G, H and D are written in terms of per capita growth rates, $xf(x)$, $xg(x, y, \beta)$, $yh(x, y, \beta)$, and $yd(y, \beta)$, respectively. We use the more general functions to simplify notation. Throughout this chapter we will assume the following about the functional responses in system (1.3). First, G and H are strictly increasing smooth functions of x, y, and β. Second, D is a strictly increasing smooth function of y and β. Note that our assumptions about D and H being increasing functions of β implicitly define a trade-off for the trait, which in general will be density-dependent. As the predator invests more in the trait and β increases, the predator birth rate will increase at the expense of a higher death rate.

The equation representing the trait dynamics in system (1.3) follows from the quantitative genetics approach derived in Lande [1982] and Abrams et al. [1993]. The theory assumes that the mean trait value (β) of a population changes at a rate proportional to both the additive genetic variance of the trait and the individual fitness gradient. This implies that the magnitude and direction of the selection pressure is determined by the fitness gradient of the trait, $\frac{\partial}{\partial \beta}\left[\frac{1}{y}\frac{dy}{dt}\right]$. Gradient dynamic approaches are a first approximation to many models and their simplicity makes them analytically tractable [Abrams, 2001, 2005]. In addition, gradient dynamics models capture a range of behavior observed at the phenotypic level without having to specify gene level processes. Thus, they are a good way to begin to understand the behavior of eco-evolutionary models, but may yield an incomplete picture when specifics about the complexities of the genetic processes matter.

The direction and magnitude of the selection pressure can be both density and frequency dependent. When selection is frequency dependent, the trait equation in system (1.3) involves the gradient with respect to the fitness of the invader's phenotype instead of the resident's phenotype,

$$\epsilon \frac{d\beta}{dt} = B(\beta) V \frac{\partial}{\partial \hat{\beta}} \left(\frac{1}{y} \left[H(x, y, \beta, \hat{\beta}) - D(y, \beta, \hat{\beta}) \right] \right) |_{\hat{\beta}=\beta} \tag{1.4}$$

We will consider the special case where selection is not frequency dependent. Thus, fitness will not depend on the frequency of trait values and an individual with a new trait $\hat{\beta}$ will invade and replace a population with mean trait β if the relative fitness of the invading individual is higher than an individual with the mean trait value. We use this special case of the theory due to its analytic tractability and as a first approach to studying the effects of rapid evolution on ecological dynamics.

1.3.2 Fast-Slow Dynamics in the Eco-Evolutionary Model (1.3)

When ϵ is a small positive value, the dynamics of system (1.3) can be understood by knowing how solutions move on the critical manifold, where solutions jump off of the critical manifold, and where they land on it. For system (1.3), points on the critical manifold, C, satisfy $d\beta/dt = 0$, or equivalently

$$C = \left\{(x, y, \beta) : \ B(\beta)[H_\beta(x, y, \beta) - D_\beta(y, \beta)] = 0, y > 0\right\}. \tag{1.5}$$

We divide C into a left, middle, and right branch, defined respectively as:

$$C_L = \{(x, y, \beta) : \ x > 0, y > 0, \beta = \beta_{min}\} \tag{1.6}$$

$$C_M = \left\{(x, y, \beta) : \ [H_\beta(x, y, \beta) - D_\beta(y, \beta)] = 0, y > 0, \beta \in (\beta_{min}, \beta_{max})\right\} \tag{1.7}$$

$$C_R = \{(x, y, \beta) : \ x > 0, y > 0, \beta = \beta_{max}\}. \tag{1.8}$$

Instead of one-dimensional curves, as in figure 1.2, now each branch is a two-dimensional surface or plane in three-dimensional space (see figure 1.3).

To understand when trajectories jump off of and onto the critical manifold, we classify points on C as attracting or repelling. For a point ρ on C_M, the value of $B[H_{\beta\beta} - D_{\beta\beta}]$ evaluated at that point, $B(\beta)[H_{\beta\beta}(\rho) - D_{\beta\beta}(\rho)]$, is the potentially nonzero eigenvalue for the fast dynamics. Because $B(\beta) \geq 0$, this eigenvalue has the same sign as $H_{\beta\beta} - D_{\beta\beta}$. When the eigenvalue is negative, the point will be attracting and trajectories will land on it. When the eigenvalue is positive, the point will be repelling and trajectories will jump from it. Similarly, $B_\beta(\rho)[H_\beta(\rho) - D_\beta(\rho)]$ is the potentially nonzero eigenvalue for the fast dynamics for points on

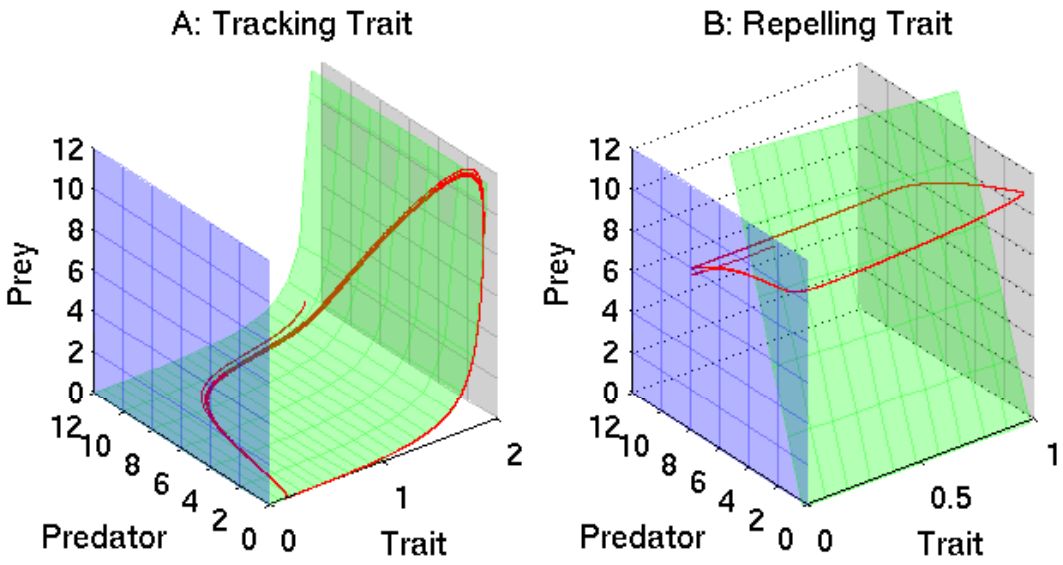

Figure 1.3: Example trajectories (red) for a predator-prey system with a tracking (A) or repelling (B) predator trait. The blue, green, and gray planes define the left, middle, and right branches of the critical manifold, respectively. See appendix A.8 for equations and parameter values.

C_L and C_R. To summarize, for a point ρ on C:

$$C_M: \quad H_{\beta\beta}(\rho) - D_{\beta\beta}(\rho) < 0 \qquad \text{Stable} \qquad (1.9)$$

$$H_{\beta\beta}(\rho) - D_{\beta\beta}(\rho) > 0 \qquad \text{Unstable} \qquad (1.10)$$

$$C_L, C_R: \quad B_\beta(\rho)[H_\beta(\rho) - D_\beta(\rho)] < 0 \qquad \text{Stable} \qquad (1.11)$$

$$B_\beta(\rho)[H_\beta(\rho) - D_\beta(\rho)] > 0 \qquad \text{Unstable} \qquad (1.12)$$

In total, landing points satisfy equation (1.9) or (1.11) and jumping points satisfy equation (1.10) or (1.12).

Solutions to system (1.3) behave in the following manner. First a trajectory quickly approaches an attracting piece of critical manifold. During this time, the population densities do not change substantially. Once near the attracting piece, the trajectory moves along the critical manifold as if it were stuck to that

surface. If the trajectory never leaves the attracting part of the surface, then it will stay near that surface for all time and go to a stable equilibrium point or periodic orbit. If instead the trajectory enters the repelling part of the surface, then the trajectory will jump away from that part of the critical manifold and land on an attracting part of the critical manifold. The trajectory then repeats the sequence.

As an intuitive example of how solutions move in our system, consider a water droplet falling from the sky onto a slanted roof suspended above a sidewalk. The direction of fast movement in the system is up and down. The sidewalk and roof are branches of the critical manifold. Due to gravity, the droplet is attracted to the roof and very quickly falls onto it. Once on the slanted roof, the drop slowly moves towards the edge of the roof. This slow movement is just like the slow movement along the critical manifold. When the drop gets to the edge of the roof, again due to gravity, the droplet will be repelled from the roof edge and be attracted to the sidewalk. The water drop then quickly falls to the sidewalk and moves slowly along it. Trajectories in our system will essentially behave the same except that it will sometimes be possible for solutions to become trapped on the critical manifold at a stable equilibrium or periodic orbit. Going back to the water drop, this situation is analogous to the drop getting caught in a divot on the roof or sidewalk.

In figure 1.3 we present two examples of how trajectories can behave in our system. When selection favors intermediate trait values, all of C_M is attracting (equation (1.9) always satisfied) and the trajectory stays near C_M for all time. When selection favors extreme values, all of C_M is repelling (equation (1.10) always satisfied) and the trajectory alternates between being near C_L and being

near C_R. We will refer to first case as a tracking trait and the second as a repelling trait.

1.4 Results

1.4.1 Local Stability Analysis

To begin understanding the effects of fast evolution, we first analyze how incorporating evolution into a predator-prey system changes the stability of the ecological dynamics. To do this, we compare the stability of an equilibrium point of system (1.3) to the stability of the same equilibrium point when we freeze evolution by setting $d\beta/dt = 0$ (see appendix A.3 for details). In this section we will consider only tracking traits (which represent stabilizing selection) and pay particular attention to cases where stable evolutionary dynamics either destabilize population dynamics that would head towards a stable equilibrium in the absence of evolution or stabilize population dynamics that would cycle in the absence of evolution.

As seen in theorem A.2 of appendix A.3, the effect evolution has on the stability of the population dynamics depends on the sign of $H_{x\beta}$. Since $H_\beta - D_\beta$ represents the strength of selection on the trait, $H_{x\beta} = H_{x\beta} - D_{x\beta}$ represents how the strength of selection and the reward for investing in the trait increases or decreases as prey density increases. When $H_{x\beta} > 0$, the trait becomes more rewarding and the strength of selection increases as prey density increases. In this case, stable evolutionary dynamics increase the region of stability of the population dynamics and the inclusion of evolution in a system with cyclic population

dynamics could lead to a equilibrium state for the populations. When $H_{x\beta} < 0$, the trait becomes less rewarding and the strength of selection decreases as prey density increases. In this case, stable evolutionary dynamics decrease the region of stability of the population dynamics and the inclusion of evolution in an ecological system at equilibrium could lead to population oscillations. This result is quite counterintuitive since the trait ($d\beta/dt$ equation) and population subsystems (system (1.3) with $d\beta/dt = 0$) would tend to stable equilibria when decoupled, but now cycle when coupled. These two results emphasize that it is not enough to understand the stability of the evolutionary and ecological processes separately in order to determine the stability of the eco-evolutionary system.

To illustrate the above ideas we examine two examples. First, consider a modified Rosenzweig-MacArthur model [Rosenzweig and MacArthur, 1963] with $F = x(r - kx)$, $G = H = bxy/(1 + cx/\beta)$ and $D = y(a\beta^2 + d)$ for some positive parameters a, b, c, d, r, and k. Here, increasing the predator's trait decreases the predator's handling time parameter at the cost of increasing the per capita death rate of the predator. Since the trait becomes increasingly rewarding as prey density increases ($H_{x\beta} > 0$), the addition of evolution to a cycling ecological model can cause the populations to head towards a stable equilibrium (figures 1.4 *A* and *B*).

For the second example, consider another modified Rosenzweig-MacArthur model where $F = x(r - kx)$, $G = H = bxy\beta/(1 + x\beta)$ and $D = y(a\beta + d)$. Here, as the predator invests more in the trait, the searching efficiency of the predator increases at the cost of an increased death rate. An increased searching efficiency implies that an individual will necessarily spend more time eating and less time

searching, but as prey density increases, the value of being an efficient searcher will decrease and having a shorter handling time will be more rewarding. Thus, investment in searching efficiency yields diminishing returns as prey density increases ($H_{x\beta} < 0$). As seen in figures 1.4 *C* and *D*, this allows for the case where the population dynamics tend to equilibrium when the trait is frozen but with the addition of stable evolutionary dynamics, the populations cycle for all time.

1.4.2 Trade-Off Curves

One special case of system (1.3) of particular interest is when the effect of the trait on the predator recruitment and death rate is density independent. Mathematically, this means that the functional forms of the terms in system (1.3) factor as

$$\begin{aligned} H(x, y, \beta) &= h(x, y)\eta(\beta) \\ D(y, \beta) &= d(y)\delta(\beta). \end{aligned} \tag{1.13}$$

This factorization allows us to write δ as a function of η (see appendix A.4), which defines a trade-off curve between the proportional increase of the predator recruitment and proportional increase of the predator death rate. Qualitative properties of the trade-off curve, defined by $\delta(\eta)$, can be used to predict qualitative properties of the population and trait time series, but the above factorization also limits the range of dynamical behavior a system can exhibit.

The concavity of the trade-off curve determines whether trait dynamics are stable or unstable (theorems A.3 and A.4 of appendix A.4). For a trait value at β, if $\delta(\eta)$ is concave up, then the trait dynamics are stable and if $\delta(\eta)$ is concave

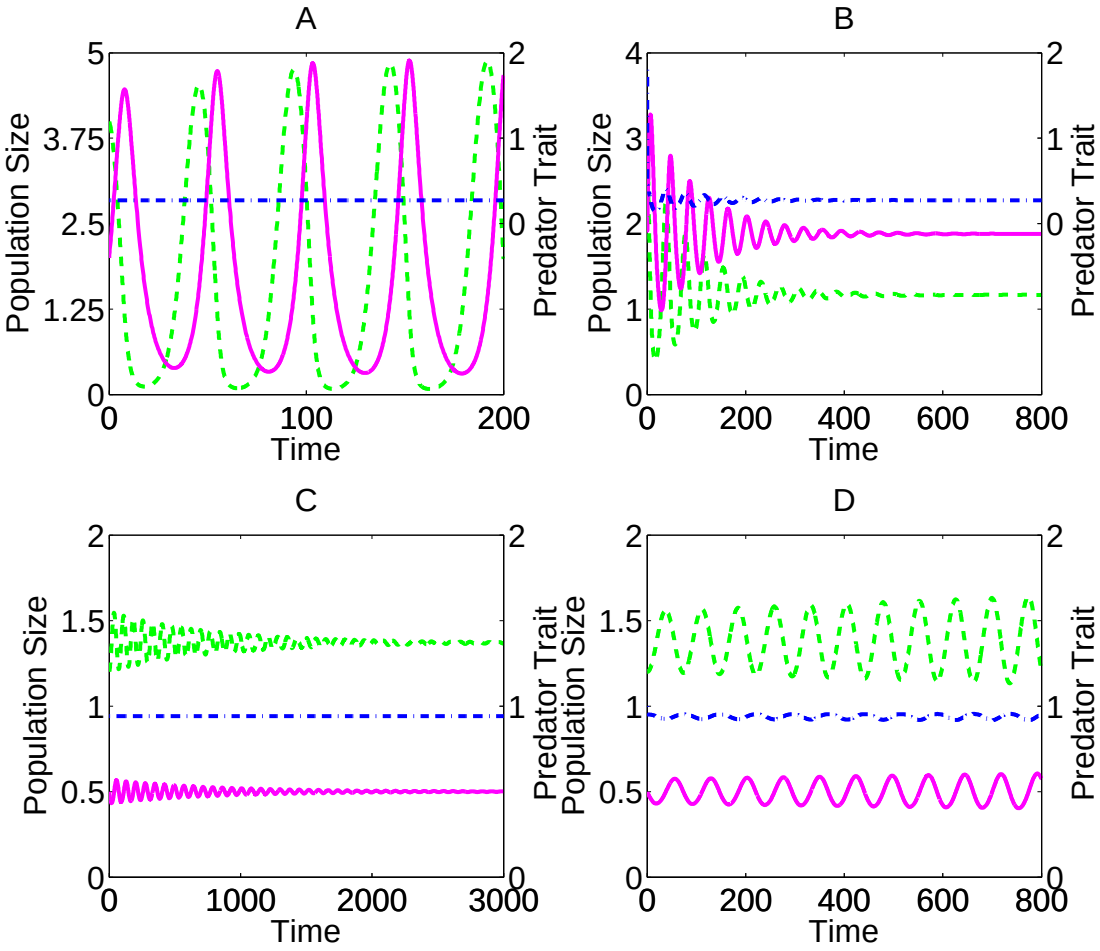

Figure 1.4: Examples of evolution (*A*-*B*) stabilizing and (*C*-*D*) destabilizing population dynamics. (*A*) Population dynamics cycle and trait dynamics tend to an equilibrium state when decoupled. (*B*) When coupled, the population and trait dynamics tend to stable equilibria. (*C*) Population and trait dynamics tend to stable equilibria when decoupled. (*D*) When coupled, the system is unstable and yields cyclic dynamics. In *A* and *B*, $a = 3$, $b = 1.86$, $c = 0.1$, $d = 1.3$, $k = 0.4$ and $r = 2.95$ and for the evolutionarily fixed dynamics $\beta \approx 0.27$. In *C* and *D*, $b = 3.82$, $c = 1$, $d = 1.21$, $k = 0.34$ and $r = 1.25$ and for the evolutionarily fixed dynamics $\beta \approx 0.94$.

down, then the trait dynamics are unstable at β. This implies that always concave up trade-off curves yield tracking traits, and always concave down trade-off curves yield repelling traits.

If the trade-off curve is always concave up, then the population dynamics ei-

ther tend to equilibrium or exhibit predator-prey oscillations where the predator lags behind the prey with a phase lag of less than one quarter of the cycle period. Examples of the second case are presented in figures 1.5 *A* and 1.5 *C* for two different trade-off curves. There are substantial quantitative differences between the oscillatory dynamics of figures 1.5 *A* and 1.5 *C*. The derivatives of the trade-off curves allow one to distinguish between the different cases. In figure 1.5 *B*, the derivative of the trade-off curve is large in magnitude and increasing very rapidly. Consequently, the large population fluctuations in figure 1.5 *A* result in only small changes in the trait. If the curve resembles a straight line, i.e. has little curvature like in figure 1.5 *D*, then, as depicted in figure 1.5 *C*, small population oscillations will yield large trait fluctuations. For the intermediate case where the derivative is small in magnitude but still increasing, substantially large population oscillations will lead to large trait oscillations.

If the trade-off curve is always concave down, either the trait value converges to one of the extreme values and evolution ceases, or the trait oscillates between the two extreme values of the trait (figure 1.5 *E*). These oscillations are known as relaxation oscillations in the fast-slow dynamical systems literature. We have numerically investigated a large number of models and our findings suggest that while possible, relaxation oscillations of the trait are not the typical behavior of systems with a concave down trade-off curve and they only occur for a few initial conditions in very small ranges of parameter space. Furthermore, our numerical investigations suggest that the relaxation oscillations in the trait will not alter the population dynamics in a way that distinguishes them from the population dynamics occurring on the β_{min}- or β_{max}-plane. Thus, when the trade-off curve is always concave down, we can assume that the ecological dynamics will behave as if the trait is frozen either at β_{min} or β_{max}.

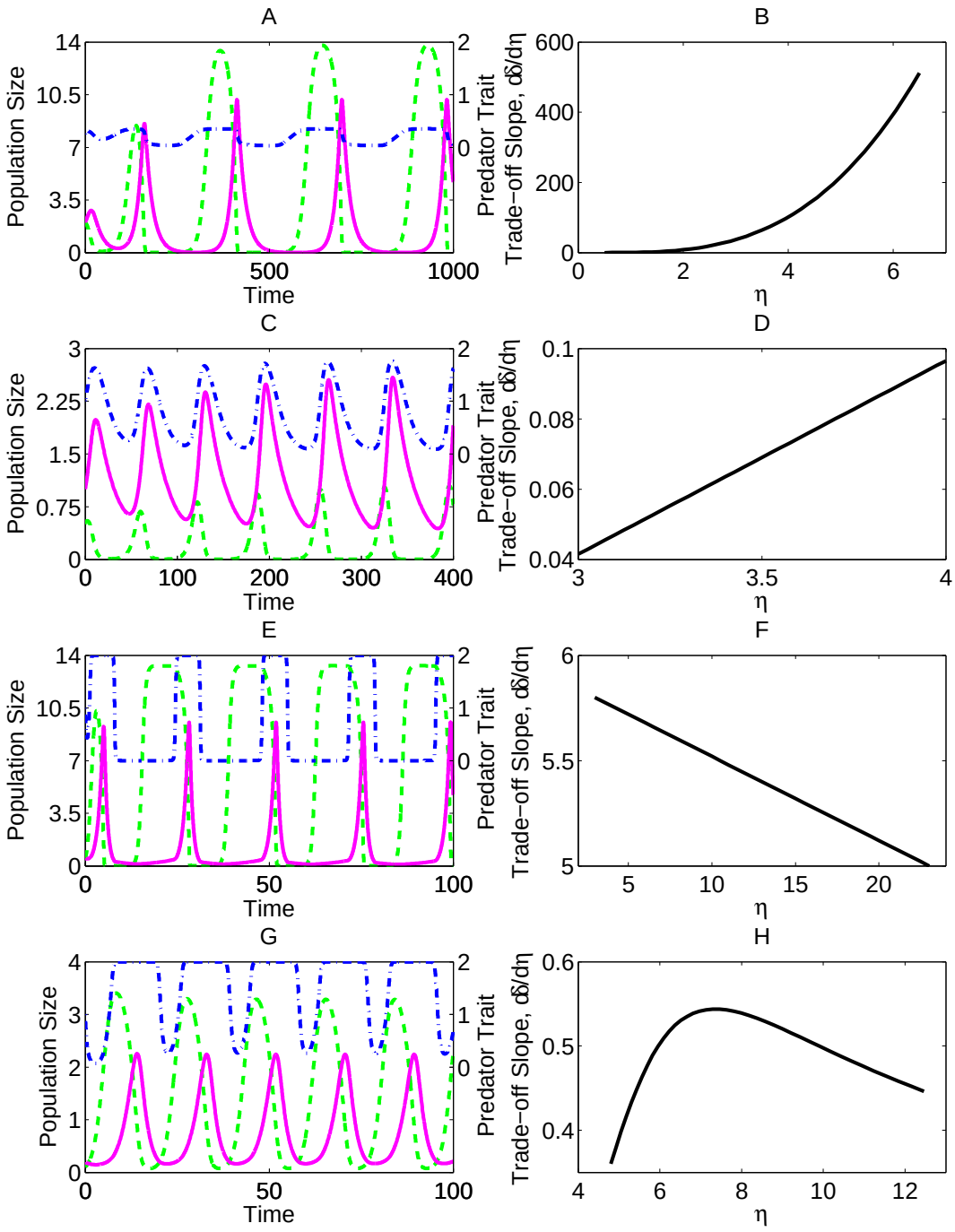

Figure 1.5: Examples of oscillating population and trait time series when a trade-off curve defines the cost for the trait. (Left Column) Predator, prey, and trait dynamics are the solid magenta, dashed green, and dot-dashed blue curves, respectively. (Right Column) Derivative of the trade-off curve ($d\delta/d\eta$) assuming the factorization in equation (1.13). The trade-off curve is (*A*-*B*) concave up, (*C*) concave down, and (*D*) s-shaped. Equations and parameters are given in appendix A.8.

Finally we consider the case when the trade-off curve does not have constant concavity and instead has a sigmoid shape (figure 1.5 *H*). Since the trade-off curve has concave up and concave down sections, all of the dynamics in figure 1.5 can be observed with this trade-off curve. In addition, time series for an s-shaped trade-off curve can be a concatenation of those seen with a concave up or concave down trade-off curve. For example, the trait dynamics near β_{max} in figure 1.5 *G* resemble the square wave-like oscillations in figure 1.5 *E* (called relation oscillations) and near β_{min}, the trait dynamics resemble those seen in figure 1.5 *C*. While rare when the trade-off curve is concave down, relaxation oscillations are much more common in systems where the trade-off curve does not have constant concavity. Thus, in general, factoring of the functional responses does not prevent relaxation oscillation type dynamics.

1.4.3 Boundary Plane Projections

In this section we present a simple graphical technique that allows one to predict the types of behavior and phenomena that arise with a repelling trait (e.g. figure 1.3 *B*). This graphical method allows us not only to determine what dynamics a particular model can exhibit, but also to distinguish between different biological mechanisms that yield new ecological behavior. Furthermore, our approach has the computational advantage that we capture all of the information about the dynamics exhibited in the three-dimensional system (1.3) with two two-dimensional plots. By using the partial information contained in these two-dimensional plots to predict the dynamics that will occur in the full three dimensional system, we can greatly reduce the amount of analysis needed to determine what types of behavior a particular model can exhibit.

To illustrate the idea behind the method, consider the trajectory in figure 1.3 *B*. Because the trait is repelling, the trajectory in figure 1.3 *B* oscillates between being very close to C_L (blue plane) and being very close to C_R (gray plane). Notice that the population densities do not change significantly when the trajectory jumps from one plane to the other. This suggests that the changes in predator and prey densities are solely determined by the behavior on the C_L and C_R planes. By understanding how the population densities change on these two planes and where the trajectory switches between planes (representing where the direction of selection switches), we can understand the behavior of the trajectory in the full three-dimensional picture.

To construct our graphic we need four pieces of information: the dynamics on C_L, the dynamics on C_R, and the points where trajectories will be repelled (jump) from each plane. The dynamics on C_L and C_R are determined by fixing the trait at β_{min} and β_{max}, respectively, in system (1.3). Trajectories on C_L or C_R will tend to stable equilibria or periodic orbits in those planes. We will refer to these stable objects as boundary attractors. The repelling points on each plane are those that satisfy equation (1.12) and the attracting points are those that satisfy equation (1.11). In our system, the repelling and attracting parts of the planes will be separated by a line defined by the intersection of C_M with C_L and C_R. In figure 1.3 *B*, the repelling part of C_L is above the intersection with C_M (large prey values, small predator values) and the attracting part is below that line (small prey values, large predator values). C_R is divided in the opposite way. Note that the division of the planes into attracting and repelling parts based on their intersection with C_M is exactly like the division of the gray curve in figure 1.2 into an attracting and a repelling piece.

The above information gives us two x, y-planes that each contain a collection of stable attractors and a line separating the plane into repelling and attracting parts. To make the graphic, we superimpose these two planes upon each other and look at one x, y-plane. Going back to figure 1.3 *B*, in essence we have removed C_M (green plane) and pushed C_L and C_R together. This collapse of three-dimensional (x, y, β) space gives us one two-dimensional (x, y) plane that contains the stable attractors, the repelling regions, and the attracting regions of both C_L and C_R.

Trajectories of the full system behave in the following way on the two-dimensional plot (see figure 1.6 *B*). The trajectory starts in the attracting region of C_L or C_R and approaches a stable attractor of that plane. While approaching the attractor, it may enter the repelling region of that plane. If it does, then the trajectory switches to following the dynamics in the opposite plane. This causes the trajectory to approach the stable object in the second plane. If the trajectory enters the repelling region of the second plane, then it will switch to following the dynamics in the first plane. When this cycle repeats indefinitely, the resulting population dynamics are a periodic orbit where the trait is cycling as well. If a trajectory stays in the attracting region of a plane for all time, then evolution will cease and the population dynamics will behave as if restricted to that plane for all time.

In the following we present how the types and positions of the stable attractors in our two dimensional graphic allow us to completely determine the dynamics exhibited in the three dimensional model. To facilitate understanding, we will assume C_L and C_R have one stable attractor each and whenever possible, that the curves separating the planes into attracting and repelling regions

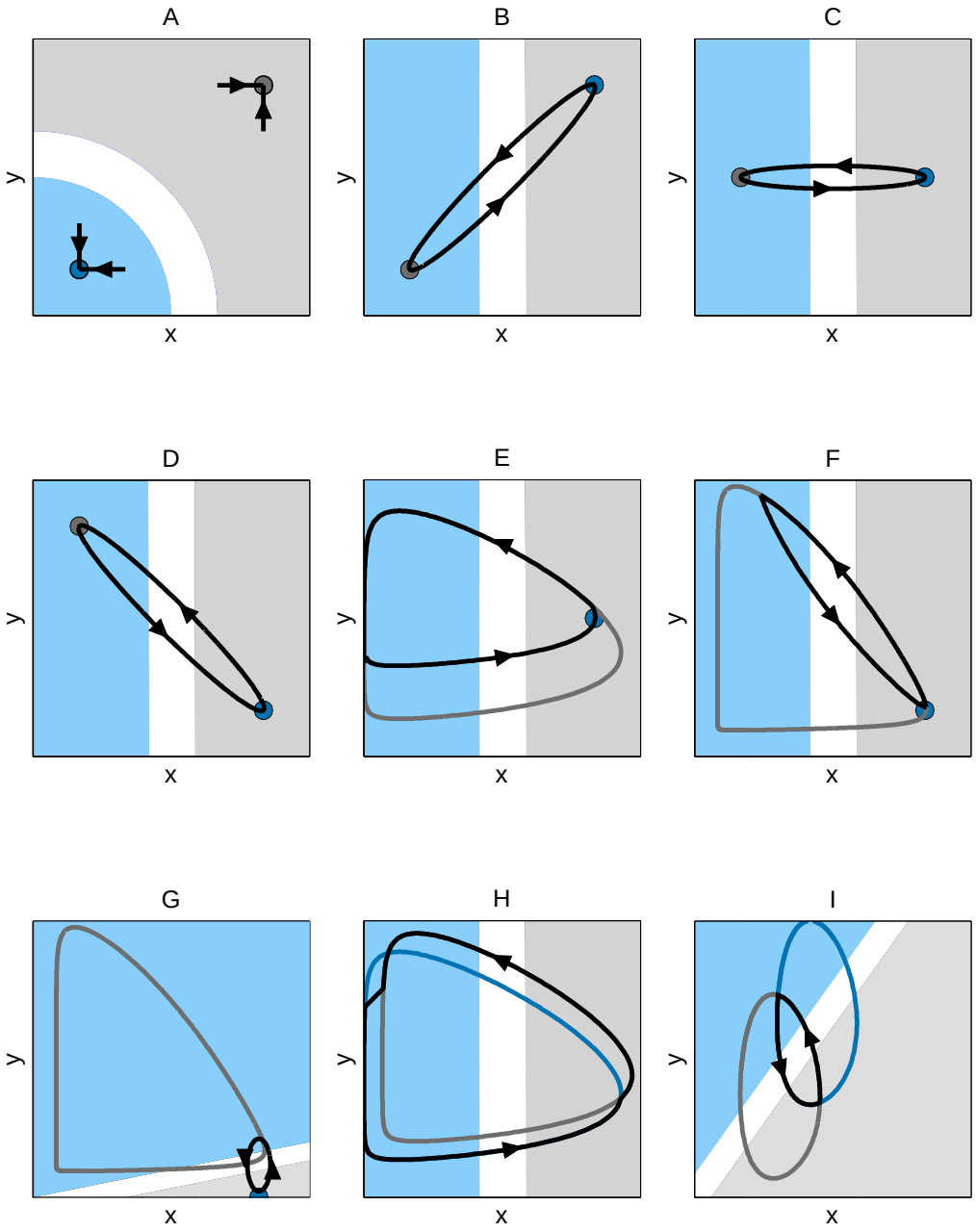

Figure 1.6: Qualitative representations of the dynamics that a predator-prey system with repelling predator trait dynamics can exhibit, projected onto the x,y-plane. Dark blue (dark gray) equilibria or periodic orbits represent the stable limiting dynamics on the β_{min}-plane (β_{max}-plane). Black curves represent the observed population dynamics of the full evolving system projected onto the x,y-plane. Light blue (light gray) regions correspond to population levels where the trait is decreasing (increasing) for all trait values. White regions correspond to population levels where the β_{min} and β_{max} planes are both locally attracting for the trait dynamics.

are parallel to the y-axis. The analysis is the same when these assumptions are relaxed. Finally, in figure 1.6, trajectories will spend some time in the repelling region of a plane and not jump immediately before switching their behavior (for example see figure 1.6 B). This behavior is common, though not the rule, and we use it to emphasize how trajectories will behave.

Equilibrium-Equilibrium Case

We begin with the simplest case where C_L and C_R only have one stable equilibrium point. If at least one of the equilibria is located in the attracting region of its respective plane then trajectories will converge to that equilibrium and evolution will cease. Cases where both equilibria are in the attracting region of their planes yield systems with bistability (figure 1.6 A). For example, the particular set up in figure 1.6 A means that the predator-prey system (1.3) would tend to one of two equilibrium states. Either both species would be scarce and the predator would have a small trait value or both species would be abundant and the predator would have a large trait value. Since only one equilibrium needs to be in the attracting region of its plane to have evolution cease, an initial check for evolutionary convergence of a repelling trait is whether any equilibria are in the attracting regions of their planes.

Now assume each boundary contains a single equilibrium contained in the repelling region of the plane. These equilibria are saddles that are attracting in the x- and y-directions but repelling in the β-direction. In our graphic, trajectories from such systems will alternate between approaching the C_L and C_R equilibria (see figures 1.6 B, 1.6 C, 1.6 D, and 1.7 B for examples). In the full three dimensional picture, trajectories behave as follows. First, the trajectory quickly

runs close to the attracting region of one of the boundary planes. Then, the trajectory slowly moves toward the equilibrium point as if it was restricted to that plane. As the trajectory approaches the equilibrium point, it will cross into the repelling region of that plane. Eventually the trajectory is repelled to the second plane where it will behave as if constrained to that plane. As the trajectory approaches the equilibrium in the second plane, it will cross into the repelling region, run away to the first boundary plane, and repeat the cycle. This yields periodic behavior like in figure 1.7 *A* and 1.7 *B*.

Qualitative properties of the above periodic orbits are determined by the relative positions of the two equilibria in *x*,*y*-plane. When one equilibrium has a greater predator density and a greater prey density than the other equilibrium, classical cycles with a predator lag less than or equal to a quarter of the period are observed (figures 1.6 *B*, 1.7 *A* and 1.7 *B*). If the predator densities of both equilibria are equal and the densities of the prey sufficiently different, then the prey will cycle substantially while the predator population will remain relatively constant (figure 1.6 *C*). This phenomena has been named cryptic dynamics [Yoshida et al., 2007]. Finally, when one equilibrium has a greater predator density and a smaller prey density than the other equilibrium, predator-prey oscillations with a lag greater than a quarter of the period result (figures 1.6 *D*, 1.7 *C* and 1.7 *D*). Cryptic dynamics and oscillations with a lag greater than a quarter of the period are not observed in non-evolving systems.

All of the equilibria in figures 1.6 *A*, 1.6 *B*, and 1.6 *C* are coexistence equilibria (both species have a positive density). Another case of interest is when one of the equilibria is an extinction equilibrium (predator density is zero). In this case, one of boundary equilibria is on the *x*-axis and in the ecological dynamics on

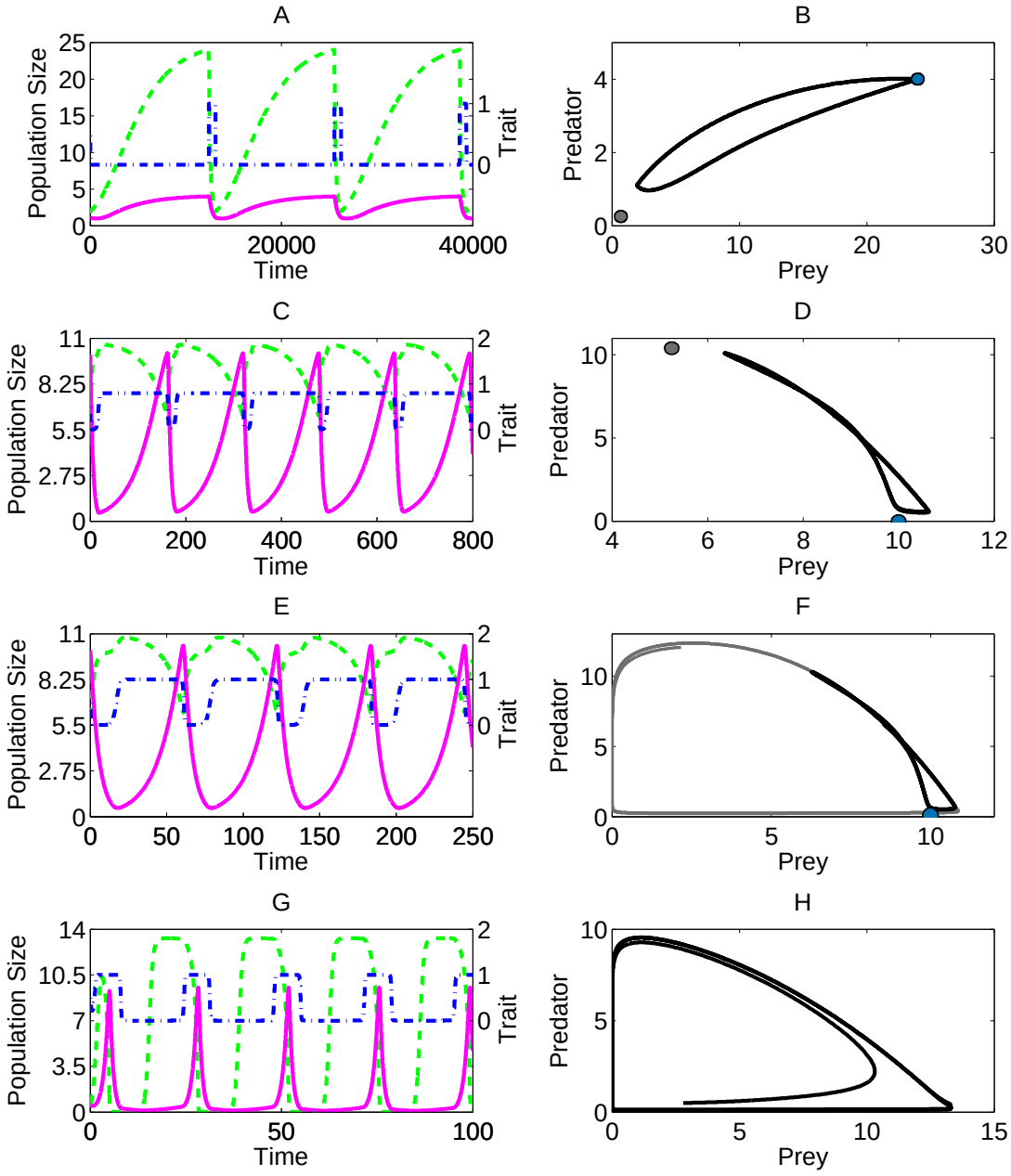

Figure 1.7: Examples of population and trait time series (left column) for (*A*) figure 1.6 *B*, (*C*) figure 1.8 *D*, (*E*) figure 1.8 *G*, and (*G*) figure 1.6 *H*. A projection of the population dynamics onto the predator,prey-plane (black curve) accompanies each example in the right column. For each projection a gray (blue) equilibrium or periodic orbit represents the stable attractor in the α_{min}- or β_{min}-planes (α_{max}- or β_{max}-planes). In plot *H*, the stable periodic orbits of the β_{min}- and β_{max}-planes lie almost exactly on top of the black orbit and are omitted.

that plane, the predator always goes extinct. When the extinction equilibrium is in the attracting part of the plane, evolution leads to Darwinian extinction [Webb, 2003, Parvinen, 2005]. If the extinction equilibrium is in the repelling region, then predator-prey cycles with a lag greater than a quarter of the period are possible. In this case, our graphic looks like figure 1.6 *D* except that the β_{min}-plane equilibrium (blue equilibrium) is on the x-axis.

Periodic Orbit Case

Assume either C_L or C_R has an equilibrium point in the repelling part of its plane and that the other has a periodic orbit partially in the repelling part of its plane. As in the previous case, the equilibrium and periodic orbit are stable in the x- and y-directions and (at least partially) repelling in the β-direction. In our graphic, trajectories will alternate between approaching the equilibrium point, and approaching and following the periodic orbit (figures 1.6 *E*, 1.6 *F*, and 1.6 *G*). In the full three-dimensional picture, trajectories behave as in the equilibrium-equilibrium case, except that now the trajectory will follow the path of the periodic orbit into the repelling region before it jumps to the other plane. Note that the equilibrium can be an extinction equilibrium.

The positions of the equilibrium point, the periodic orbit, and the repelling regions of each boundary plane in the x, y-plane affect the observed population oscillations. When a trajectory follows the boundary periodic orbit for a large proportion of its cycle (figure 1.6 *E*), the predator lags behind the prey with a lag less than one quarter of the period. When a trajectory follows the boundary periodic orbit for a small proportion of its cycle, the lag becomes greater than a quarter of the period and completely out-of-phase cycles are possible (fig-

ures 1.6 *F* and 1.7 *E*). Cryptic dynamics can be observed when the equilibrium is below the right bend of the boundary periodic orbit and trajectories follow the periodic orbit for a brief amount of time (figure 1.6 *G*).

Finally assume C_L and C_R both have a periodic orbit partially in their repelling regions. In our graphic, trajectories alternate between following each limit cycle for a portion of its orbit. This yields a periodic orbit that is a concatenation of the two periodic orbits (figure 1.6 *H*). The orientation of the two limit cycles determines if the new periodic orbit will have a predator lag less than a quarter of the period (figures 1.6 *H* and 1.7 *G*) or a lag that is greater than a quarter of the period (figure 1.6 *I*). Note that the orientation of the limit cycles presented in figure 1.6 *I* is the only one through which out-of-phase oscillations can occur in the case where both boundary planes have a periodic orbit.

When Do These Oscillatory Dynamics Occur?

Our graphic shows that three qualitatively different types of population oscillations can arise in predator-prey systems with predator evolution. While quarter-phase lag cycles (figure 1.6 *E*) are observed in the population dynamics of non-evolving systems, out-of-phase oscillations (figures 1.6 *D* and 1.6 *F*) and cryptic dynamics (figures 1.6 *C* and 1.6 *G*) can not be seen unless evolution is present. Figures 1.7 *D* and 1.7 *F* depict why this is the case. When out-of-phase cycles or cryptic dynamics occur in the three-dimensional system, the population dynamics projected onto the two-dimensional plane run along a single curve in both directions. Such behavior cannot occur in a two-dimensional system where such behavior would violate the uniqueness property of solutions to a system of two ordinary differential equations.

Even when evolution is present, most systems with a repelling trait cannot exhibit all three types of behavior. First, in order to have both of the boundary attractors partially in the repelling regions of their respective planes, we need $H_{x\beta} > 0$ (see appendix A.5). This means that as prey density increases, the trait must become increasingly rewarding and the strength of selection for larger trait values, $H_\beta - D_\beta$, must increase. If $H_{x\beta} < 0$, then the trait will always converge to either β_{min} or β_{max}. A second condition for trait oscillations is that if the predator functional responses, H and D, factor as in equation (1.13), then they must define an s-shaped trade-off curve (see section 1.4.2).

As shown in appendix A.5, the dynamics in figures 1.6 *B*, 1.6 *C*, and 1.6 *D* require additional constraints. First, the predator functional responses cannot factor as in equation (1.13). Second, the oscillations in those cases can only be seen when H is not an everywhere increasing function of x. This implies that any standard functional response like type I, II or III will not be sufficient to see such dynamics. Instead, the prey must interfere with the predator's ability to capture prey when the prey are at high densities (e.g. a type IV functional response, Kot 2001).

Finally, in general, when one boundary has an extinction equilibrium or a periodic orbit and the other has a coexistence equilibrium, there are fewer mathematical constraints on when these oscillations will arise (as compared to when both planes have only coexistence equilibria or periodic orbits). This trend suggests that the oscillations seen in this section are found most often when the β_{min}- and β_{max}-planes are on the opposite sides of a bifurcation that depends on the value of β. For example, in figure 1.6 *E* the β_{min}-plane contains an attracting periodic orbit and the β_{max}-plane contains an attracting equilibrium point. If we

treat β as a parameter, then as β increases toward β_{max}, the population cycles that were present when $\beta = \beta_{min}$ disappear to give rise to an equilibrium state. We expect that bifurcations in the ecological dynamics depending on the trait value are the main mechanisms through which rapid trait evolution gives rise to dynamics that cannot occur in the absence of evolution.

1.4.4 Predator-Prey Model with Prey Evolution

The effects of predator and prey evolution are nearly equivalent. In this section, we present the differences that arise when the prey is the evolving species. This analysis shows that sometimes only ecological data and information are needed to determine which species is evolving in a predator-prey system. In the following α is the mean prey trait, where smaller values of α protect the prey more (e.g. make is less edible) but come at a large cost. The prey evolution model and all results about it that agree with the predator evolution model are contained in appendix A.6.

Boundary Plane Projections

Using the method in Section 1.4.3, a superposition of the dynamics on the α_{min}- and α_{max}-boundary planes can be constructed. All of the dynamics presented in figure 1.6 with predator evolution are possible in figure 1.8 with prey evolution. Additional types of dynamical behavior are also possible when the prey is the evolving species. When the α_{min}-equilibrium is an extinction equilibrium, that is freezing the prey trait at α_{min} would lead to predator extinction, dynamics like those in figures 1.8 *B* and 1.8 *E* are possible. These two cases are not possible

with predator evolution when an extinction equilibrium is present.

Prey evolution also generates dynamics like those in figures 1.8 *C* and 1.8 *D* with fewer biological assumptions than the predator evolution case. With predator evolution, predation interference caused by the prey (e.g. type IV functional response) was necessary to get figures 1.6 *C* and 1.6 *D*. With prey evolution, such dynamics arise naturally and without extra assumptions about the system. This observation is of use to experimentalists working with predator-prey systems where it is unclear which species is evolving. If such interference is known to be absent from a system, then out-of-phase population cycling or cryptic dynamics lends evidence toward the prey being the evolving species.

Phase Relations with Tracking Traits

Ecological oscillations where the predator lags behind the prey with a lag that is less than one quarter of the period are typical of evolutionarily fixed system [Bulmer, 1975]. Predator-prey cycles where the lag is greater than one quarter of the period, like in figure 1.1, suggest that evolution is occurring in the system. Such oscillations are easily generated with a repelling trait (see section 1.4.3). Following Bulmer [1975], we investigate when such oscillations can arise with a tracking trait.

As shown in appendix A.7, a tracking predator trait cannot change the lag and in such cases the ecological processes dictate the lag in the population dynamics. The same is not true for prey evolution. When the prey trait is tracking, the lag between the predator and prey oscillations depends on the quantity (see

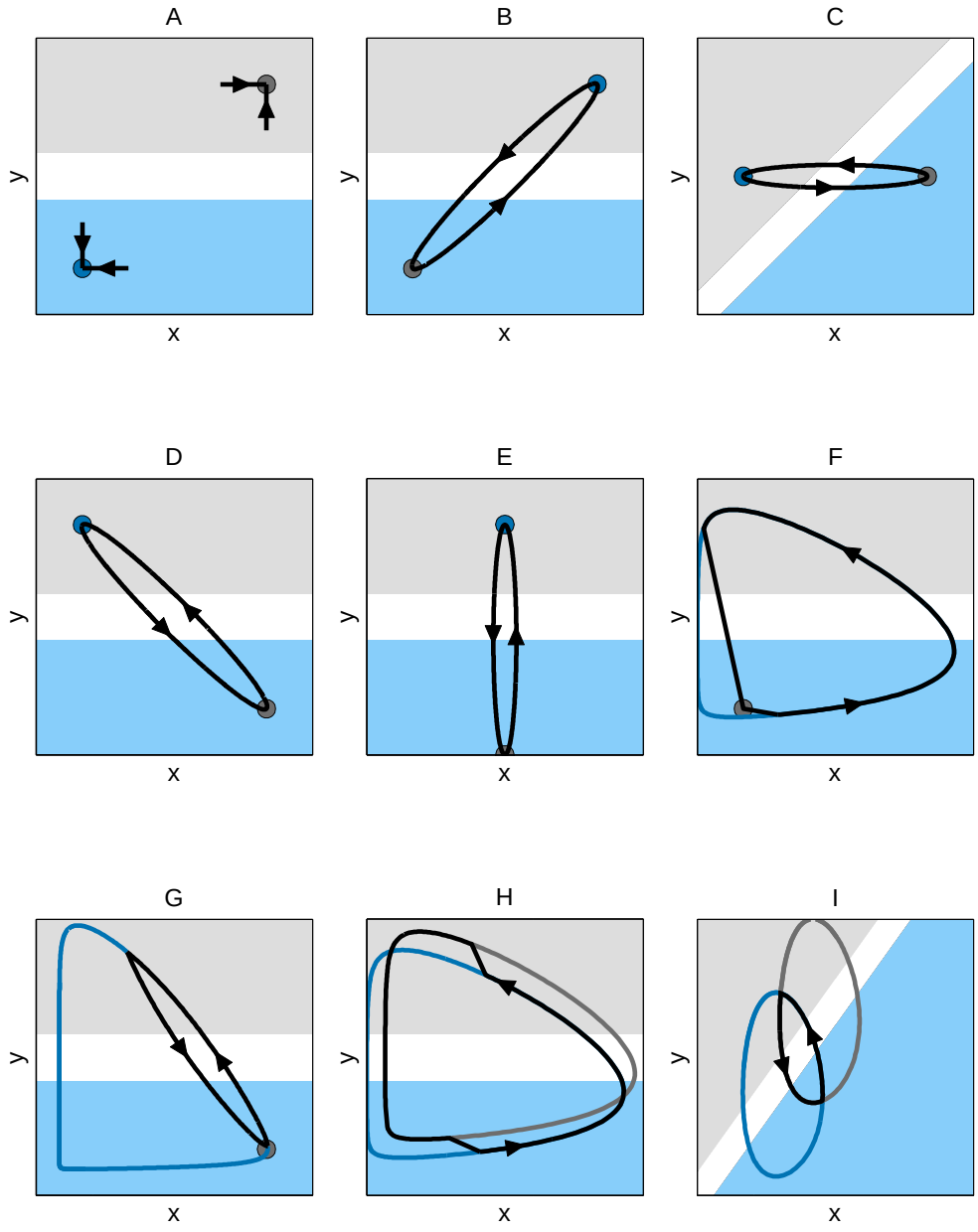

Figure 1.8: Qualitative representations of the dynamics that a predator-prey system with repelling prey trait dynamics can exhibit, projected onto the x,y-plane. Dark blue (dark gray) equilibria or periodic orbits represent the stable limiting dynamics on the α_{max}-plane (α_{min}-plane). Black curves represent the observed population dynamics of the full evolving system projected onto the x,y-plane. Light blue (light gray) regions of the x,y-plane correspond to population levels where the trait is increasing (decreasing) for all trait values. White regions correspond to population levels where the β_{min} and β_{max} planes are both locally attracting for the trait dynamics. In this figure and figure 1.6, blue (gray) signifies the direction of selection being better (worse) for the non-evolving species.

appendix A.7)

$$Q = H_y - D_y + \frac{H_\alpha G_{y\alpha}}{F_{\alpha\alpha} - G_{\alpha\alpha}}. \tag{1.14}$$

The sign of Q determines whether the lag is greater or less than a quarter of the period of the oscillations. When Q is negative, the lag is less than a quarter of the period and tends to zero as Q tends to negative infinity. When Q is positive, the lag is greater than a quarter of the period and tends to half of the period as Q tends to positive infinity. When evolution is absent, $Q = H_y - D_y$. Thus, the sign of $H_\alpha G_{y\alpha}/(F_{\alpha\alpha} - G_{\alpha\alpha})$ determines how the lag changes with the addition of prey evolution. Since we expect $H_y - D_y \leq 0$ [Bulmer, 1975] and assume $F_{\alpha\alpha} - G_{\alpha\alpha} < 0$ and $H_\alpha > 0$, the change in the lag due to evolution is determined by the sign of $G_{y\alpha}$.

The quantity $G_{y\alpha} = -(\partial/\partial y)(F_\alpha - G_\alpha)$ describes how the strength of selection increases or decreases as the number of predators increases. When the trait becomes increasingly rewarding as predator density increases, $G_{y\alpha} > 0$ and prey evolution decreases the phase delay between the predator and prey oscillations. When the trait becomes less rewarding as predator density increases, $G_{y\alpha} < 0$ and prey evolution increases the phase delay between predator and prey oscillations. In particular, if $G_{y\alpha} < 0$ and $H_\alpha G_{y\alpha}/(F_{\alpha\alpha} - G_{\alpha\alpha})$ is large enough, then the phase difference between the oscillations will be greater than a quarter of the period.

We propose two biological mechanisms through which the magnitude of $H_\alpha G_{y\alpha}/(F_{\alpha\alpha} - G_{\alpha\alpha})$ will be large enough. First, assume that a small investment in the prey trait causes a large decrease in the predator's ability to consume and convert prey. Mathematically, this would imply that H_α is very large. In the second mechanism, assume the trade-off in the trait is nearly linear. This results

in lack of curvature in the fitness gradient and $F_{\alpha\alpha} - G_{\alpha\alpha}$ being very small.

The above results in combination with those from section 1.4.4 imply that population oscillations with a lag greater than a quarter period will most likely be the result of prey evolution. Thus, if such oscillations are observed and an experimentalist is deciding on which species to investigate closer for signs of rapid evolution, without extra information, the prey species is the better starting point. In addition, if tracking prey evolution is determined to be the cause of the oscillations, then the driving mechanism can be determined by measuring the effect evolution has on predator consumption (H_α) and the curvature of the trade-off curve ($F_{\alpha\alpha} - G_{\alpha\alpha}$).

1.5 Discussion

Throughout the last two decades theoreticians have studied particular models and systems to understand the effects of rapid evolution on population dynamics in predator-prey systems. To gain insight into how new phenomena arise in such systems due to rapid evolution, we examined the extreme case where evolutionary processes are much faster than their ecological counterparts. In using this approach, we are not positing that evolution occurs at instantaneous rates. Rather, the information obtained by studying the fast limit illuminates eco-evolutionary dynamics that occur when evolutionary and ecological process have comparable time scales.

The main benefit from the analytical tractability and generality gained by working in the fast evolution limit is a better understanding of the links between individual-level mechanisms and population-level phenomena in eco-

evolutionary dynamics. Our approach shows that qualitative properties of a trade-off curve predict how population dynamics affect oscillations in the trait and the range of phenotypes observed (figure 1.5). In addition, since trade-off curves lead to a particular factorization of predator functional responses, the shape of the trade-off curve can determine the range of ecological and evolutionary dynamics that can occur.

Explicit assumptions about the predator and prey functional responses also play an important role in determining the range of behavior systems can exhibit. With prey evolution, assumptions about the trait's effect on predator recruitment and the curvature of its trade-off determine if out-of-phase oscillations can arise from a tracking trait. For predator evolution, more complex interactions between the predator and prey species (e.g. type IV functional response) are necessary to realize specific mechanisms through which new behaviors, such as cryptic dynamics, arise. With either species evolving, oscillatory dynamics of the trait, completely out-of-phase oscillations, and the destabilization of ecological dynamics by a stable trait are only possible in systems with predator satiation and a complex density-dependent trade-off for the trait.

Finally, by comparing the effects of predator and prey evolution, we observed that predator-prey oscillations where the predator lags behind the prey by more than quarter of the period are much more common in systems where the prey is the evolving species. In some cases, extra ecological information about the system, like the absence of a type IV functional response, will suffice to infer that prey evolution is occurring. Thus, we can make predictions about evolutionary processes from purely ecological data.

Some of the above conclusions also act as cautionary notes for experimen-

talist and modelers. First, while rapid evolution in a predator-prey system can allow for population dynamics that are not possible in evolutionarily fixed systems, one must be careful about assumptions that prevent these dynamics from occurring. Because of their simplicity, functional responses that factor as in equation (1.13) have been used in the literature to investigate the effects of evolution [e.g. Khibnik and Kondrashov, 1997, Law et al., 1997]. Biologically, this implies that a trade-off curve exists and that the effects of the trait are independent of the densities of the predator and prey species. In this case, the oscillations in figures 1.6, 1.7, and 1.8 and the destabilization of ecological dynamics by a stable trait in figures 1.4 *C* and 1.4 *D* are not possible. Thus, simplifying biological assumptions used in data collection and model selection can lead to an incomplete understanding of a system and leave new or unique behavior unexplained.

A second cautionary note is sounded by figures 1.4 *C* and 1.4 *D*, where the stability of the eco-evolutionary dynamics cannot be predicted from the behavior of the decoupled evolutionary and ecological processes. It is very generally true that the dynamics of interspecific population interactions and coevolution cannot be predicted by understanding each component separately. The phenomenon in figure 1.4 has been observed for specific cases of our model. Abrams [1992] examined a particular family of functional forms for the predator recruitment term, H, and found that destabilization of population dynamics with a stable trait required sufficiently rapid evolution and a nonlinear dependence of H on the predator trait. Our generalization of the second condition is $H_{x\beta} < 0$ from Section 1.4.1. Abrams and Matsuda [1997b] also noted that predator satiation was necessary to destabilize population dynamics, though their results are not directly comparable since their system does not satisfy equa-

tions (1.9) or (1.10).

When new phenomena do arise, our analysis offers analytical conditions and graphical methods that allow one to identify mechanisms driving the ecological dynamics in an evolving system. Given time series data for a system where selection favors extreme phenotypes, the graphics in figures 1.6 and 1.8 allow one to identify the potential mechanisms that are driving the dynamics. With further ecological information about the dynamics exhibited by the extreme phenotypes (e.g. equilibrium-equilibrium case) or ecological processes (e.g. absence of a type IV functional response), the correct mechanism and the evolving species can be deduced.

This graphic can also be applied to predator-prey systems where selection is frequency dependent. Two of the mechanisms presented in section 1.7 have been observed experimentally where frequency dependent selection was present. Out-of-phase cycles were generated from the scenario in figure 1.8 *G* in Yoshida et al. [2003] and cryptic dynamics generated by the scenario in figure 1.6 *G* (but where the prey is evolving) were observed by Bohannan and Lenski [2000]. Thus, our projection method can yield information about the dynamics possible in systems with frequency dependent and independent selection, but it is unclear if any new dynamics can arise with frequency dependent selection.

The Bohannan and Lenski [2000] and Yoshida et al. [2003] studies also demonstrate how the analysis at the fast evolution limit can yield insight for biological systems where ecological and evolutionary changes are occurring at the same rate. In both systems, evolution was not occurring faster than the population dynamics, yet the theory still accurately predicted the dynamics. In this

study we have emphasized this point numerically by only presenting numerical simulations where $\epsilon \geq 0.1$ - a value considered large for fast-slow systems theory.

The previous two points suggest that similar analyzes could be useful in other areas where eco-evolutionary dynamics are important. One area where ecological and evolutionary processes can have comparable time scales is host-pathogen systems [Earn et al., 2002, Grenfell et al., 2004]. Recent studies have begun to emphasize the need to understand the interplay between these processes when considering vaccination strategies and the evolution of drug resistance and virulence [Grenfell et al., 2004, Gandon and Day, 2007]. Studying the fast evolution limit could yield insight into the complicated behavior observed in these systems.

Finally, we consider the advantages and disadvantages of applying the theory presented in this study to predator-prey and other exploiter-victim systems. Since gradient dynamics approaches are a first approximation to many models, they capture a rage of behavior observed at the phenotypic level without having to specify specific gene level processes [Abrams, 2001, 2005]. In addition, gradient dynamic approaches allow one to study how ecological and evolutionary processes influence each other at any separation of time scales. Their simplicity and versatility makes them a good way to begin understand the types of behavior exhibited by eco-evolutionary models. The disadvantage of this approach arises when specifics about the genetic processes matter and assumptions in the theory break down (e.g. near evolutionary branching points or when invasion of a new trait value does not guarantee that individuals with that trait value will persistence). Because of their simplifying assumptions, gradient dynamic

approaches cannot account for these complexities and more detailed models are needed.

This study exemplifies how fast-slow dynamical systems theory offers a clear viewpoint through which the effects of evolution on ecological dynamics can be studied. The reduction in dimension and the resulting analytical tractability of this methodology makes it a powerful tool for understanding the interplay between ecological and evolutionary processes. Furthermore, while the theory requires a large separation of time scales, it still offers understanding about cases where that assumption is relaxed. Thus, we think the approach followed in this study is a step forward towards developing a general theory for eco-evolutionary dynamics.

CHAPTER 2

COMPARING THE EFFECTS OF EVOLVED AND INDUCED DEFENSES ON PREDATOR-PREY INTERACTIONS USING FAST-SLOW DYNAMICAL SYSTEMS THEORY

2.1 Abstract

Interspecific interactions depend not only on the population densities of the interacting species, but on their phenotypes as well. Phenotypic variation can be plastic or heritable and both mechanisms can drive phenotypic change at rates comparable to or faster than those of ecological dynamics (e.g., changes in population abundances or spatial distributions). In this study we compare the effects rapidly induced and rapidly evolving defenses have on community dynamics by considering the fast phenotypic change limit using fast-slow systems theory. Our approach allows us to study phenotypically plastic and evolving systems with one overarching theory, thus capturing the effects rapidly induced defenses have on ecological dynamics and how those effects differ from the effects of evolving defenses. Our results show that rapidly induced defenses tend to stabilize community dynamics and that some behaviors observed in rapidly evolving systems cannot be produced by phenotypic plasticity.

2.2 Introduction

Interactions between trophic levels are known to be influenced not only by population densities, but also the behavioral, life history, and morphological traits

of the interacting individuals. This interplay between populations, mediated by ecologically important traits (trait-mediated interactions: Bolker et al. 2003), is expected to have important consequences at the individual, population and community levels [Lima, 1998, Agrawal, 2001, Bolker et al., 2003, Werner and Peacor, 2003, Miner et al., 2005, Preisser et al., 2005, Berg and Ellers, 2010].

It is also increasingly recognized that changes in ecologically important species' traits can occur fast enough to affect interspecific interactions while they are taking place [Tuda, 1998, Werner and Peacor, 2003, Agrawal et al., 2007]. Rapid phenotypic changes in populations can arise as a consequence of trait evolution at ecological rates (eco-evolutionary dynamics: Fussmann et al. 2007, Kinnison and Hairston 2007) or phenotypic plasticity in individuals within the population [Tollrian and Harvell, 1999]. For example, the evolution of species' traits has been shown to occur in fewer than 6 generations in birds [Grant and Grant, 2002], crustaceans [Hairston and Dillon, 1990], fish [Conover and Munch, 2002], mammals [Pelletier et al., 2007], and reptiles [Sinervo et al., 2000]. Similarly, the onset of defenses induced by the presence of a predator can be observed after time spans ranging from a few hours [Green and Ryan, 1972, Haukioja, 1980, Kuhlmann and Heckmann, 1985, Kusch, 1993] to a few weeks [Agrawal et al., 1999, Relyea and Auld, 2004].

The shared rapidity in response exhibited in these systems suggests that rapid evolution and rapidly induced defenses could have similar effects on community level dynamics. Despite this similarity though, most theoretical work investigating the effects of rapidly evolving traits and phenotypic plasticity has progressed independently. Studies of eco-evolutionary dynamics have shown that rapidly evolving species' traits can yield complex dynamics, some of which

are unobservable in evolutionarily fixed systems [Yoshida et al., 2007, Jones et al., 2009] and cannot be captured in phenotypically plastic models [Shertzer et al., 2002]. Furthermore, rapid evolution has the potential to either stabilize or destabilize population dynamics [Abrams, 1992, Abrams and Matsuda, 1997b, Cortez and Ellner, 2010]. In contrast, most theoretical studies of inducible defense systems suggest that phenotypic plasticity tends to stabilize population dynamics [Okuyama and Ruyle, 2003, Vos et al., 2004b, Ramos-Jiliberto et al., 2007, 2008, Serizawa et al., 2008]. This conclusion is not supported universally [Ramos-Jiliberto, 2003, Ramos-Jiliberto and Garay-Narváez, 2007], but even systems destabilized by induced defenses do not exhibit the full spectrum of dynamics observed in rapidly evolving systems (e.g., out-of-phase oscillations or cryptic predator-prey cycles in which one species cycles while the other remains constant).

In total, the current theory suggests that these two means of adaptive change, though both occurring at rates comparable to those of ecological processes, do not have the same effects on community dynamics. But due to the specificity of the models and the independent routes through which they have been investigated, it is difficult to compare the effects evolving and inducible defenses have on community level dynamics and to determine why differences are observed. A general theory encompassing the dynamics exhibited by both rapidly evolving and phenotypically plastic communities would aid in determining how differences and similarities between these systems arise.

To begin to develop such a theory, we focus on predator-prey systems and consider the limit where phenotypic change occurs faster than changes in population densities. This limit has been used previously to study the effects rapidly

evolving traits have on population dynamics in predator-prey systems [Cortez and Ellner, 2010]. Here we apply the same theory to predator-prey systems where changes in predator density induce a rapid defensive response in a phenotypically plastic prey population. We note that the rapid evolution of plasticity is also possible in nature, but that case is beyond the scope of this study.

Our approach follows from fast-slow systems theory (an area known as singular perturbation theory, Arnold et al. 1995) where some variables change much faster than others, creating a separation of time scales in the system. In order to reduce the complexity of the dynamics and gain analytically tractability, the theory focuses on the limit where the fast variables are changing instantaneously with respect to the slower variables. The understanding gained in the fast limit yields insight into the dynamics that occur when there is not a separation of time scales between the variables. Thus, using fast-slow systems theory, we study the limit where induced responses are instantaneous and gain understanding about the consequences of induced defenses when the response time is less extreme. Our approach allows us not only to capture the effects phenotypic plasticity has on interspecific interactions, but also to compare directly the effects that rapid evolution and rapidly induced defenses have on community level dynamics.

In the following we explore how phenotypic plasticity and evolution can be studied under one unifying theory. Our analysis shows that rapidly induced defenses stabilize community dynamics and synchronize population oscillations in predator-prey systems. This analysis emphasizes the different effects inducible and evolving defenses have on community level dynamics. In particular, we observe that inducible defenses cannot generate many types of dy-

namics observed in rapidly evolving systems. Finally, we address how the fast induction limit yields insight into the effects phenotypic plasticity has when the rates of adaptive change are comparable to the rates of change of ecological processes.

2.3 Models

2.3.1 Predator-Prey Model with Phenotypic Plasticity

We begin with a general predator-prey model where an individual prey can be in one of two classes, x_1 or x_2, with phenotypes α_1 and α_2, respectively. As a convention, we will assume $\alpha_2 > \alpha_1$ and that a smaller value of the trait implies a decreased susceptibility to predation. This decrease in predation susceptibility comes at a fitness cost, thus creating a trade-off. We assume that individuals switch their class depending on the current predator density, y. Individuals switch to class i at rate $\epsilon^{-1}P_i(y)$, where $P_1(y) + P_2(y) = 1$ and ϵ is a positive constant. Thus, if the predator density was fixed at a value y, a fraction $P_1(y)$ of the total prey population would be defended. Note that as the function $P_1(y)$ becomes steeper, the switch between classes will resemble an abrupt 0-1 transition. In simulations we will consider more gradual switches as some experimental data suggests this is the case [Gilbert and Waage, 1967, Kusch, 1993, Buskirk and Arioli, 2002], but our analytical results do not differ.

Under the above assumptions our model is

$$\begin{aligned}
\frac{dx_1}{dt} &= F_1(x_1, x_2) - G_1(x_1, x_2, y) + \epsilon^{-1} x_2 P_1(y) - \epsilon^{-1} x_1 P_2(y) \\
\frac{dx_2}{dt} &= F_2(x_1, x_2) - G_2(x_1, x_2, y) - \epsilon^{-1} x_2 P_1(y) + \epsilon^{-1} x_1 P_2(y) \\
\frac{dy}{dt} &= H_1(x_1, x_2, y) + H_2(x_1, x_2, y) - D(y).
\end{aligned} \tag{2.1}$$

F_i is the growth rate of class i in the absence of predation, G_i is the predation rate on class i, H_i is the product of the prey to predator conversion and predation rate on class i, and D is the death rate of the predator population. We assume D is increasing in y and assume G_i and H_i are increasing in x_i and y. Typically the functions F_i, G_i, H_i and D are written in terms of per capita growth rates, e.g. $F_i = x_i f_i(x_1, x_2, y)$. Here and throughout the rest of the text we use the more general functions to simplify notation. The positive constant ϵ^{-1} represents the rate at which adults can switch between phenotypes. Since we assume induced changes in phenotype occur rapidly, ϵ will be very small, making ϵ^{-1} very large.

Before continuing, we address two key assumption made about system (2.1). First, the phenotype of a phenotypically plastic individual can either be determined at birth (e.g. *Daphnia* helmet size, Agrawal et al. 1999) or switched after birth (e.g. tadpole gut and tail length, Relyea and Auld 2004). Model (2.1) corresponds to a switch-after-birth scenario. We address a switch-before-birth scenario in appendix B.5. Second, we implicitly assume in system (2.1) that young are born expressing their parent's phenotype. We address the consequences of relaxing this assumption in appendix B.1.2. In the fast induction limit, the effects of these two assumptions are small and the dynamics exhibited in all cases are qualitatively the same. We have chosen the specific case given by system (2.1) to simplify the comparison of induced and evolved defense systems.

As seen in appendix B.1, system (2.1) is approximated by the following

predator-prey model with an average phenotype α,

$$\begin{aligned}
\frac{dx}{dt} &= F(x,\alpha) - G(x,y,\alpha) \\
\frac{dy}{dt} &= H(x,y,\alpha) - D(y) \\
\epsilon\frac{d\alpha}{dt} &= \epsilon A(\alpha)V\frac{\partial}{\partial\alpha}\left[\frac{1}{x}\frac{dx}{dt}\right] + (\alpha_2 - \alpha)P_2(y) - (\alpha - \alpha_1)P_1(y).
\end{aligned} \tag{2.2}$$

Here, our new state variables are $x = x_1 + x_2$, the total prey population density, and $\alpha = (\alpha_1 x_1 + \alpha_2 x_2)/x$, the average trait of the prey population. $F(x,\alpha) = F_1(x_1,x_2) + F_2(x_1,x_2)$ represents the growth rate of the total prey population, where we use the reverse transformations $x_1 = \frac{\alpha_2-\alpha}{\alpha_2-\alpha_1}x$ and $x_2 = \frac{\alpha-\alpha_1}{\alpha_2-\alpha_1}x$ to evaluate F_i. $G = G_1 + G_2$ and $H = H_1 + H_2$ are similarly defined. $A(\alpha)V$ represents the population variance of the trait. $A(\alpha) = 0$ at α_1 and α_2 because the trait variance is zero at α_1 and α_2 (see appendix B.1).

The population dynamics of system (2.2) are equivalent to those in system (2.1). Thus, the error we introduce by approximating system (2.1) with system (2.2) arises only in the trait equation. We discuss this error and the class of functions for which the trait equation is exact in appendix B.1.1. For example, our approximation is exact when $F_i(x_1,x_2) = x_i r(\alpha_i)[1 - kx]$ and $G_i(x_1,x_2) = x_i g(\alpha_i)y/(1+hx)$ where $x = x_1 + x_2$ and the functions $r(\alpha)$ and $g(\alpha)$ describe how an individual prey's growth and predation rate depend on its trait value. In general, the introduced error in the trait equation is multiplied by the small positive constant ϵ ($0 \le \epsilon < 1$). Thus, in the limit where phenotypic change is fast, the error will be negligible.

The last two terms on the right side of the $d\alpha/dt$ equation in system (2.2) represent the changes in the mean trait value due to phenotypic plasticity (i.e., direct transfer between prey classes). The first term represents the individual fitness gradient and has been used to model changes in evolutionary traits (see

the next subsection). In this model, that term represents changes in the mean trait value due to the birth and predation of individuals in each prey class. This term is multiplied by the small constant ϵ and consequently, as one would expect from our initial assumptions, changes in the mean phenotype of the prey population are dominated by phenotypic plasticity, not the birth and death of individuals. The ϵ multiplying the $d\alpha/dt$ in the trait equation creates a separation of time scales between the trait and population dynamics and classifies system (2.2) as a fast-slow system. Mathematically, this ensures that changes in the mean trait value are faster than changes in population densities.

2.3.2 Predator-Prey Model with Fast Evolution

We compare system (2.2) to a predator-prey system where the mean trait of the prey population, α, evolves at a rate much faster than the rate of the ecological dynamics. This model has been studied in Cortez and Ellner [2010] and we only briefly introduce it here. Our model is

$$\begin{aligned} \frac{dx}{dt} &= F(x,\alpha) - G(x,y,\alpha) \\ \frac{dy}{dt} &= H(x,y,\alpha) - D(y) \\ \epsilon\frac{d\alpha}{dt} &= A(\alpha)V\frac{\partial}{\partial\alpha}\left[\frac{1}{x}\frac{dx}{dt}\right] \end{aligned} \tag{2.3}$$

where all terms are interpreted as in system (2.2). The trait dynamics in this system follow from the quantitative genetics approach derived in Lande [1982] and Abrams et al. [1993]. Here the mean trait value changes in the direction of increasing fitness, determined by the fitness gradient $\frac{\partial}{\partial\alpha}\left(\frac{1}{x}\frac{dx}{dt}\right)$. We note that system (2.3) has been shown to approximate a particular two-prey, one-predator system analogous to system (2.1) where there is no direct transfer between the

two prey clonal classes (i.e., $P_i = 0$, Abrams and Matsuda 1997b).

As in the model with phenotypic plasticity (2.2), system (2.3) is a fast-slow system where changes in the mean trait value occur much faster than changes in the population densities. The difference between systems (2.2) and (2.3) lies in the equations describing the trait dynamics, $d\alpha/dt$. In the fast evolution system (2.3), changes in the the mean trait are dominated by and depend only on the fitness gradient. The birth and death rates of individuals in each class determine the rate at which the mean trait value changes. In system (2.2), changes in the mean trait value due to births and deaths are negligible since individuals rapidly switch their phenotypes.

2.4 Results

2.4.1 Fast-Slow Dynamics in systems (2.2) and (2.3)

When ϵ is a small positive value, the dynamics of systems (2.2) and (2.3) behave in a way that is qualitatively different from models without a separation of time scales. In particular, solutions to the systems spend nearly all of their time near an object called the critical manifold and the rest jumping between different pieces of the critical manifold.

The critical manifold, C, of system (2.2) is a two-dimensional surface whose points satisfy $d\alpha/dt = 0$ when $\epsilon = 0$, $C = \{(x, y, \alpha) : \ (\alpha_2 - \alpha)P_2(y) - (\alpha - \alpha_1)P_1(y) = 0\}$. Equivalently, C is given by the equation $\alpha = \alpha_1 P_1(y) + \alpha_2 P_2(y)$. An example of a typical critical manifold for an inducible defense system is given in figure 2.1 A.

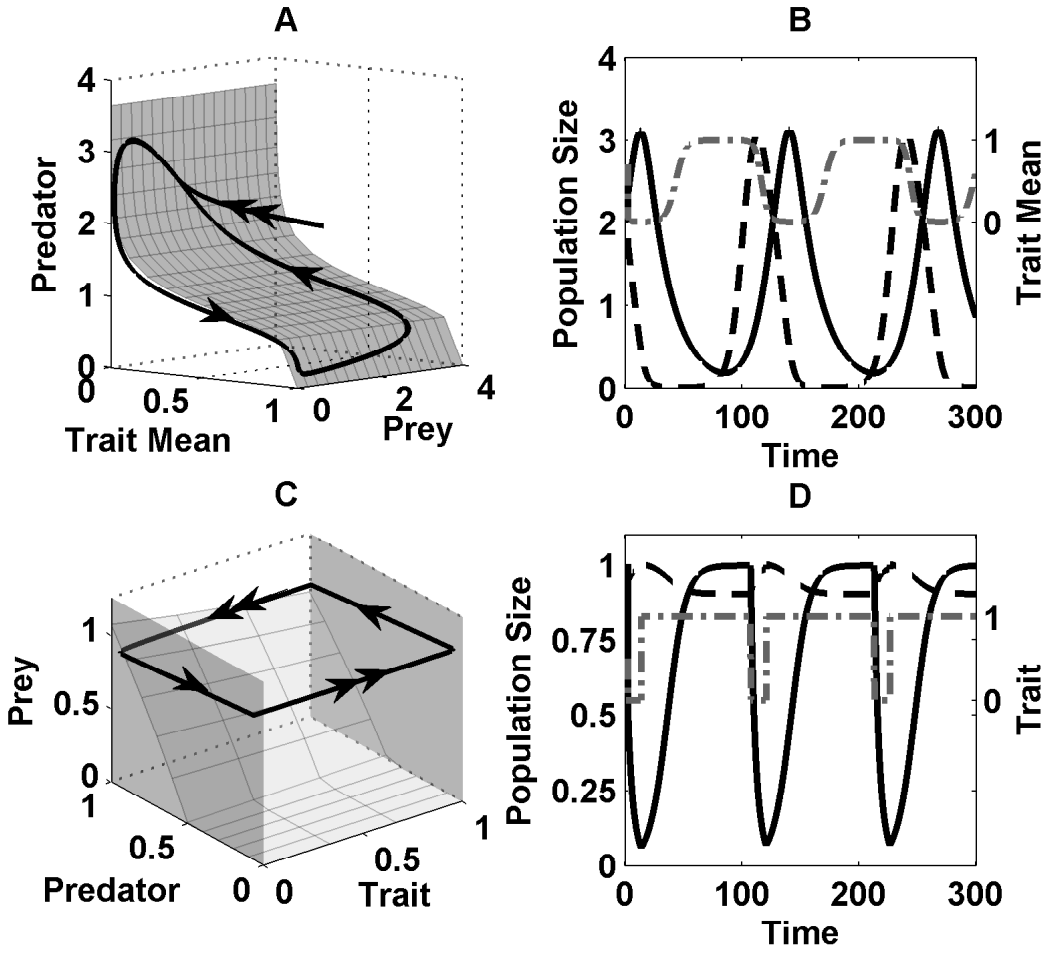

Figure 2.1: Comparison of (*A*,*B*) predator-prey oscillations in an inducible defense system and (*C*,*D*) cryptic oscillations in an evolving defense system. (*A*,*C*) Trajectory (black) and critical manifold (gray sheets) in phase space. Double arrow indicates fast motion towards or away from the critical manifold and single arrows indicate slow motion near the critical manifold. (*B*,*D*) Predator (solid black), prey (dashed black), and trait mean (gray dash-dot) time series for the trajectory. In (*C*,*D*), populations are scaled to 0-1 to emphasize that predator oscillations are driven by fluctuations in the prey trait rather than oscillations in prey abundance. In particular, the variation in the prey abundance is so small, compared to typical measurement errors and small variability in population processes, that in most cases it would be undetectable.

Solutions stay near a piece of the critical manifold or jump from it depending on the stability of the fast dynamics near that piece. For system (2.2), this stability is determined by a eigenvalue of the fast dynamics, $Q_I = \frac{\partial}{\partial \alpha}[(\alpha_2 - \alpha)P_2(y) - (\alpha - \alpha_1)P_1(y)] = -1$ (see appendix B.2 for details). The constant negative sign of Q_I has two important consequences for the behavior of system (2.2). First, solutions to system (2.2) will always approach the critical manifold and once near it, never jump away from it. figure 2.1 *A* demonstrates this behavior. Starting from some initial condition, the solution quickly runs towards the critical manifold with the values of x and y remaining nearly constant. Once near the critical manifold, the solution behaves as if it were on the critical manifold and remains near it for all time.

The second consequence of the constant negative sign of Q_I is that the dynamics of system (2.2) can be understood solely by understanding how trajectories behave on the critical manifold. Thus, in the fast induction limit, the behavior of the three-dimensional system (2.2) is determined by the behavior on a two dimensional surface. In addition, because C is two-dimensional, chaos dynamics are not possible and all solutions will eventually either exhibit periodic oscillations or go to steady state [Strogatz, 1994].

Consider the critical manifold of system (2.2). As seen in figure 2.1 *C*, the critical manifold is composed of three two-dimensional surfaces. The eigenvalue that describes the stability of the fast dynamics near a piece of the critical manifold is given by $Q_E = \frac{\partial}{\partial \alpha}\left[A(\alpha)V\frac{1}{x}\frac{\partial}{\partial \alpha}\frac{dx}{dt}\right]$; for details see Cortez and Ellner [2010]. In contrast to the constant negative sign of Q_I, in general the sign of Q_E will be positive and negative at different parts of the critical manifold. The variable sign of Q_E marks an important distinction between inducible and evolved defense

systems.

Positive values of Q_E allow for solutions to jump between two pieces of the critical manifold. This behavior can result in completely out-of-phase oscillations or cryptic cycles (one species oscillates and the other remains effectively constant). For example, the cryptic cycles in figure 2.1 *C* repeatedly jump between the left and right pieces of the critical manifold. Because the sign of Q_I is always negative, such dynamics cannot arise in rapidly induced defense systems. Thus, some dynamics exhibited by rapidly evolving traits cannot be observed in rapidly induced systems.

2.4.2 Local Stability Analysis

To begin to understand how inducible defenses affect community dynamics, we first analyze how adding of phenotypic plasticity to a fixed-defense predator-prey system changes the stability of the ecological dynamics. We do this by comparing the stability of an equilibrium point of system (2.2) to the stability of an associated equilibrium point where the defense is fixed. Mathematically, this is done via fast-slow theory by substituting the defining equation for the critical manifold from the previous section, $\alpha = \alpha_1 P_1(y) + \alpha_2 P_2(y)$, into the first two lines of system (2.2). The stability of this new system is then compared to the stability of a system with a fixed defense (see appendix B.3 for details).

We consider two types of stability. The first deals with whether the coexisting predator and prey tend to equilibrium or oscillate when fixed defenses are replaced with inducible defenses. As shown in appendix B.3, the effect phenotypic plasticity has on this kind of stability is determined by the quan-

tity $(\alpha_2 - \alpha_1)dP_1/dy$, i.e., the product of the difference in defense level and the rate at which the fraction of defended individuals changes with predator density. This quantity is zero when $P_1(y) = 0$ or $P_2(y) = 0$, and positive otherwise. $(\alpha_2 - \alpha_1)dP_1/dy$ is zero when the equilibrium density of the predators is so large that all prey are defended (in class x_1), or so small such that all prey are undefended (in class x_2). In these two cases, phenotypic plasticity has no effect on the ecological dynamics. Note that this holds even when cycles around the equilibrium are large enough to induce a response in the prey.

The quantity $(\alpha_2 - \alpha_1)dP_1/dy$ is greater than zero when at equilibrium there is a mix of strategies (in the case of prey classes) or individuals are not completely defended or undefended (in the case of a continuous trait value). For the first type of stabilization, phenotypic plasticity always dampens predator-prey oscillations. Thus, populations that would cycle when the defense is fixed experience a reduction in the amplitude of their oscillations and possibly tend to equilibrium when phenotypic plasticity is present (figure 2.2). Since rapidly induced defenses never destabilize the population dynamics nor cause oscillations, cyclic dynamics are a consequence of instability in the ecological dynamics and not due to adaptive changes in the trait.

The second type of stability deals with the coexistence of the two species. In this case, replacing fixed defenses with inducible defenses could result in predator extinction. The effect phenotypic plasticity has on the coexistence of the two species depends on the quantity $(\alpha_2 - \alpha_1)dP_1/dy\left(\frac{\partial \dot{x}}{\partial x}\right)$, where the first two terms are the same as in the previous case and the third term represents the stability of the ecological dynamics when the defense is fixed (see appendix B.3 for details). As above, when $P_1(y) = 0$ or $P_2(y) = 0$, all individuals are defended or unde-

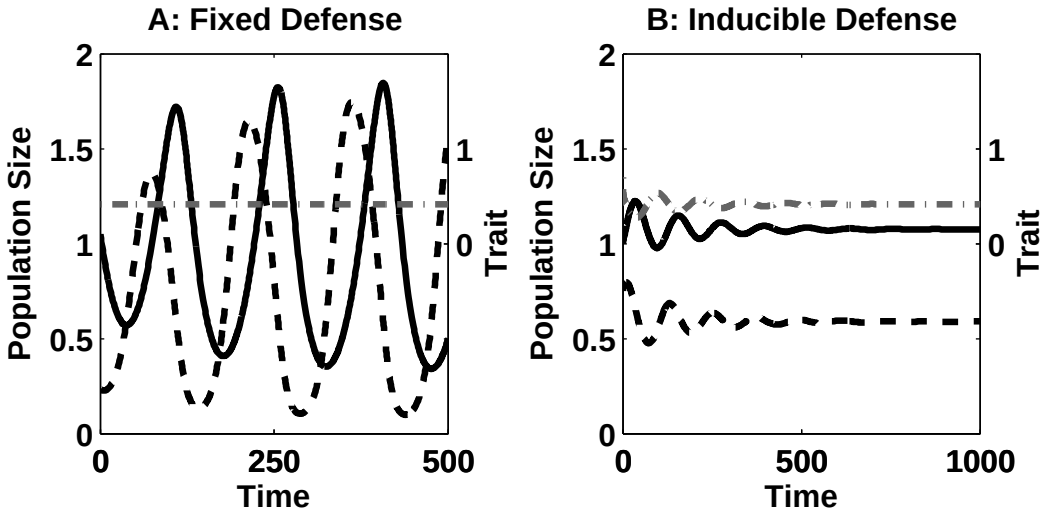

Figure 2.2: An example of inducible defenses stabilizing population oscillations. (*A*) Predator (solid black) and prey (dashed black) populations cycle when the defense (dashed-dot gray) is fixed. (*B*) Population and trait dynamics tend to equilibrium with an inducible defense.

fended at equilibrium and plasticity neither promotes or nor inhibits extinction. When $(\alpha_2 - \alpha_1)dP_1/dy$ is greater than zero, the effect phenotypic plasticity has on coexistence depends on the stability of the ecological dynamics when the defense is fixed. If the populations oscillate when the defense is fixed, then $\frac{\partial \dot{x}}{\partial x}$ is positive and induced defenses promote predator extinction. If the ecological dynamics are at equilibrium when the defense is fixed, then $\frac{\partial \dot{x}}{\partial x}$ is typically negative and inducible defenses tend to inhibit predator extinction. In total, phenotypic plasticity cannot destabilize ecological systems already at equilibrium and it dampens or eliminates oscillations and increases the chance for predator extinction in unstable systems.

2.4.3 Population Phase Lags

In purely ecological predator-prey systems, predator oscillations lag behind prey oscillations by less than a quarter of the period [Bulmer, 1975]. Previous work has shown that adding fast predator evolution to a purely ecological predator-prey model will not change the lag [Cortez and Ellner, 2010]. In contrast, fast prey evolution increases or decreases the lag depending on whether the reward for the investing in the trait increases or decreases, respectively, as the number of predators increases; see Cortez and Ellner [2010] for details. Here we discuss how phenotypic plasticity affects phase relations in predator-prey oscillations.

As shown in appendix B.4, the effect inducible defenses have predator-prey phase lag is determined by the sign of $-(\alpha_2 - \alpha_1)H_\alpha dP_1/dy$, i.e., the product of the difference in defense level, the effect the trait has on predator population growth, and the rate at which the fraction of defended individuals changes with predator density. Since this values is always negative or zero, inducible defenses only decrease the lag between the predator and prey oscillations. Thus, phenotypic plasticity synchronizes oscillations in predator-prey systems and prevents oscillations in which the lag is greater than a quarter of a period. Two examples comparing the effects of phenotypic plasticity and evolution on phase relations are given in figure 2.3. There are two points to make about this comparison. First, rapid evolution and phenotypic plasticity have different effects on the phase relations of predator-prey oscillations. While rapidly induced defenses only decreases the lag (figure 2.3 *B*), rapid evolution can also increase the lag and yield oscillations where the lag is greater than a quarter of the period (e.g., the completely out-of-phase oscillations in figure 2.3 *D*).

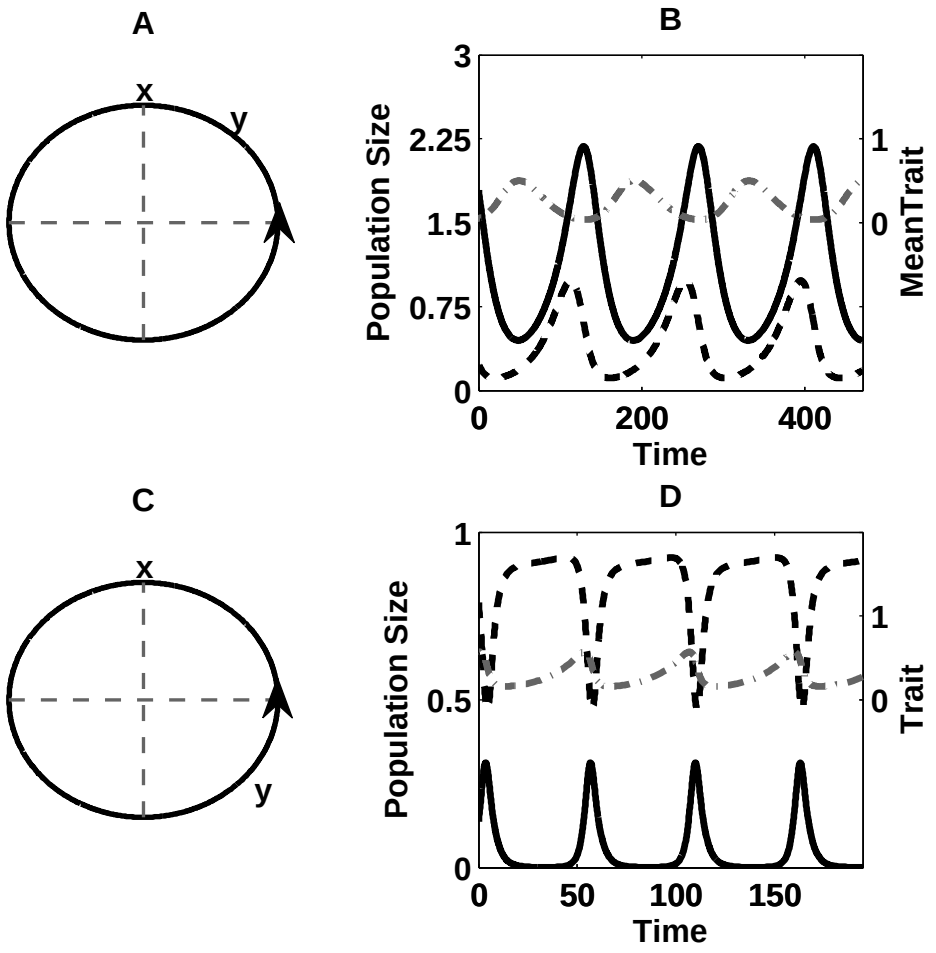

Figure 2.3: Predicted phase relations for predator-prey oscillations from (*A*,*B*) an inducible defense system and (*C*,*D*) an evolved defense system. (*A*,*C*) Predicted phase relations. The circle represents one period of the cycles. x and y mark when the prey and predator reach their peak during the cycle. The arrow denotes counter-clockwise rotation and marks the phase difference for each system when the defense level is fixed. The inducible defense decreases the phase difference (*A*) and the evolved defense increases the phase difference (*C*). (*B*,*D*) Predator (solid black), prey (dashed black) and trait mean (gray dash-dot) time series.

Second, our results suggest that oscillations where the lag is greater than a quarter of the period or cryptic dynamics (figure 2.1 *C* and *D*) are not possible in phenotypically plastic models. Out-of-phase and cryptic dynamics are observed in rapid evolution models either through the change in phase relations described above or through mechanisms that require the constant Q_I from section 2.4.1 to be positive. This qualitative difference implies that if out-of-phase oscillations or cryptic dynamics are observed, then evolution, and not phenotypic plasticity, is the likely cause.

2.5 Discussion

In this study we considered the limit where prey can change their phenotype instantaneously to gain insight into the effects rapidly induced defenses have on community dynamics and to determine how those effects differ from the effects evolutionary processes have. Our results show that rapidly induced defenses promote stability in predator-prey systems and that rapidly induced defenses cannot produce some dynamics observed in rapidly evolving systems.

The stabilizing effect of inducible defenses has been observed in previous studies of predator-prey and other higher order trophic systems (e.g. Underwood 1999, Vos et al. 2004a,b, Ramos-Jiliberto et al. 2007), but this trend does not hold universally (e.g. see Ramos-Jiliberto 2003, Ramos-Jiliberto and Garay-Narváez 2007). When induction of the defense is fast, our analysis shows that induced defenses always promote stability in predator-prey systems. This conclusion is independent of when the phenotypic change occurs during the life history of an organism, i.e., switch-before-birth (appendix B.5) or switch-after-

birth (system (2.2 and appendix B.1.2). The forms of the trait equations in systems (2.2), (B.1.10) of appendix B.1.2, and (B.5.3) of appendix B.5 suggest why the effects of phenotypic plasticity are independent of timing in the fast induction limit and why stabilization is not observed in all models when the rate of induction is not nearly instantaneous.

In the fast induction limit, the trait dynamics of all three models for phenotypic change have the same governing equation. In particular, the trait equation becomes $0 = (\alpha_2 - \alpha)P_2(y) - (\alpha - \alpha_1)P_1(y)$ when $\epsilon = 0$. This equivalence is a consequence of assuming that the mean value of the trait changes faster than the population dynamics. The assumption that an individual can switch phenotypes almost instantaneously after birth independent of whether it was born expressing its parent's phenotype (system (2.2)) or not (system (B.1.10) of appendix B.1) and the assumption that the turnover of individuals in the prey population is fast relative to changes in population size (appendix B.5) are equivalent mathematically. Thus, in the limit where phenotypic change is faster than ecological dynamics, we expect the effects of phenotypic plasticity to be independent of when the defense is induced during the life history of an organism.

But when the rate of phenotypic change is comparable to rates of ecological change, these differences in timing do matter. In system (2.2), births and deaths of individuals within each prey class have a minimal effect on the rate at which the mean trait value changes when phenotypic change is fast (ϵ is small). As the separation of time scales between the the ecological and adaptive processes becomes less pronounced (ϵ approaches 1), gains and losses within each class will influence the rate of change of the mean trait value more. Since the effects of recruitment and loss of prey on the mean trait are different between

systems (2.2), (B.1.10), and (B.5.3), we should expect to see differences in the effects of phenotypic plasticity on community dynamics.

In particular for system (2.2), as the rates of adaptive and ecological processes become comparable, we can expect inducible defenses to be destabilizing in some cases. Evolutionary traits have the potential to be destabilizing [Abrams and Matsuda, 1997b, Cortez and Ellner, 2010] and terms similar to those that govern the trait dynamics in evolutionary models are also present in our phenotypically plastic models (e.g., the gradient terms multiplied by ϵ in the trait equation of system (2.2)). Similarly, while rapidly induced defenses only synchronize predator-prey oscillations, rapidly evolving traits can also desynchronize cycles and increase the lag between the predator and prey oscillations when costs for defense are small [Cortez and Ellner, 2010]. Weak costs for inducible defenses have been observed in many systems [Buskirk and Steiner, 2009], suggesting that inducible defenses can also desynchronize population dynamics when the rate of induction is comparable to the rates of ecological processes. Thus, it may be possible for plastic traits to destabilize population dynamics when the rate of induction is comparable to rates of ecological processes. This conclusion emphasizes an advantage of considering fast adaptation limit. While the fast induction limit does not capture all of the effects phenotypic change has on population dynamics, it does illuminate how and when additional effects can arise.

The above suggests that without a separation of time scales, the effects of evolution and phenotypic plasticity should be similar. However, some dynamics observed in evolutionary predator-prey models cannot be observed in inducible defense models. Evolution has been shown experimentally and theoret-

ically to yield completely out-of-phase or cryptic oscillations in predator-prey systems [Yoshida et al., 2007, Jones et al., 2009, Cortez and Ellner, 2010]. The reason these types of oscillations cannot arise due to rapidly induced defense is depicted in figure 2.4.

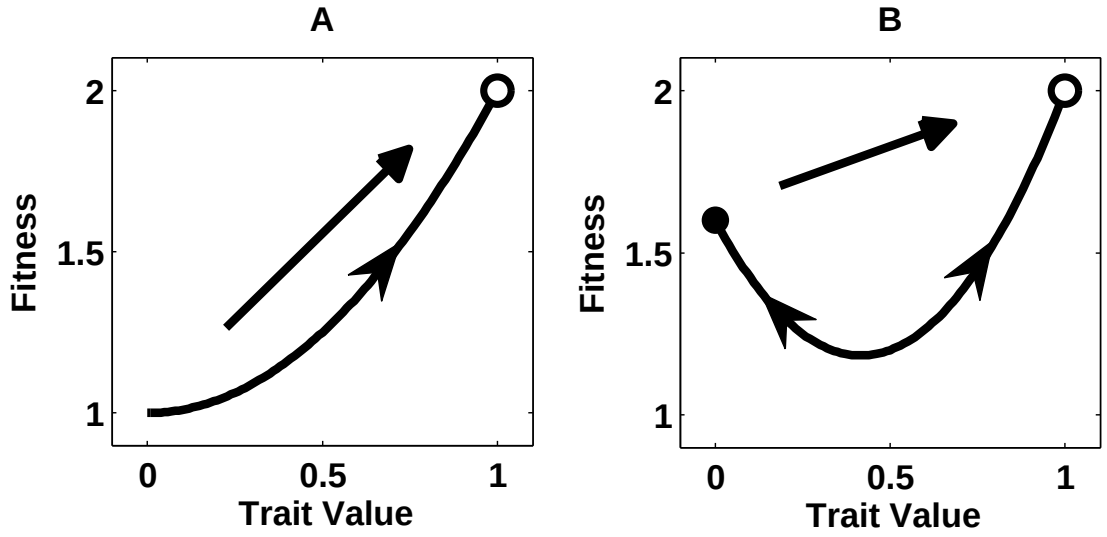

Figure 2.4: Phenotypic differences between evolutionary and plastic adaptation. An individual's trait value determines its fitness (solid black curve). Plasticity only depends on which trait value is most fit under current conditions (open circles) and a plastic trait tends towards the global fitness maximum (triangular arrow). Evolution can climb the fitness curve towards any local fitness maximum (open or closed circles) and which max the trait tends to depends on the current trait value (v-backed arrows). (*A*) Because a unique local fitness maximum is necessarily a global fitness maximum, plastic and heritable adaptation tend towards the same trait value. (*B*) The separation of multiple local fitness maxima by a fitness valley yields a u-shaped fitness curve. This results in evolutionary bistability and selection potentially favoring a trait value that is not globally maximal (left v-backed arrow).

Phenotypic change in plastic systems results in individuals having the phenotype with the greatest fitness given the current conditions. Thus, the induction or reduction of the trait always results in the trait converging to the highest peak in the fitness landscape (dashed line and triangular arrow in figure 2.4). In contrast, evolution is driven by the slope of the fitness curve, i.e. the fitness

gradient, so it cannot cross a fitness valley to reach a higher peak. Often the trait dynamics for both mechanisms of adaptive change will behave similarly. This occurs when selection drives the trait in the direction of increasing fitness and arrives at the highest fitness peak (figure 2.4 *A* and right v-backed arrow of figure 2.4 *B*). Out-of-phase and cryptic oscillations occur in eco-evolutionary models when bistability arises and two local fitness maxima of the trait are separated by a fitness minimum of the trait (figure 2.4 *B*). In such situations, selection drives the trait in the direction of increasing fitness but depending on which side of the valley it started on, the trait may arrive at a value that is a local, but not global, fitness maximum (left v-backed arrow of figure 2.4 *B*). Because phenotypic plasticity always chooses the most fit trait value, bistability cannot arise and hence, out-of-phase and cryptic oscillations are not possible in inducible defense systems.

The above conclusions do depend on the type of trait and may not hold for all phenotypically plastic traits. Some studies of learned behavioral traits where individuals can learn from other conspecifics have used models that are nearly identical to the evolutionary trait model (2.3) (e.g., Abrams and Matsuda 2004). Since fitness valleys can arise in such systems and the trait dynamics depend on the fitness gradient, plastic behavioral traits may be able to generate the complex dynamics seen in evolutionary models.

The theory presented in this study can also be applied to phenotypically plastic predator traits (e.g., inducible offenses [Agrawal, 2001] or foraging theory [Křivan, 2007]). For two species predator-prey systems where the predator's phenotype depends on prey density, rapidly induced offenses stabilize population dynamics (appendix B.6). Stabilization has been observed in optimal forag-

ing systems with multiple prey types [Yamauchi and Yamamura, 2005, Křivan, 2007] and in higher trophic systems [Uchida et al., 2007], but destabilization is also possible [Abrams, 1992]. Our results suggest that these differences in predictions can be understood using similar analysis and may be due to the rate of induction and to whether the adaptive process depends on the fitness gradient. Our approach may also be fruitful in understanding the community dynamics in systems where both inducible defenses and inducible offenses are present (e.g. Feng et al. 2009, Kishida et al. 2009) and how they differ from eco-coevolutionary dynamics.

This work demonstrates that the mechanisms through which adaptive changes arise play an important role in determining what effects they have on community dynamics. The fast phenotypic change limit and the general theory presented here allows us to capture the different effects phenotypic plasticity and evolution have on ecological systems. We have observed that rapidly induced defenses tend to stabilize population dynamics and that they cannot generate some of the dynamics observed in rapidly evolving systems. Thus, this work begins to unify the theory of adaptive change and to determine how the effects of adaptive change depend on the underlying driving process.

CHAPTER 3

DYNAMICS IN THE VICINITY OF A TRANSVERSAL INTERSECTION OF THE CRITICAL MANIFOLD IN 1-FAST, 2-SLOW DYNAMICAL SYSTEM

3.1 Abstract

Multiple time scale ecological and evolutionary models generically yield fast-slow dynamical systems where two critical manifolds intersect transversally along a curve. In addition, due to biological constraints, one of the manifolds is often invariant in the system. This study presents the dynamics that occur in the vicinity of the transversal intersection in a class of biologically motivated 1-fast, 2-slow dynamical systems. Our analysis shows that chaotic and other complicated dynamics occur in parameter space $O(\epsilon)$-close to Hopf bifurcations of the system. Furthermore, the dynamics occur in an $O(\epsilon)$-neighborhood of the intersection curve, where the fast-slow structure breaks down. In regions of parameter space farther from the Hopf bifurcations, solution behavior can be predicted from the singular flows away from the intersection curve and from previous results of 1-fast, 1-slow dynamical systems near the intersection curve.

3.2 Introduction

The rates of change of ecological and evolutionary processes for different species can differ by many orders of magnitude within a single system. For example, bacteria and viruses have generation times on the order of hours or

days and evolve over days or weeks, while their hosts may have generation times measured in years and evolve over time spans measured in tens or hundreds of years. Because it is often difficult, if not impossible, to collect data with the proper sampling interval in such systems, mathematical models have been key to exploring and understanding the dynamics that can be exhibited by ecological and evolutionary systems with multiple time scales.

Systems of ordinary differential equations are one common approach used to model multiple time scale ecological and evolutionary dynamics. The separation of time scales is explicitly denoted by writing the system as

$$\begin{aligned} \epsilon \dot{x} &= F(x, y, \epsilon) \\ \dot{y} &= G(x, y, \epsilon) \end{aligned} \tag{3.1}$$

where ϵ is a small positive parameter that represents the separation of time scales between the fast and slowly varying variables, $x \in \mathbb{R}^n$ and $y \in \mathbb{R}^m$ respectively. System (3.1) is a fast-slow system and is analyzed using singular perturbation or Fenichel theory [Fenichel, 1979, Arnold et al., 1995]. The theory focuses on understanding the dynamics that occur when $\epsilon = 0$ and how that information can be used to predict and understand the dynamics that occur when ϵ is small and positive.

Intuitively, one can think about the behavior of system (3.1) as being composed of slowly varying dynamics and periodic rapid transitions. The slow evolution of solutions occurs near an object called the critical manifold or critical set, $C = \{(x, y) : F(x, y, 0) = 0\}$. Rapid transitions occur when solutions leave the vicinity of the critical manifold, often rapidly approaching another part of C. Thus, solutions to the fast-slow system (3.1) can be thought of as the concatenation of the dynamics near the critical manifold and the fast transitions between

different regions of the critical manifold.

Fast-slow systems theory has been used to understand the ecological and evolutionary dynamics in a variety of biological systems with multiple time scales. For purely ecological systems, previous studies have used fast-slow systems theory to understand the oscillatory dynamics in bitrophic systems with two species [Rinaldi and Muratori, 1992a,b, Rinaldi and Gragnani, 2004, Buric et al., 2006] and bitrophic systems with three species where two slow predators compete for a single fast prey [Liu et al., 2003, Deng and Loladze, 2007]. Similarly, the theory has been used in studies of the different oscillatory and chaotic dynamics observed in tritrophic systems where there may be two or three time scales [Muratori, 1991, Muratori and Rinaldi, 1992, Lenbury and Likasiri, 1994, Feo and Rinaldi, 1998, Deng, 2001, Mehidi, 2001, Deng and Hines, 2002, 2003, Ginoux et al., 2005, Vidal, 2006, Jiang and Yang, 2009]. Most of the studies focus on fast prey, slow predator systems, but fast predator or parasite systems have also been studied [Rinaldi and Muratori, 1992a, Buric et al., 2006].

Beyond purely trophic models, fast-slow dynamical systems have been used to investigate the ecological dynamics of metacommunities [Goldwyn and Hastings, 2008, Rinaldi, 2009], pathogen and parasite systems [Lenbur et al., 1999, Lenbury et al., 2000, Poggiale et al., 2001], and systems with a slowly varying environmental variable [Lenbury and Tumrasvin, 2000, Boudjellaba and Sari, 2009]. Multiple time scale systems are also commonplace in studies of eco-evolutionary dynamics where either the population dynamics are fast [Schecter, 1985, Marrow et al., 1992, 1996, Abrams and Matsuda, 1997b, Khibnik and Kondrashov, 1997, Decole et al., 2006] or the evolutionary dynamics are fast [Cortez and Ellner, 2010].

A shared characteristic of all the models in the above studies involves the critical manifold, C. Due to biological constraints and assumptions (e.g. non-negative population size, density dependent interactions, or finite resource allocation), the functions describing the dynamics of the fast variables in system (3.1) have a particular form, namely $F(x, y, \epsilon) = xf(x, y, \epsilon)$. As a consequence, the critical manifold is composed of two manifolds, one defined by $x = 0$ and another defined by $f(x, y, 0) = 0$, that generically intersect transversally along a curve. Furthermore, the subspace $x = 0$ is invariant in the system. The transversal intersection of the critical manifolds is important because many of the complex dynamics observed in ecological and evolutionary models involve solutions passing by the intersection. In fact, nearly all of the complex dynamics observed in the above biological studies are due to global return mechanisms where solutions must pass through an ϵ-neighborhood of the transversal intersection (e.g., Lenbury and Likasiri 1994, Deng and Hines 2002, Ginoux et al. 2005, Deng and Loladze 2007).

In this study, we focus on the behavior of solutions and the dynamics that arise in the vicinity of the transversal intersection of the critical manifold. The behavior of solutions near the transversal intersection of critical manifolds in 1-fast, 1-slow dynamical systems has been investigated previously by Schecter [1985] and Krupa and Szmolyan [2001]. Here we focus on 1-fast, 2-slow dynamical systems in the biologically motivated case where one sheet of the critical manifold is invariant in the full system (i.e., $F = xf$ from the example above). Our analysis shows that complex behavior arises near the transversal intersection of the critical manifold. These dynamics occur in regions of parameter space near to where Hopf bifurcation of the system occurs $O(\epsilon)$-close to the intersection of the critical manifolds.

3.3 Canonical Form

We begin with a biologically motivated 1-fast, 2-slow system, $x \in \mathbb{R}$ and $y \in \mathbb{R}^2$ in system (3.1), where the $x = 0$ plane is invariant. Examples from the literature include predator-prey systems with one fast prey and two slow predators [Liu et al., 2003, Deng and Loladze, 2007, Jiang and Yang, 2009] and predator-prey systems where the ecological dynamicss of the two species are slow but one species evolves rapidly [Cortez and Ellner, 2010]. Our system has the form

$$\begin{aligned} \epsilon \dot{x} &= F(x, y, z, \epsilon) \\ \dot{y} &= G(x, y, z, \epsilon) \\ \dot{z} &= H(x, y, z, \epsilon) \end{aligned} \tag{3.2}$$

and we assume it satisfies the following conditions

$$F(0, y, z, \epsilon) = 0 \quad \text{for all } y, z \text{ and for all } \epsilon \geq 0 \tag{C1}$$

$$\frac{\partial F}{\partial x}(0, 0, 0, 0) = 0 \tag{C2}$$

$$\left(\frac{\partial^2 F}{\partial x \partial y}(0, 0, 0, 0)\right)^2 + \left(\frac{\partial^2 F}{\partial x \partial z}(0, 0, 0, 0)\right)^2 \neq 0 \tag{C3}$$

$$\frac{\partial^2 F}{\partial x^2}(0, 0, 0, 0) \neq 0. \tag{C4}$$

Condition (C1) guarantees that the $x = 0$ plane is a branch of the critical manifold and invariant in the full system. Condition (C2) allows for a second branch of the critical manifold to cross the $x = 0$ plane. Conditions (C3) and (C4) ensure that the second branch is not tangent to the fast flow and that the two branches of the critical manifold intersect transversally.

Under assumptions (C1) through (C4), system (3.2) can be transformed into

$$\begin{aligned} \epsilon\dot{x} &= x\,[x - y] + xf(x, y, z, \epsilon) \\ \dot{y} &= z + g(x, y, z, \epsilon) \\ \dot{z} &= \lambda + ax + by + cz + h(x, y, z, \epsilon) \end{aligned} \tag{3.3}$$

where $f, g, h = O(\epsilon, \epsilon u, u^2, uv)$ for $u, v \in \{x, y, z\}$ (see appendix C.1). Here $f = O(\epsilon, \epsilon x)$ means that all terms of f are of order ϵ, ϵx, or higher. We will restrict our attention to the truncated system

$$\begin{aligned} \epsilon\dot{x} &= x(x - y) \\ \dot{y} &= z \\ \dot{z} &= \lambda + ax + by + cz. \end{aligned} \tag{3.4}$$

The fast flow of system (3.4) is $\dot{x} = x(x - y)$, $\dot{y} = \dot{z} = 0$. The equilibria of the fast flow define the critical set of system (3.4), $C = \{(x, y, z) : \ x(x - y) = 0\}$. C is composed of a vertical and a horizontal two-dimensional manifold,

$$C_V = \{(x, y, z) : \ x = 0\} \tag{3.5}$$

$$C_D = \{(x, y, z) : \ x = y\}. \tag{3.6}$$

As see in figure 3.1, we denote the attracting and repelling branches of each manifold by C_V^a, C_V^r, C_D^a, and C_D^r, where the subscripts V and D denote the particular manifold each branch belongs to and the superscripts a and r denote the stability or instability of the branch, respectively. C_V is invariant in system (3.4) and C_D intersects it transversally along the intersection curve $C_I = C_D \cap C_V = \{(x, y, z) : \ x = 0, y = 0\}$.

For $\lambda \neq 0$, two equilibria always exist in system (3.4)

$$p_D = (\frac{-\lambda}{a + b}, \frac{-\lambda}{a + b}, 0) \in C_D \qquad p_V = (0, \frac{-\lambda}{b}, 0) \in C_V. \tag{3.7}$$

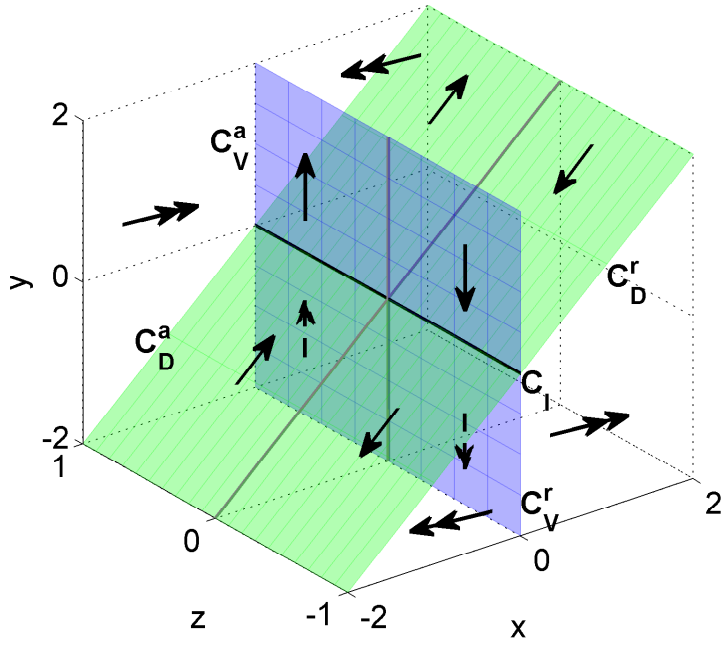

Figure 3.1: Qualitative picture of the slow-fast dynamics of system (3.4) near the intersection curve. The critical manifolds are the blue veritcal (C_V) and green diagonal (C_D) planes. The attracting and repelling branches of the manifolds are denoted by the superscripts a and r, respectively. The two manifolds intersect transversally along the curve C_I. The directions of the slow and fast flows are given by the single and double arrows, respectively.

The two equilibria are always a nonzero distance apart except when they coalesce at $\lambda = 0$.

3.4 Slow Flows and the Intersection Curve

In this section we focus on the slow flows of system (3.4) and how they influence the dynamics near the intersection curve for small values of ϵ. For a qualitative picture of the slow and fast flows, see figure 3.1. We will implicitly assume throughout the following that ϵ is sufficiently small.

Setting $\epsilon = 0$ in system (3.4) yields a differential algebraic equation (DAE). The algebraic constraint of the DAE ensures that solutions to the DAE are either on C_V or C_D. The flow of the DAE defines the slow flow associated with each manifold of the critical set. The slow flow on C_V is

$$\begin{aligned} \dot{y} &= z \\ \dot{z} &= \lambda + by + cz. \end{aligned} \tag{3.8}$$

The unique equilibrium of this subsystem is $p_V = (0, -\lambda/b, 0)$ and its eigenvalues are $\mu_\pm = \frac{1}{2}c \pm \frac{1}{2}\sqrt{c^2 + 4b}$.

The slow flow on C_D is

$$\begin{aligned} \dot{y} &= z \\ \dot{z} &= \lambda + (a+b)y + cz. \end{aligned} \tag{3.9}$$

The unique equilibrium of this subsystem is $p_D = (\frac{-\lambda}{a+b}, \frac{-\lambda}{a+b}, 0)$ and its eigenvalues are $\eta_\pm = \frac{1}{2}c \pm \frac{1}{2}\sqrt{c^2 + 4(a+b)}$. Except along the intersection curve, for ϵ small enough, the behavior of solutions on the critical manifold approximates the behavior of solutions near the critical manifold to first order.

Along the intersection curve, C_I, the slow flow is given by $\dot{y} = z$ and $\dot{z} = \lambda + cz$. When $\epsilon = 0$, the flow is not well defined along the curve because in the singular limit both C_V and C_D are invariant. Thus, it is conceivable that for positive ϵ, solutions approaching the intersection curve along a sheet of the critical manifold could exit following the same sheet, or transfer and then exit following a different sheet. For example, consider the trajectories in figure 3.2 that have been projected onto the x, y-plane. In figure 3.2 *B*, the trajectory approaching C_I along C_V^a with $x < 0$ could exit the vicinity of the intersection curve either along C_D^a (dashed red curve) or C_V^r (solid red curve). In the following we discuss how

solutions behave in the vicinity of the intersection curve when ϵ is sufficiently small.

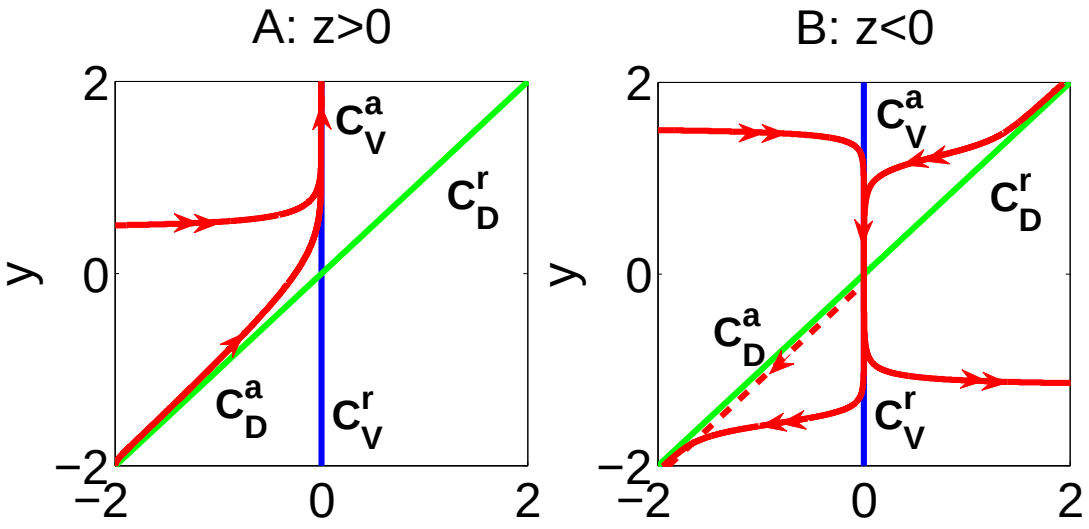

Figure 3.2: Examples of solutions that approach the intersection curve at (A) positive values of z and (B) negative values of z, projected to the x, y-plane. The critical manifolds are labeled as in figure 3.1 and solutions are in red. (A) All solutions that approach the intersection curve leave the vicinity of the intersection curve along C_V^a. (B) All solutions that approach the intersection curve along C_V^a have canard-like behavior and exit along C_V^r (solid red line). Solutions with $x < 0$ do not exit along C_D^a (dashed red line).

Consider the flow of system (3.4) near the point $\rho = (0, 0, z_0) \in C_I$ where $z_0 < 0$. We will first introduce two cases and then show how the dynamics near this point can be inferred from previous studies. For the first case, assume the x-coordinate of the solution is positive. All solutions of this type will approach the intersection curve along C_V^a and exit along the repelling branch C_V^r (see figure 3.2 B). The distance for which a trajectory remains near the repelling sheet will be discussed below. In the second case we assume the x-coordinate of the solution approaching the intersection curve is negative. These solutions also approach the intersection curve along C_V^a, but then can either exit along the attracting sheet C_D^a (figure 3.2, dashed red curve) or the repelling sheet C_V^r (figure 3.2,

solid red curve). One might expect solutions to follow the attracting branch, but this is not the case. To see this result, we show that for small enough ϵ, our system behaves qualitatively like a special case of the two-dimensional analog of our model that was analyzed by Krupa and Szmolyan [2001].

First we transform our system in the following way.

LEMMA 3.1. *Assume $\rho = (0, 0, z_0) \in C_I$ where $z_0 \neq 0$. Then locally the flow near ρ is given by*

$$\begin{aligned} \dot{x} &= x(x - y) \\ \dot{y} &= \hat{\epsilon}(1 + \hat{g}(y, \hat{z})) \\ \dot{\hat{z}} &= \hat{\epsilon}(0 + \hat{h}(x, y, \hat{z})) \end{aligned} \tag{3.10}$$

where $g = O(y, z)$ and $h = O(x, y, z)$.

Proof. Let $\theta = \arctan\left(\frac{\lambda + cz_0}{z_0}\right)$ and $\hat{\epsilon} = \epsilon z_0$. The coordinate change $\hat{z} = -\sin(\theta)y + \cos(\theta)(z - z_0)$ where

$$\begin{aligned} \hat{g}(y, \hat{z}) &= \frac{-\tan(\theta)}{z_0} y + \frac{\csc(\theta)}{z_0} \hat{z} \\ \hat{h}(y, \hat{z}) &= \frac{a\cos(\theta)}{z_0} x + \frac{\cos(\theta)}{z_0} [b + \sin(\theta) - \tan^2(\theta)] y + \frac{1 - \tan(\theta)}{z_0} \hat{z} \end{aligned}$$

and a rescaling of time yields the result. □

Remark: The above transformation only retains the fast-slow structure present in system (3.4) when ϵ is sufficiently small. In particular, the terms $\tan(\theta)$ and $\csc(\theta)$ in the proof of the previous lemma tend to positive or negative infinity as $z \to 0$. This transformation and the following analysis does not hold at $z = 0$ for any ϵ because the slow flow is tangent to the intersection curve.

The above tells us that near the point $\rho = (0, 0, z_0)$, $\dot{x} = O(x^2, y^2)$, $\dot{y} = O(\epsilon)$, and $\dot{z} = O(\epsilon u)$ for $u \in \{x, y, z\}$. For sufficiently small ϵ, the $O(\epsilon)$ and $O(x^2, y^2)$ terms will

dominate and z will remain essentially constant. Thus, for sufficiently small ϵ, the dynamics in system (3.10) will behave like the dynamics on the center manifold $W^c = \{(x, y, \hat{z}) : \hat{z} = 0\}$. The dynamics on W^c are given by

$$\begin{aligned} \dot{x} &= x(x - y) \\ \dot{y} &= \hat{\epsilon}(1 + \hat{g}(y, 0)). \end{aligned} \tag{3.11}$$

System (3.11) is a special case of a model presented in Krupa and Szmolyan [2001],

$$\begin{aligned} \dot{x} &= x^2 - y^2 + \bar{\lambda}\epsilon + h_1(x, y, \epsilon) \\ \dot{y} &= \epsilon(1 + h_2(x, y, \epsilon)) \end{aligned} \tag{3.12}$$

where $\bar{\lambda} = 1$ and $h_1 = 0$ (see appendix C.2 for details). The critical manifold of system (3.12) consists of two lines ($y = x$ and $y = -x$) that intersect transversally at a non-normally hyperbolic point located at the origin. When $\bar{\lambda} = 1$, the line $x = y$ is invariant in the truncated system and solutions that approach the non-normally hyperbolic point along the attracting branch of the line $x = y$ do not exit along the attracting branch of the line $y = -x$. Instead, the solutions exit along the repelling branch of the line $y = x$ and have canard like behavior.

Returning to the two cases from above, the results in Krupa and Szmolyan [2001] imply that for ϵ small enough, solutions approaching the intersection curve along C_V^a on either side of the z, y-plane will exit following C_V^r and have canard like behavior. The distance a solution will follow the repelling sheet of C_V can be determined via a variational equation or Pontryagin's delay of lost stability (for particular examples in the literature see Schecter 1985, Deng 2001, Boudjellaba and Sari 2009).

Now consider the flow of system (3.4) near the point $\rho = (0, 0, z_0) \in C_I$ where $z_0 > 0$. Using the above reduction, one can show that all solutions approaching

the intersection curve with $z_0 > 0$ exit the vicinity of the intersection curve along C_V^a (see figure 3.2 *A* for examples). This follows from the invariance of C_V and that $\dot{y} > 0$ near ρ for the slow flows on both C_V and C_D. Thus, for positive values of z, solutions will approach the intersection curve along C_D^a or C_V^r and leave the vicinity of the intersection curve along C_V^a.

3.5 Normal Form Dynamics

This section investigates the dynamics exhibited by system (3.4). In particular, we will focus on the stability and bifurcations of the equilibrium p_D and the periodic orbits it gives birth to after undergoing Hopf bifurcation.

Bifurcation diagrams for different parameter regimes are given in figure 3.3. We only present diagrams for nonnegative values of c due to symmetry. In particular, reversing time by $t \to -t$ is equivalent to the transformation $(x, y, \lambda, c) \to (-x, -y, -\lambda, -c)$. In addition, we will only present the numerical examples for $\epsilon = 0.1$. ϵ can be scaled out of system (3.4) with the rescaling $(Z, A, B, C, \lambda) = (\epsilon z, \epsilon^2 a, \epsilon^2 b, \epsilon c, \epsilon^2 \lambda)$. Thus, the dynamics presented here qualitatively represent the behavior exhibited by system (3.4) for other values of ϵ.

We note a few bifurcations that will be present in all cases. When $\lambda = 0$, p_D and p_V coalesce at a transcritical bifurcation. Along the line $b = -a$, the equilibrium p_D does not exist except when $\lambda = 0$. Similarly, p_V does not exist when $b = 0$ except when $\lambda = 0$.

We begin by relating the stability of p_D in system (3.4) to the stability of the equilibria of the slow flows (3.8) and (3.9) via the Routh-Hurwitz Criteria. We

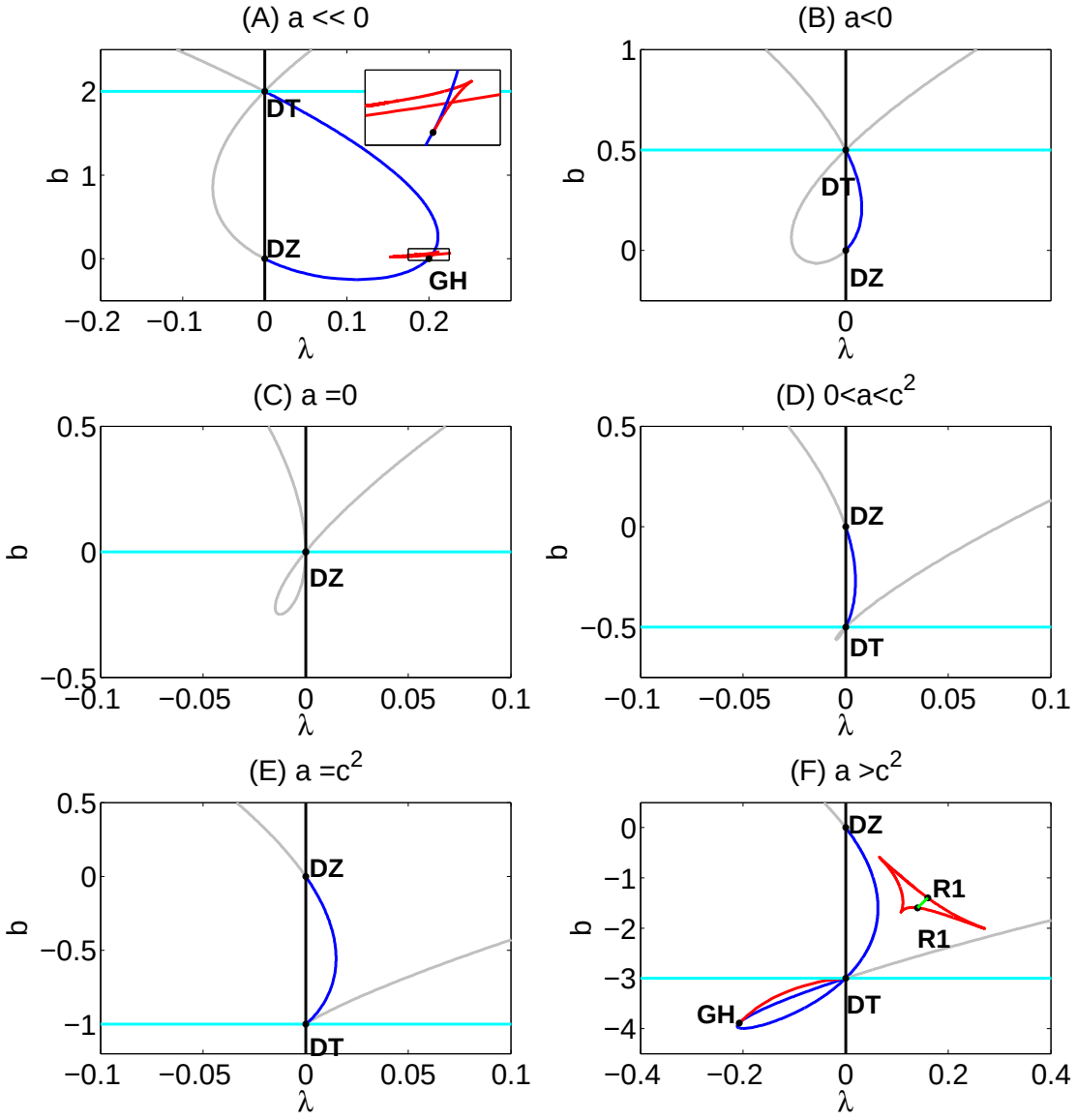

Figure 3.3: Bifurcation diagram for system (3.4) for varying values of a, b and λ with $(c, \epsilon) = (1, 0.1)$. Curve color corresponds to the following bifurcations: black - transcritical; blue - Hopf; cyan - p_D does not exist; gray - neutral saddle (trace =0); green - Neimark-Sacker; red - saddle node of limit cycles. DZ, GH, and DT denote double zero, generalized Hopf, and degenerate transcritical bifurcations (see section 3.5.2). R1 denotes 1:1 strong resonance points. (A) The mini-panel magnifies the boxed region.

then investigate when Hopf bifurcations occur in the system. Finally, using numerical continuation, we explore the bifurcations periodic orbits undergo.

3.5.1 Equilibria stability and the slow flows

Here we show when the stability of the equilibria can be completely determined by information contained in the fast and slow flows. We begin with the stability of the equilibrium on the invariant manifold, p_V. For all values of ϵ, the stability of p_V in the full system (3.4) is determined by the eigenvalues $\mu_\pm$ and the sign of λ/b. Thus, the stability of p_V is independent of ϵ and is completely determined by its stability in the fast and slow subsystems.

The stability of p_D in system (3.4) is more complicated. We begin analyzing the stability of p_D via the Routh-Hurwitz Criteria by considering the limits where $|\lambda| \gg \epsilon$ and $|\lambda| \ll \epsilon$. This viewpoint allows us to relate the stability of p_D in the full system to its stability and the stability of p_V in the fast and slow flows. The stability of p_D for intermediate value of λ can also be understood using the Routh-Hurwitz Criteria, though the analysis is more complicated and less intuitive. We address this case in the next section. The main conclusions of this section are as follows. For values of λ much larger than ϵ, the stability of p_D is determined by its stability in the slow and fast flows. For values of λ much smaller than ϵ, the stability of p_D is given by the stability of p_V in the slow flow (3.8) and the opposite stability of p_V in the fast flow.

We first recall the Routh-Hurwitz criteria. After a transformation of time, the

Jacobian evaluated at p_D is given by

$$J = \begin{bmatrix} \frac{-\lambda}{a+b} & \frac{\lambda}{a+b} & 0 \\ 0 & 0 & \epsilon \\ \epsilon a & \epsilon b & \epsilon c \end{bmatrix}. \tag{3.13}$$

The characteristic polynomial for this matrix is

$$\rho(\gamma) = \gamma^3 - \left(\epsilon c - \frac{\lambda}{a+b}\right)\gamma^2 - \left(\epsilon^2 b + \frac{\epsilon c \lambda}{a+b}\right)\gamma - \epsilon^2 \lambda. \tag{3.14}$$

The Routh-Hurwitz criteria tells us that the number of roots of $\rho(\gamma)$ (or equivalently the number of eigenvalues of J) with positive real part is given by the number of sign changes in the sequence $\{1, A_1, A_1(A_1A_2 - A_3), A_3(A_1A_2 - A_3)^2\}$ where

$$\begin{aligned} A_1 &= -\epsilon c + \frac{\lambda}{a+b} \\ A_2 &= -\epsilon^2 b - \frac{\epsilon c \lambda}{a+b} \\ A_3 &= -\epsilon^2 \lambda. \end{aligned} \tag{3.15}$$

Note that sign of last term in the sequence is determined solely by the sign of A_3. The number of roots with negative real part is the given by the number of sign changes in the sequence $\{1, -A_1, A_1(A_1A_2 - A_3), -A_3(A_1A_2 - A_3)^2\}$.

When λ is large in magnitude, the terms with λ in equation (3.15) dominate. In this case, the signs of two of the eigenvalues are determined by the signs of $\eta_\pm$. The sign of the last eigenvalue is determined by sign of $x^* = -\lambda/(a+b)$. Note that the sign of x^* is the same as the sign of the normal hyperbolicity condition evaluated at p_D (i.e. the stability p_D in the fast flow). Thus, in this case the stability of p_D can be deduced solely by understanding its stability in the fast and slow flows.

In the limit where $\lambda \ll \epsilon$, the terms with ϵ in equation (3.15) dominate. In this case, the signs of two of the eigenvalues are determined by the signs of $\mu_\pm$.

The sign of the last eigenvalue is determined by the sign of $-\lambda/b$. Note that the y coordinate of p_V is $-\lambda/b$ and recall that the stability of p_V in the x-direction is given by the sign λ/b. Thus, in the case where $\lambda \ll \epsilon$, the stability of p_D in system (3.4) can be determined solely from the stability of p_V in the slow flow (3.8) and the fast flow. In particular, the signs of two of the eigenvalues are given by the signs of $\mu_\pm$ (i.e. the stability of p_V in the slow flow (3.8)) and the sign of the last eigenvalue is given by $-\lambda/b$ (the opposite sign of the nonzero eigenvalue of p_V in the fast flow). When $\lambda = 0$, the signs of two of the eigenvalues are given by the signs of $\mu_\pm$ and the last eigenvalue is zero. With a center manifold reduction, the (nonlinear) stability of the equilibrium in the x-direction can be shown to be determined by the sign of $(a + b)/b$.

3.5.2 Hopf bifurcation

Hopf bifurcations of p_D occur when $A_1A_2 - A_3 = 0$ and $A_2 > 0$. Solving $A_1A_2 - A_3 = 0$ for λ yields

$$\lambda = \epsilon\frac{(a+b)}{2c}\left[a + c^2 \pm \sqrt{(a+c^2)^2 + 4c^2b}\right]. \tag{3.16}$$

Thus, Hopf bifurcation of the system occurs $O(\epsilon)$-close to the origin, and in particular, the intersection curve. Numerical examples of where Hopf bifurcation exist in parameter space are given in figure 3.3.

Degenerate Hopf bifurcation occurs in system (3.4) when the first Lyapunov coefficient vanishes or the real eigenvalue vanishes. Generalized Hopf bifurcations occur when the first Lyapunov coefficient vanishes and the second Lyapunov does not vanish. Numerically, generalized Hopf bifurcations are observed in system (3.4) only when $a+b < 0$. In the unfolding, the Hopf bifurcation

switches from subcritical to supercritical as it passes through the generalized Hopf point along the Hopf curve. Two periodic orbits exist in an adjoining region of parameter space and these periodic orbits annihilate in a saddle-node of limit cycles bifurcation.

Degenerate Hopf bifurcations where the real eigenvalue vanishes occur when the trace of the Jacobian (3.13) is zero, i.e. when $A_1 = 0$. For positive values of ϵ, this occurs when $\lambda = 0$ and either $c = 0$, $a + b = 0$, or both vanish. When $\lambda = 0$, $c = 0$, and $a + b \neq 0$, no equilibria exist in the system. When $\lambda = 0$ and $a+b = 0$, the line $\{(x, y, z) : x = y, z = 0\}$ is composed of equilibria. The eigenvalues of these equilibria are zero and $\frac{\epsilon}{2}\left(c \pm \sqrt{c^2 + 4b}\right)$. Thus, degenerate Hopf bifurcations where the real eigenvalue vanishes only occur when $\lambda = 0$, $a+b = 0$, $b < 0$, and $c = 0$. Under these constraints, the Hopf bifurcation coincides with the transcritical bifurcation of p_D and p_V.

It is expected that the line of equilibria passing through the degenerate Hopf point will not persist when higher order terms are added to system (3.4). The effects of higher order terms were investigated by keeping all quadratic terms of system (3.3) and truncating terms of order three or greater. Through linear transformations, that system can be transformed into the following at the transcritical-Hopf bifurcation.

$$\begin{aligned} \dot{u} &= g_1 u^3 + g_2 u|v|^2 + g(u, v, \bar{v}) \\ \dot{v} &= \epsilon\beta i v + h_1 uv + h_2 u^2 v + h_3 v|v|^2 + h(u, v, \bar{v}) \end{aligned} \tag{3.17}$$

where $u \in \mathbb{R}$, $v \in \mathbb{C}$, $\beta = \sqrt{-b}$, $g, h = O(\|(u, v, \bar{v})\|^4)$ and the coefficients $g_j \in \mathbb{R}$ and $h_j \in \mathbb{C}$ are linear combinations of the quadratic terms of the $\dot{y}$ and $\dot{z}$ equations of system (3.3). We make a few notes about the form of system (3.17). First, generically only one quadratic term of system (3.3) does not vanish at the

transcritical-Hopf bifurcation. Thus, generically system (3.3) does not satisfy two of the degeneracy conditions for the fold-Hopf normal form (see Kuznetsov 2000). The coefficient on the remaining quadratic term is $h_1 = 1/2 + O(\epsilon)$. Second, generically the line $\{(x, y, z) : x = y, z = 0\}$ is not composed of equilibria at the transcritical-Hopf bifurcation. Finally, the behavior of system (3.3) at a transcritical-Hopf point must be studied on a case-by-case basis that includes all quadratic terms.

In figure 3.3, Hopf curves terminate at degenerate transcritical (DT) and double zero bifurcations (DZ). At DT bifurcations, $\lambda = a + b = 0$ and the line $\{(x, y, z) : x = y, z = 0\}$ is composed of equilibria. While the equilibrium point at the origin is present for all parameter values, the line of equilibria does not persist when quadratic terms are included in system (3.4). The nonlinear stability of the equilibrium at the origin is determined by the coefficients of the quadratic terms in the $\dot{y}$ and $\dot{z}$ equations of system (3.3).

Double zero bifurcations correspond to parameter values where two eigenvalues vanish. They arise in system (3.4) when $\lambda = b = 0$, and $a \neq 0$. At such points, the equilibrium exists at the origin, the eigenvector for the nonzero eigenvalue of the Jacobian is $(0, 1/c, 1)^T$, and the generalized eigenvectors for the zero eigenvalue are $(0, 1, 0)^T$ and $(-\frac{c}{\epsilon a}, 0, 1/\epsilon)^T$. The Jordan Normal Form for this bifurcation is

$$\begin{pmatrix} 0 & 1 & 0 \\ 0 & 0 & 0 \\ 0 & 0 & \epsilon c \end{pmatrix}.$$

When system (3.4) undergoes a double zero bifurcation, the line $\{(x, y, z) : x = z = 0\}$ consists of equilibria. In addition, after a center manifold reduction

and subsequent transformations leading to the Bogdanov-Takens normal form [Kuznetsov, 2000], system (3.4) becomes

$$\begin{aligned} \dot{u} &= v \\ \dot{v} &= -uv \end{aligned} \tag{3.18}$$

where the u^2 coefficient of the $\dot{v}$ equation in system (3.18) is zero. By addressing the effects of higher order terms, we investigate if these are generic properties of our class of systems.

If all quadratic terms of system (3.3) are kept, the behavior of system (3.4) on the center manifold at the double zero bifurcation is determined by

$$\begin{aligned} \dot{u} &= v + \sigma_1 u^2 + \sigma_2 uv + \sigma_3 v^2 \\ \dot{v} &= -uv \end{aligned} \tag{3.19}$$

where σ_i are rational functions of the linear and quadratic coefficients of system (3.3). Clearly the line of equilibria passing through the origin does do not exist generically in system (3.19). The u^2 coefficient of the $\dot{v}$ equation is generically zero though. This occurs because one of the generalized eigenvectors for the zero eigenvalue is contained in the invariant plane $x = 0$. system (3.19) always has an equilibrium at the origin that is half-stable in the invariant line $v = 0$. When $\sigma_1 < 0$, the equilibrium has an infinite number of homoclinic orbits and when $\sigma_1 > 0$, there are no homoclinic orbits (see figure 3.4).

3.5.3 Periodic orbits

Periodic orbits arise in system (3.4) either through Hopf bifurcation of system (3.4) or saddle-node bifurcations. Here we present some of the saddle-node, period doubling and torus bifurcations of the periodic orbits observed

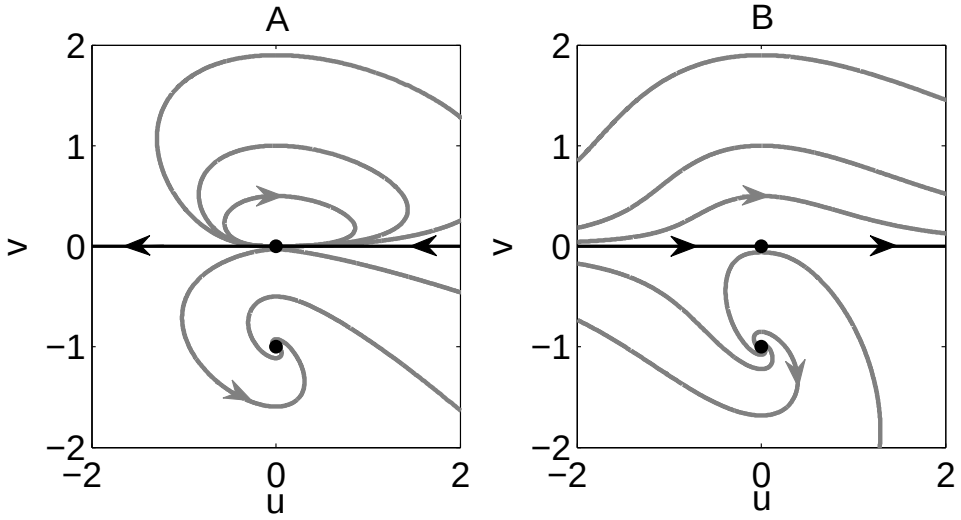

Figure 3.4: Example solutions to system (3.19) when (*A*) $\sigma_1 < 0$ and (*B*) $\sigma_1 > 0$. system (3.19) describes the dynamics on the center manifold of equilibrium p_D at double zero bifurcations ($\lambda = b = 0$, $a \neq 0$) in system (3.4). The equilibrium of system (3.19) at the origin is always half stable on the invariant line $v = 0$. When $\sigma_1 < 0$, that equilibrium has an infinite number of homoclinic orbits.

via continuation as one or two parameters are varied. We will consider three parameter regimes where periodic orbits are observed. These cases correspond to figures 3.3 *A*, $\lambda < 0$ in 3.3 *F*, and $\lambda > 0$ in 3.3 *F*. Note that periodic orbits do not exist for $\epsilon = 0$ except when $b < 0$ and $\lambda = c = 0$. At these values, the unique equilibrium point of the system is neutrally stable with one zero eigenvalue and a complex pair eigenvalues with zero real part.

In the first case, $\lambda > 0$, $c > 0$, $a + b < 0$, and $a < 0$ is sufficiently large in magnitude. As shown in figure 3.5, up to four periodic orbits are observed in phase space. The two periodic orbits in figure 3.5 *A* and the outer and inner most periodic orbits of figure 3.5 *B* emerge via subcritical and supercritical Hopf bifurcations of p_D, respectively. In the vicinity of the generalized Hopf point, these two periodic orbits annihilate in a saddle-node of limit cycles bifurcation. The other two periodic orbits in figure 3.5 *B* emerge from a saddle-node of limit

cycles bifurcation. Each of these two periodic orbits annihilate with one of the two periodic orbits that emerged from the Hopf bifurcations at a saddle-node of limit cycles bifurcation.

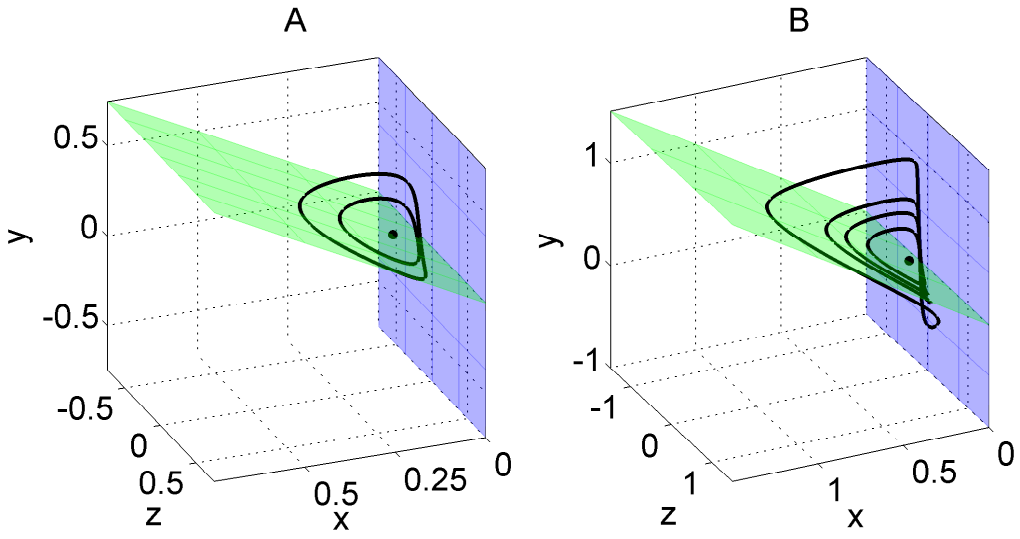

Figure 3.5: Periodic orbits of system (3.4) for $(a, b, c, \epsilon) = (-2, -0.079, 1, 0.1)$ and either (A) $\lambda \approx 0.2091$ or (B) $\lambda \approx 0.2106$. Parameter values correspond to the regions in the mini panel of figure 3.3 A. The two periodic orbits in (A) and the inner and outermost periodic orbits in (B) emerged from Hopf bifurcations of p_D (black dot). The remaining two periodic orbits in (B) emerged from a saddle node of limit cycles.

In the second case where periodic orbits are observed, $a + b < 0$ and $a > 0$ are sufficiently large in magnitude and $\lambda < 0 < c$ (figure 3.3 F). Up to two periodic orbits are observed in the vicinity of the generalized Hopf bifurcation. These periodic orbits are small and remain outside of a neighborhood of size 2ϵ of the intersection curve (figure 3.6 B). For $a + b < 0$ small in magnitude, the periodic orbits are sufficiently large that they enter a 2ϵ-neighborhood of the intersection curve. Once within this neighborhood, the unstable manifold of p_D begins to fold over on itself (figures 3.6 C and 3.6 D) and more complicated dynamics arise. We study the resulting dynamics using sections transverse to the flow. In

figure 3.7, we present returns to a particular family of sections as λ varies with $(a, b, c) = (3, -3.1, 1)$. The sections are defined by $x = -\lambda/(a + b)$ and $z < 0$. Note that due to the exponential attraction of solutions to the slow manifold, returns to the sections are essentially one-dimensional.

For small values of λ, returns between the outermost periodic orbit and the equilibrium point p_D converge to the smaller stable periodic orbit (figure 3.7 *B*). Returns outside of the outermost periodic orbit eventually escape to $x = -\infty$. As λ becomes more negative, the folding of the unstable manifold of p_D induces a quadratic map on returns to the section. Points of higher period arise in the return map as λ becomes more negative, until a period three orbit is born (figure 3.7 *D* and *E*). The birth of a three-orbit implies the existence of a chaotic set in a 1-dimensional map [Li and Yorke, 1975]. Thus the birth of a three orbit in the return map implies the emergence of a chaotic set in system (3.4). As λ increases in magnitude, the returns to the section become unbounded and for λ large enough in magnitude, most trajectories are lost to $x = \infty$ (figure 3.7 *F*). In total, in this region a chaotic regime separates regimes where solutions in the vicinity of the equilibrium point are bounded and unbounded.

In the third region where periodic orbits are observed, $a, c, \lambda > 0$ and $a + b > 0$ (figure 3.3 *F*). A stable periodic orbit emerges from a supercritical Hopf bifurcation for small λ. As λ increases, the periodic orbit eventually undergoes period doubling and torus bifurcations. These bifurcations occur within a region of b, λ-parameter space bounded by three saddle-node of limit cycles curves (see figure 3.3 *F*). Two of the saddle-node curves contain 1:1 strong resonance points. These resonance points are connected by a curve of Niemark-Sacker bifurcations. A complete unfolding of strong 1:1 resonant points is unknown to

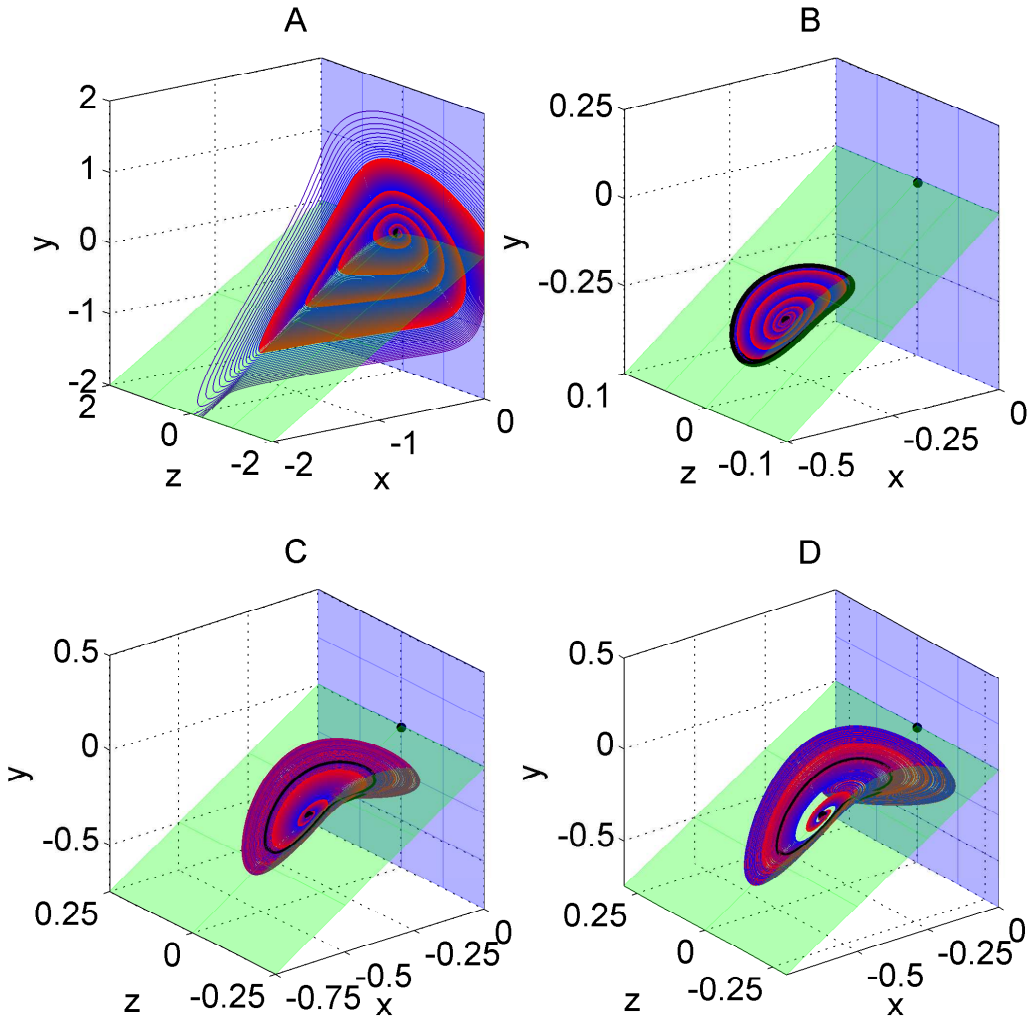

Figure 3.6: Unstable manifold of the equilibrium p_D for $(a, b, c, \epsilon) = (3, -3.1, 1, 0.1)$ when (A) $\lambda = -0.005$, (B) $\lambda = -0.031$, (C) $\lambda = -0.033$, and (D) $\lambda = -0.03338$. All panels contain p_D (black dots) and panels $(B\text{-}D)$ contain the stable periodic orbit that emerged via supercritical Hopf bifurcation (black, closed orbit). Due to its size, the saddle-type periodic orbit that emerged via subcritical Hopf bifurcation is only included in (B), where it is very close to the stable orbit. (A) No periodic orbits exist. (B) For small values of λ, the orbits remain outside of a 2ϵ-neighborhood of the intersection curve. $(C\text{-}D)$ For larger values of λ, the periodic orbit enters the 2ϵ-neighborhood and and the unstable manifold of p_D folds over on itself.

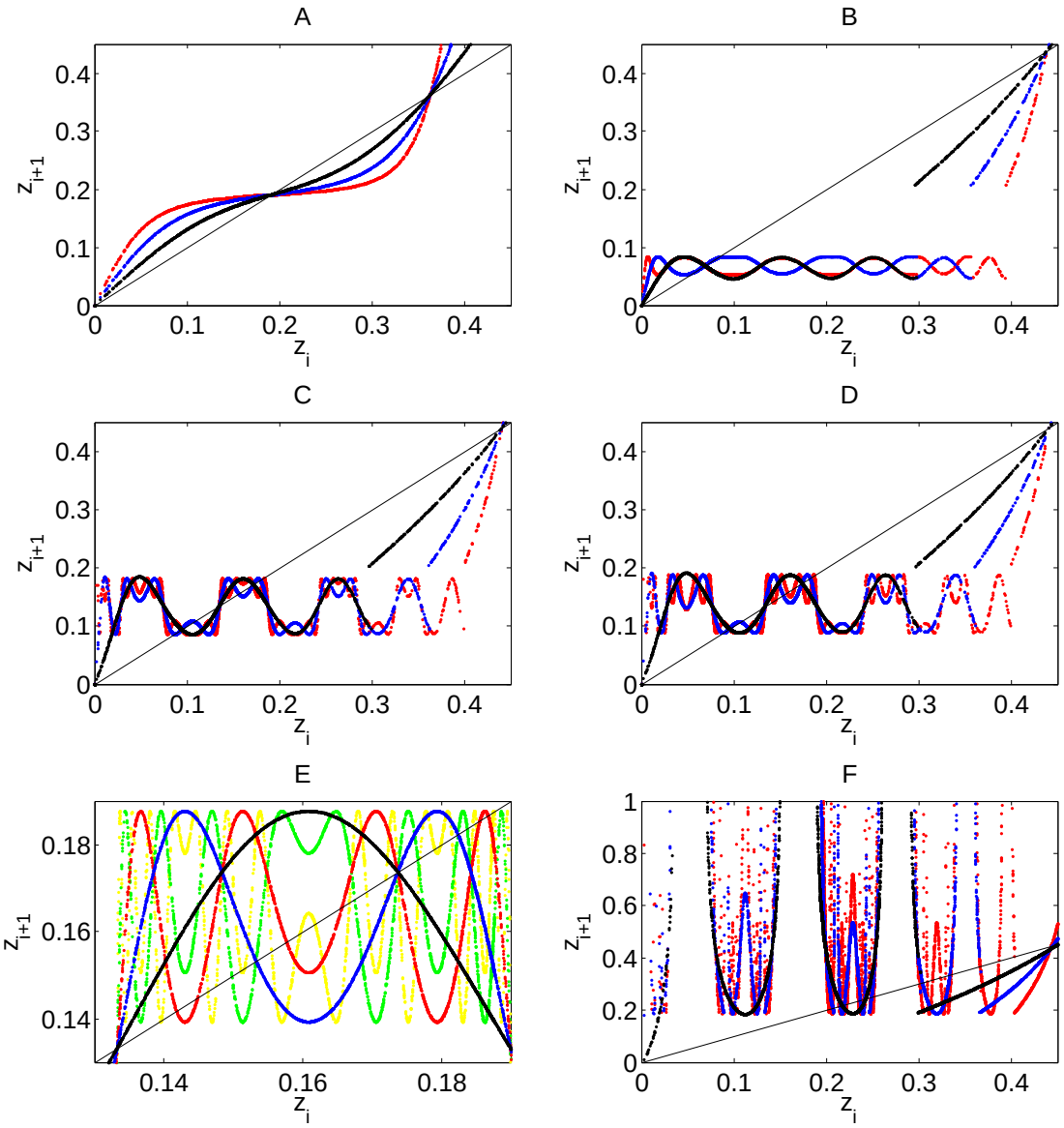

Figure 3.7: Induced maps for the returns to the sections defined by $x = -\lambda/(a+b)$ and $z < 0$. Only z coordinates are recorded since returns are essentially one dimensional. Parameter values are $(a, c, \epsilon) = (3, 1, 0.1)$ for all panels, (A) $b = -3.5$ and $\lambda = -0.15$,$(B\text{-}F)$ $b = -3.1$, (B) $\lambda = -0.32$, (C) $\lambda = -0.3333$, $(D\text{-}E)$ $\lambda = -0.3338$, and (F) $\lambda = -0.0348$. The equilibrium is located at $(0, 0)$ and the thin black line defines the line $z_i = z_{i+1}$. The maps induced by first, second, third, fourth, and fifth returns to the section are in black, blue, red, green, and yellow, respectively. Panel (E) is an enlargement of the chaotic region in panel (D). The existence of a three-orbit in panels (D) and (E) implies the existence of a chaotic set in system (3.4).

the author, but the general unfolding is expected to have regions of parameter space involving a torus break up, phase-locking Arnold tongues, and an infinite number of saddle cycles [Kuznetsov, 2000]. figure 3.8 shows some examples of periodic orbits that emerge in the region enclosed by the three saddle-node of limit cycle curves.

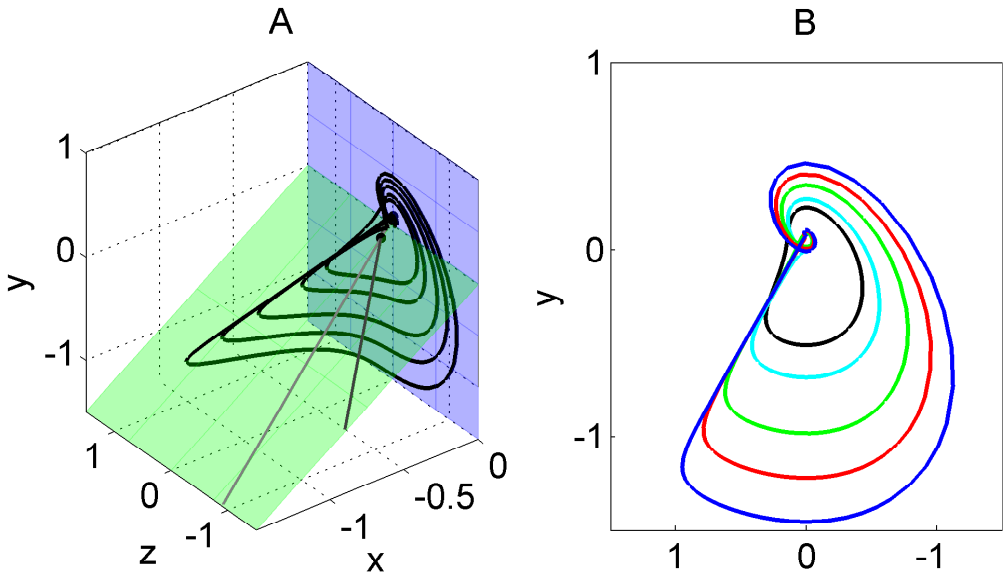

Figure 3.8: Five periodic orbits of system (3.4) for $(a, b, c, \lambda, \epsilon) = (3, -1.5, 1, 0.1233059, 0.1)$ in (A) phase space and (B) projected to the z, y-plane. Parameters correspond to the region enclosed by the three saddle-node of limit cycles curves in figure 3.3 F. (A) Equilibria are black dots and the stable and unstable manifolds of p_D in the slow flow (3.9) are the gray and black lines, respectively. (B) The black orbit emerged from a subcritical Hopf bifurcation at $\lambda \approx 0.063$. The blue and green orbits and the red and blue orbits emerged from limit point cycle bifurcations at $\lambda \approx 0.111$ and $\lambda \approx 0.123$, respectively.

3.6 Geometric Analysis and Invariant Manifolds

The critical manifolds of system (3.4) are normally hyperbolic away from the intersection curve. The stability of each branch of the manifolds is seen in fig-

ure 3.1. Away from the intersection curve, the normal hyperbolicity of a critical manifold implies that there exist invariant slow manifolds that are within an $O(exp(-c/\epsilon))$-distance of each other and that are within an $O(\epsilon)$-neighborhood of the critical manifold [Fenichel, 1971, 1979]. The critical and slow manifolds separate phase space into regions where solutions flow towards or away from $x = \pm\infty$ and $x = 0$. Phase space is further subdivided by the stable and unstable manifolds of equilibria and periodic orbits of the system. In this section we address the behavior of solutions in phase space and how that behavior is influenced by the stable and unstable manifolds of these invariant sets.

3.6.1 Stable and unstable slow manifolds

We begin with regions of parameter space where periodic orbits are absent. In these regions, the qualitative behavior of a solution can be predicted by naïvely following the fast and slow flows of system (3.4) away from the intersection curve and by following the appropriate behavior from section 3.4 near the intersection curve. Examples of solutions from different regions of parameter space are shown in figure 3.9. In all cases, the solutions essentially follow the slow flow when away from the intersection curve and behave like one of the trajectories in figure 3.2 when in the vicinity of the intersection curve.

In figures 3.9 *A* and *C*, the solutions split into two groups with qualitatively different dynamics. In particular, the solutions in (*A*) either tend to $x = 0$ (left three trajectories) or $x = -\infty$ (right three trajectories) and the solutions in (*C*) either rotate around p_D and p_V once (left four trajectories) or do not rotate at all (right three trajectories). In both cases, p_D is a saddle in the slow flow (3.9)

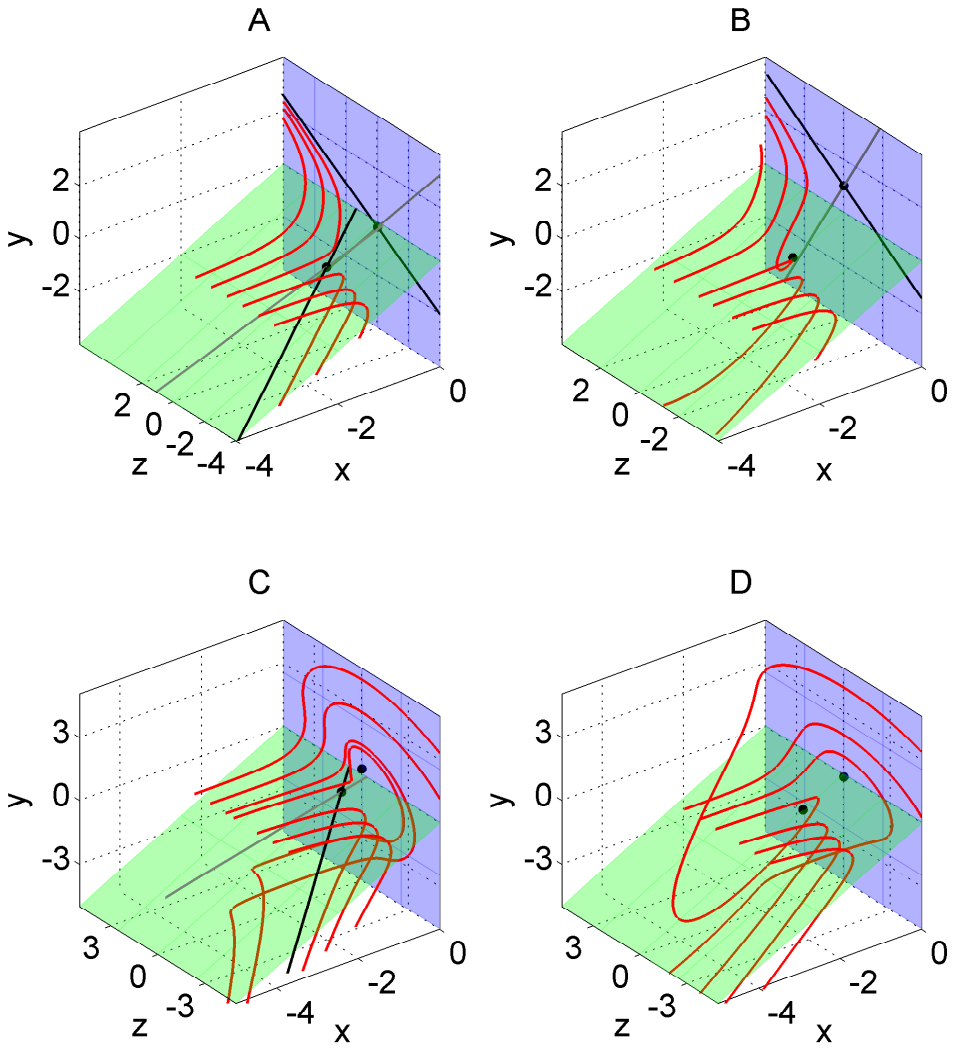

Figure 3.9: Examples of solution behavior in regions of parameter space where periodic orbits do not exist. All trajectories (red) follow the slow flow far from the intersection curve and behave like one of the trajectories in figure 3.2 near the intersection curve. When either of the equilibria (black dots) are saddles in the slow flows (3.8) and (3.9), their stable and unstable manifolds (gray and black lines, respectively) are included. In all panels $c = 1$ and $\epsilon = 0.1$. The other parameters are (A) $(a, c, \lambda) = (-2, 2.5, -0.005)$, (B) $(a, c, \lambda) = (-2, 1.5, -0.5)$, (C) $(a, c, \lambda) = (3, -2, 0.5)$, and (D) $(a, c, \lambda) = (3, -3.5, -0.5)$.

and we denote its stable manifold in that flow by W_0^s. For $\epsilon > 0$, there exists an associated one-dimensional stable submanifold, W_ϵ^s, in the slow manifold of C_D. The attracting manifold, W_a^s, of the stable manifold W_ϵ^s is the object that splits the trajectories in figures 3.9 *A* and *C*.

In other regions of parameter space where p_D is a node in the slow flow (3.9) or C_D is repelling, the divergence of solutions is determined in an analogous way by the weak stable or unstable manifold of p_D and its attracting or repelling manifold. Consider the example in figure 3.6 *A*. In the full system (3.4), p_D is a saddle with a single negative eigenvalue and complex conjugate pair with positive real part. In the slow flow (3.9), p_D is a node source. The behavior of solutions that approach C_D through the plane $x = -3$ is presented in figure 3.10 *A*. The red line defines the intersection of the attracting sheet of the weak unstable manifold with the plane $x = -3$. Solutions passing through the plane with more negative values of z turn around and head off to $x = -\infty$ without a rotation around p_D. Solutions with more positive values of z rotate around p_D at least once before heading off to $x = -\infty$. The number of rotation is determined by the sectors of rotations outlined in black.

3.6.2 Stable and unstable manifolds of invariant sets

The attracting and repelling manifolds of the stable and unstable manifolds of p_D also split trajectories in regions of parameter space where periodic orbits exist, but additional behavior is observed due to the presence of the periodic orbits. In this section we focus on the three regions of parameter space from before where periodic orbits arise: $\lambda < 0$ in 3.3 *F*, $\lambda > 0$ in figure 3.3 *A*, and $\lambda > 0$

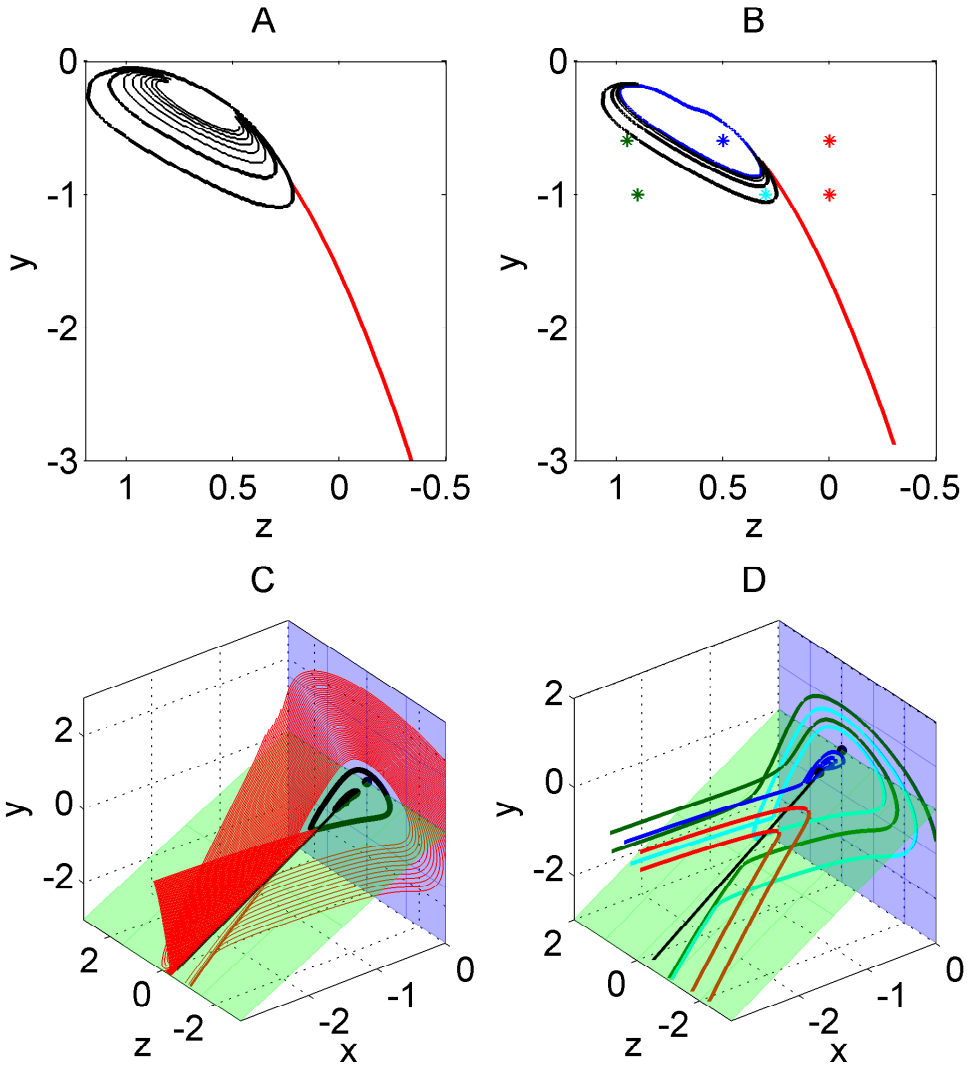

Figure 3.10: Divergence of solutions for $(a, b, c, \epsilon) = (3, -3.1, 1, 0.1)$ when (A) $\lambda = -0.005$ and $(B\text{-}D)$ $\lambda = -0.033$. (A,B) Solution behavior determined by its intersection with the plane $x = -3$. The red curve divides the solutions into those that undergo at least one rotation around p_D (more positive values of z) and those that do not (more negative values of z). Black curves define the boundaries of the sectors of rotation. In (B) solutions within the blue curve converge to a stable object in a neighborhood of p_D. Colored star points correspond to trajectories in (D). (C) Trajectories (red) that intersect the weak unstable manifold (black line) of p_D in system (3.9). These trajectories split solutions to system (3.4) into those that undergo at least one rotation about p_D and those that do not. These trajectories define the red curve in (B). (D) Examples of solutions to system (3.4) that undergo one rotation (dark green), two rotations (cyan), no rotations (red), or converge to a stable object in the neighborhood of p_D (blue).

in 3.3 *F*.

First, consider the region in 3.3 *F* where $\lambda < 0$ and the foliations of the fast flow. For small values of λ, the attracting manifold of the weak unstable manifold of p_D defines the boundary between trajectories of the fast foliations that do and do not make at least one rotation around p_D. As seen in figure 3.10 *A*, solutions that undergo at least one rotation are further subdivided by sectors of rotation that define the number of times they rotate around p_D. Note that for small values of λ, all solutions eventually escape to $x = -\infty$. As λ decreases, p_D undergoes Hopf bifurcations and attracting invariant sets emerge. These sets are bounded by the saddle-type periodic orbit that emerged from the subcritical Hopf bifurcation. As shown in figure 3.10 *B* and *D*, the emergence of the attracting invariant sets results in some trajectories becoming trapped within a neighborhood of p_D and not escaping to $x = -\infty$. For those solutions that do escape to $x = -\infty$, solutions that intersect the weak unstable manifold of p_D in the slow flow (3.9) divide the solutions that undergo at least one rotation and those that do not. Note that unlike in the cases were periodic orbits do not exist, these solutions are not contained in an attracting or repelling manifold.

Now we focus on the unstable manifold of the equilibrium after the supercritical Hopf bifurcation. For values of λ close to the bifurcation value, the unstable manifold of p_D and the 2-dimensional stable manifold of the stable periodic orbit are the same (figure 3.6 *B*). As λ becomes more negative, the stable periodic orbit grows and enters a 2ϵ-neighborhood of the intersection curve (figure 3.6 *C*). Upon entry of this neighborhood, the unstable manifold of p_D begins to fold over on itself, eventually yielding the quadratic map shown in figure 3.7.

There are two points to make about dynamics that occur in this region of

parameter space. First, due to the proximity of the equilibrium point to the intersection curve, a separation of time scales does not exist near the equilibrium point. In the slow flow, p_D is a node source, yet in the full three dimensional model, p_D is a node sink. Thus, unlike the examples in figure 3.9, solutions do not behave as one would expect from the singular limits of system (3.4). Only for λ large enough do solutions begin to escape to $x = -\infty$ and the dynamics begin to resemble the fast-slow structure (figure 3.7 *F*). Hence, the chaotic dynamics define the boundary between where the slow-fast structure of system (3.4) is retained near the equilibrium and where it no longer persists.

The second point to emphasize about the behavior in this region of parameter space is that the chaotic dynamics only arise after the stable periodic orbit enters an $O(\epsilon)$-neighborhood of the equilibrium point. Since a separation of time scales does not exist in this region of state space, one must do a full analysis of the three-dimensional system in order to understand the behavior of the system. This point also applies to the dynamics that occur for smaller values of λ, before the birth of the chaotic set. For example, for parameters near the supercritical Hopf bifurcation, the unstable manifold of the periodic orbit that emerges from the subcritical Hopf bifurcation is exactly half of the stable manifold of the stable periodic orbit (figure 3.7 *A*). For regions of parameter space farther away, a break is observed in the induced return map (figure 3.7 *B*) and it is unclear if this equivalence holds.

For the second region of parameter space where periodic orbits are observed ($\lambda > 0$ in figure 3.3 *A*), we will consider the behavior of the system in reverse time. When no periodic orbits exist, all solutions tend to the equilibrium point. Otherwise, all solutions either converge to a limit cycle or the equilibrium. De-

spite the proximity of the invariant sets to the intersection curve, the behavior in this region of parameter space is well behaved in the sense that stable and unstable manifolds of the equilibrium and periodic orbits behave as one would expect in a two-dimensional system. It is expected that this is partially due the stability of the equilibrium being the same in the full system (3.4) and in the slow flow (3.9). In both systems, the equilibrium has one real negative eigenvalue and a pair of complex eigenvalues with negative real part. Note again though that the dynamics in this region of parameter space cannot be inferred from the singular limits of system (3.4) due to proximity of the invariant sets to the intersection curve.

The last region of parameter space where periodic orbits are observed is found in figure 3.3 F where $\lambda > 0$. As in the first case of this section, one can determine the behavior of trajectories approaching the critical manifolds by looking at the attracting manifold of the stable manifold of p_D and by determining which solutions interact with the invariant sets. Since p_D is a saddle equilibrium in the full system and its unstable direction aligns with the unstable direction defined by the slow flow, most solutions approaching the critical manifolds escape to $x = -\infty$. The behavior of solutions that do not escape to infinity resembles the behavior of solutions in the vicinity of Shil'nikov homoclinic orbits. For example, the periodic orbits in figure 3.8 resemble what one would expect when a Shil'nikov snake arises from a saddle-focus homoclinic orbit [Kuznetsov, 2000]. While a Shil'nikov homoclinic structure cannot be the underling mechanism, because the equilibrium p_V lies in an invariant plane and homoclinic orbits of that type are impossible, the actual mechanism may be closely related to it.

3.7 Discussion

This study presents the dynamics that occur in the vicinity of the transversal intersection of the critical manifold in a class of biologically motivated 1-fast, 2-slow dynamical systems. Our analysis shows that complex dynamics occur in parameter space $O(\epsilon)$-close to Hopf bifurcations of the system. In addition, while some of the dynamics near the transversal intersection can be inferred from the fast and slow subsystems, most of the complex behavior exhibited by system (3.4) is not predicted by the singular limits. This lack of predictive power is a consequence of the dynamics occurring in an $O(\epsilon)$-neighborhood of the intersection curve.

This study was motivated by a class of fast-slow biological models where two critical manifolds transversally intersect along a curve and one of the manifolds is generically invariant in the full system. Previous studies of such ecological and evolutionary models have explored and documented parameter regimes where complex dynamics like chaos and mixed mode-oscillations can be found (e.g., Muratori and Rinaldi 1992, Lenbury and Likasiri 1994, Deng and Hines 2003, Ginoux et al. 2005). In all cases, solutions only remain in the vicinity of the intersection curve for brief periods of time and have the canard-like behavior seen in figure 3.2. In addition, if equilibria are involved in the dynamics (e.g. homoclinic orbits, Feo and Rinaldi 1998), the equilibria exist far away from the intersection curve. Thus, the dynamics in previous studies arise from global phenomena where solutions pass by the intersection curve as part of global return.

We have shown that chaotic dynamics also occur in the vicinity of the in-

tersection curve and these dynamics arise from local bifurcations and phenomena. Numerical continuation calculations presented here show that one chaotic regime arises as a consequence of the secondary bifurcations of periodic orbits (figure 3.3 F where $\lambda > 0$). Another chaotic regime is observed in regions of parameter space where invariant manifolds of periodic orbits enter an $O(\epsilon)$-neighborhood of the intersection curve (figure 3.6). In phase space, all of these dynamics occur $O(\epsilon)$-close to Hopf bifurcations of the equilibrium p_D. Thus, both the Hopf bifurcations and the more complicated bifurcations leading to chaotic dynamics occur when particular invariant sets and manifolds are $O(\epsilon)$-close to the intersection curve.

The proximity of the invariant sets and manifolds to the intersection curve have important consequences for how one must study the dynamics of a system with a transversal intersection of the critical manifold. For a typical fast-slow system, the behavior of solutions in the singular limits is studied so to gain insight into the dynamics that occur in the full system when ϵ is small. While the slow flows do yield insight into the behavior of solutions that pass through the vicinity of the intersection curve (figure 3.2), the singular limits fail to capture any of the complex behavior that occurs in parameter space $O(\epsilon)$-close to Hopf bifurcations of p_D. Even the Hopf bifurcations of p_D are not captured in the singular limit. Because all of these bifurcations occur when the equilibria or periodic orbits are within an $O(\epsilon)$-neighborhood of the intersection curve, the fast-slow structure is lost and one must analyze the full three dimensional model in order to completely understand the behavior of solutions in the vicinity of the intersection curve.

APPENDIX A

APPENDIX OF CHAPTER 1

A.1 Equivalence of Predator and Prey Evolution

Here we prove that a predator-prey model with predator evolution can be transformed into a model with prey evolution by a reversal in time. The general predator-prey model with predator evolution is

$$\begin{aligned} \frac{dx}{dt} &= F(x) - G(x,y,\beta) \\ \frac{dy}{dt} &= H(x,y,\beta) - D(y,\beta) \\ \epsilon\frac{d\beta}{dt} &= B(\beta)Vy^{-1}[H_\beta(x,y,\beta) - D_\beta(y,\beta)]. \end{aligned} \tag{A.1.1}$$

Reversing time, using the substitution $\tau = -t$, yields

$$\begin{aligned} \frac{dx}{d\tau} &= -F(x) + G(x,y,\beta) \\ \frac{dy}{d\tau} &= -H(x,y,\beta) + D(y,\beta) \\ \epsilon\frac{d\beta}{d\tau} &= B(\beta)Vy^{-1}\frac{\partial}{\partial\beta}(-H(x,y,\beta) + D(y,\beta)). \end{aligned} \tag{A.1.2}$$

After the following substitutions,

$$\begin{aligned} &\bar{y} = x \quad \bar{x} = y \quad \alpha = \beta \\ &\bar{F} = D \quad \bar{G} = H \quad \bar{H} = G \\ &\bar{D} = F \quad A = B \end{aligned}$$

system (A.1.2) becomes

$$\begin{aligned} \frac{d\bar{x}}{d\tau} &= \bar{F}(\bar{x},\alpha) - \bar{G}(\bar{x},\bar{y},\alpha) \\ \frac{d\bar{y}}{d\tau} &= \bar{H}(\bar{x},\bar{y},\alpha) - \bar{D}(\bar{y}) \\ \epsilon\frac{d\alpha}{d\tau} &= A(\alpha)V\bar{x}^{-1}\frac{\partial}{\partial\alpha}(\bar{F}(\bar{x},\alpha) - \bar{G}(\bar{x},\bar{y},\alpha)) \end{aligned} \tag{A.1.3}$$

which is a predator-prey system with prey evolution.

Two points should be noted here. First, the time reversing transformation switches the stability of all invariant sets. That is, stable (unstable) objects, like equilibrium points, in system (A.1.1) become unstable (stable) objects in system (A.1.3). Second, the existence of a transformation between systems (A.1.1) and (A.1.3) does not imply that all dynamics observed in the prey evolution model can be observed in the predator evolution model. D is assumed to be an increasing function of y and β while F is only assumed to be an increasing function of α. Since D and F swap roles after the transformation, in order for the systems to be equivalent F would have be assumed to be increasing in x. Such an assumption does not hold when the prey are assumed to have a logistic growth function or when an Allee effect is present. Consequently, most results for the predator evolution case will hold in the prey evolution case with a change in notation. The opposite will not always be the case.

A.2 Fast-Slow Systems

When $\epsilon \ll 1$ (ϵ is positive and much smaller than one), system (1.3) is a fast-slow dynamical system. The trait is the fast variable and the populations are the slow variables. In the following we will consider two related dynamical systems where we have set $\epsilon = 0$: one describing the slow dynamics of system (1.3) (the slow flow) and another describing the fast dynamics of system (1.3) (the fast flow). These two systems are known as singular limits of the dynamics system. The dynamics exhibited by these singular limits tell us about the dynamics of the full system (1.3) when $\epsilon \ll 1$.

Setting $\epsilon = 0$ in system (1.3) yields the slow flow:

$$\begin{aligned} \frac{dx}{dt} &= F(x) - G(x, y, \beta) \\ \frac{dy}{dt} &= H(x, y, \beta) - D(y, \beta) \\ 0 &= B(\beta) V y^{-1} [H_\beta(x, y, \beta) - D_\beta(y, \beta)]. \end{aligned} \tag{A.2.1}$$

system (A.2.1) is a differential algebraic equation - a differential equation (first two equations) with an algebraic constraint (third equation). It describes the population and trait dynamics of system (1.3) when the state variables are constrained by the algebraic equation of system (A.2.1). In this limit, the trait dynamics respond instantaneously to the dynamics of the population variables.

To derive the fast flow we rewrite our system in terms of the fast time scale, $\tau = t/\epsilon$.

$$\begin{aligned} \frac{dx}{d\tau} &= \epsilon(F(x) - G(x, y, \beta)) \\ \frac{dy}{d\tau} &= \epsilon(H(x, y, \beta) - D(y, \beta)) \\ \frac{d\beta}{d\tau} &= B(\beta) V y^{-1} [H_\beta(x, y, \beta) - D_\beta(y, \beta)]. \end{aligned} \tag{A.2.2}$$

Setting $\epsilon = 0$ yields the fast flow

$$\begin{aligned} \frac{dx}{d\tau} &= \frac{dy}{d\tau} = 0 \\ \frac{d\beta}{d\tau} &= B(\beta) V y^{-1} [H_\beta(x, y, \beta) - D_\beta(y, \beta)]. \end{aligned} \tag{A.2.3}$$

system (A.2.3) describes the dynamics of the trait when the populations are held constant.

The set of equilibrium points of the fast flow when $\epsilon = 0$ is called the critical manifold and given by the set of points

$$C = \left\{ (x, y, \beta) : \ B(\beta)[H_\beta(x, y, \beta) - D_\beta(y, \beta)] = 0, y > 0 \right\}. \tag{A.2.4}$$

This set has a left, a middle and right branch defined respectively as:

$$C_L = \{(x, y, \beta) : \ x > 0, y > 0, \beta = \beta_{min}\} \tag{A.2.5}$$

$$C_M = \left\{(x, y, \beta) : \ H_\beta(x, y, \beta) - D_\beta(y, \beta) = 0, y > 0, \beta \in (\beta_{min}, \beta_{max})\right\} \tag{A.2.6}$$

$$C_R = \{(x, y, \beta) : \ x > 0, y > 0, \beta = \beta_{max}\} \tag{A.2.7}$$

Notice that any equilibrium point of the full system (1.3) must be a point in the critical manifold. Also notice that the critical manifold is the set of points to which the slow flow (A.2.1) is constrained by its algebraic equation.

As explained in the main text, the dynamics of system (1.3) can be understood by knowing what solutions do near the critical manifold, where they jump away from it, and where they land near it. The slow flow describes how solutions move on the critical manifold, which in turn tells us how solutions near the critical manifold behave. The fast flow allows us to understand where a solution will jump away from the critical manifold and where it will approximately land.

Consider a point ρ on the critical manifold, C. If ρ is a landing point, then ρ is a stable equilibrium point of the fast flow (A.2.3). If ρ is a jumping point, then ρ is an unstable equilibrium point of the fast flow. The stability of ρ can be determined by computing the eigenvalues of the Jacobian at each point. We are guaranteed that two of the eigenvalues will be zero (because the population dynamics are constant), the third eigenvalue is

$$B_\beta(\rho)[H_\beta(\rho) - D_\beta(\rho)] + B(\rho)[H_{\beta\beta}(\rho) - D_{\beta\beta}(\rho)]. \tag{A.2.8}$$

Negative values tell us that ρ is attracting (stable) in the fast flow and positive values tell us that ρ is repelling (unstable) in the fast flow. For a point ρ on C_M, ρ is stable when equation (1.9) is satisfied and unstable when (1.10) is satisfied.

Similarly, a point ρ on C_L or C_R is attracting when equation (1.11) is satisfied and repelling when (1.12) is satisfied. Note that due to the function $B(\beta)$, a trajectory running away from a repelling part of the critical manifold will eventually approach an attracting part of the critical manifold. Thus a solution that jumps away from C must land on it somewhere else.

In addition to the dynamics presented in the main text, other phenomena are observed in fast-slow dynamics system. We briefly point out when such cases can arise. Points on C satisfying one of the inequalities in equations (1.9) through (1.12) are said to be normally hyperbolic. Where the critical manifold is normally hyperbolic, we can use Fenichel theory [Arnold et al., 1995] to piece together what the dynamics of the full system (1.3) look like from the information contained in the fast and slow flows. Points where none of the inequalities hold are non-normally hyperbolic points. Two classes of non-normally hyperbolic points arise in our model and each allows for a broad spectra of phenomena.

The first class of non-normally hyperbolic points that can arise in our system satisfies $H_{\beta\beta}(\rho) - D_{\beta\beta}(\rho) = 0$. These points are known as folds in the fast-slow systems literature and yield phenomena like canards and mixed mode oscillations. An example of such a point is the apex of the prey nullcline in figure 1.2. The other class of non-normally hyperbolic points in our system arises when two branches of the critical manifold intersect non-tangentially. These points lie on C_L and C_R, satisfy $H_\beta(\rho) - D_\beta(\rho) = 0$, and are the result of the transverse intersections of C_M with C_L or C_R. An example is the intersection of the prey nullcline with the predator axis in figure 1.2. When the trait is repelling, these points also allow for the existence of canard-like trajectories and relaxation oscillations. For example, the trajectory in figure 1.2 B does not jump away from the repelling

region of C_L right away and instead follows the flow on the repelling branch for some time. The distance a particular trajectory will follow the repelling branch can be determined using variational equations or Pontryagin's delay of lost stability (for particular examples Schecter 1985, Deng 2001, Boudjellaba and Sari 2009). A detailed analysis of all possible dynamics that can occur in the vicinity of such points is not currently available in the literature, but it is the focus of current and future studies (M. H. Cortez and J. Guckenheimer, unpublished manuscript).

In the main text we focus on systems where either equation (1.9) or equation (1.10) is always satisfied for all points on C_M. This case prevents fold points from arising. Since C_M intersects C_L and C_R transversally in our system (the intersection of the green plane with the blue and gray planes in figure 1.3), the second class of non-normally hyperbolic points will always be present. In the main text we will only consider systems where equilibria are far from the intersections of two branches of the critical manifold. It is possible to construct systems where these conditions do not hold, but the dynamics that arise near the intersection curves are beyond the scope of this study.

A.3 Local Stability Analysis

Here we show how adding evolution to a non-evolving ecological system changes the stability of the ecological dynamics. In particular, we focus on cases where adding evolution induces cycling in an ecological system at equilibrium or causes a cycling ecological system to to go equilibrium. To do this we compare the equilibria of the evolving system and the evolutionarily fixed

system. In the following, we limit our focus to equilibria on C_M that satisfy equation (1.9). Equilibria that don't satisfy equation (1.9) behave like saddles or sources in the full system and do not offer much insight into the effects of evolution on the local stability of the population dynamics. Also, equilibria on C_L or C_R do not change stability when evolution is added to the system because on those planes β is held constant at either β_{min} or β_{max}.

Let $p = (\bar{x}, \bar{y}, \bar{\beta})$ be an equilibrium point of model (1.3). Consider the associated equilibrium point, $q = (\bar{x}, \bar{y})$, of the non-evolving system

$$\begin{aligned} \frac{dx}{dt} &= F(x) - G(x, y, \bar{\beta}) \\ \frac{dy}{dt} &= H(x, y, \bar{\beta}) - D(y, \bar{\beta}) \end{aligned} \tag{A.3.1}$$

where β is a parameter fixed at the value $\bar{\beta}$. system (A.3.1) represents the population dynamics of the full system (1.3) where the predator trait value has been fixed at the equilibrium trait value $\bar{\beta}$. Since system (A.3.1) is a planar vector field, the stability of the equilibrium point q is completely determined by the trace and the determinant of the Jacobian matrix at the equilibrium, respectively $\text{tr}(J_{NE}|_q)$ and $\det(J_{NE}|_q)$. If q is stable, then $\det(J_{NE}|_q) > 0$ and $\text{tr}(J_{NE}|_q) < 0$. If either inequality is reversed then q will be unstable.

We are interested in how the stability of the coexistence equilibrium q changes as a consequence of adding predator evolution. Recall (see appendix A.2) that an equilibrium point of system (1.3) must be a point on the critical manifold and that for small ϵ the dynamics of the full model behave locally like the dynamics on the critical manifold. Thus, to understand the stability of a coexistence equilibrium point of the full system (1.3), we look at the stability of the same equilibrium point when the dynamics are constrained to the critical manifold. Using the trace and determinant of systems (1.3) and

(A.3.1) evaluated at their respective equilibrium, we can express the stability of the equilibrium, p, of the full system in terms of the equilibrium, q, of the non-evolving system (A.3.1). This will give us an equation that describes the stability of evolving system in terms of the stability of the evolutionarily fixed system plus a perturbation. If the perturbation is stabilizing then evolution stabilizes the population dynamics and if the perturbation is destabilizing then evolution destabilizes the population dynamics. We emphasize here that the mathematical theory we are using only holds when $\epsilon << 1$, but the results may hold when ϵ is larger.

In the following, we will only consider equilibria that have positive determinants for both the Jacobian of system (A.3.1) and the Jacobian of system (1.3) restricted to the critical manifold. Situations where the determinant changes sign can lead to evolutionarily driven extinction, a topic that has been discussed elsewhere in the literature [Parvinen, 2005, Webb, 2003].

There are two cases to consider when comparing the local stability of equilibria of systems (A.3.1) and (1.3). If the predator per capita consumption and death rates depend linearly on the same function of y, $H(x,y,\beta) = d(y)h(x,\beta)$ and $D(y,\beta) = d(y)\delta(\beta)$, then the critical manifold will be constant with respect to y. That is, a point (x,y,β) is on the critical manifold if and only if $(x,\bar{y},\beta)$ is on the manifold for all positive $\bar{y}$. An example of such a case is the Rosenzweig-MacArthur model [Rosenzweig and MacArthur, 1963] where $d(y) = y$. If the predator functional responses do not have the same linear dependence on a function of y or have nonlinear dependences on y then the critical manifold will vary with y. In the following, we present the relationships between the trace and determinant of the Jacobian for system (A.3.1) and the Jacobian for system (1.3)

restricted to C_M for both cases.

Before stating the theorems we make a note about the notation used throughout the proofs. Let $G(x, y, z)$ be a function where y and z could be functions of x. We write $\partial G/\partial x$ to denote the partial derivative of G with respect to x. We contrast this with the notation G_x, where we are denoting the partial derivative of G with respect to its first argument. The following illustrates the difference,

$$\frac{\partial G}{\partial x} = G_x + G_y \frac{\partial y}{\partial x} + G_z \frac{\partial z}{\partial x}.$$

Often the arguments of G will be independent of each other and the notations will imply the same result, i.e. $\partial G/\partial x = G_x$. When this is not the case, we will stick to the above convention.

THEOREM A.1. *Assume C_M, defined by equation (A.2.6), depends only on x and β. That is, C_M is constant with respect to y. Let $p = (\bar{x}, \bar{y}, \bar{\beta})$ be a coexistence equilibrium point of system (1.3) on C_M and assume equation (1.9) is satisfied at p. Let $q = (\bar{x}, \bar{y})$ be the associated equilibrium point of the non-evolving system (A.3.1). Let $J|_p$ denote the Jacobian for system (1.3) restricted to C_M, evaluated at p and $J_{NE}|_q$ denote the Jacobian for system (A.3.1) evaluated at q. Then the following relations hold between the trace and determinant of $J|_p$ and $J_{NE}|_q$:*

$$\det(J|_p) = \det(J_{NE}|_q) + \left. \frac{H_{\beta x}}{H_{\beta\beta} - D_{\beta\beta}} [G_\beta (H_y - D_y) - G_y H_\beta] \right|_p$$

$$\operatorname{tr}(J|_p) = \operatorname{tr}(J_{NE}|_q) + \left. G_\beta \frac{H_{\beta x}}{H_{\beta\beta} - D_{\beta\beta}} \right|_p$$

Proof. Because equation (1.9) is satisfied at p, the implicit function theorem allows us to write β locally as a function of x, $\beta(x)$. For notational ease in the following, we will not explicitly denote this dependence of β on x.

For system (1.3) constrained to the critical manifold, the Jacobian evaluated at p is

$$J|_p = \begin{pmatrix} F_x - \frac{\partial}{\partial x}G & -\frac{\partial}{\partial y}G \\ \frac{\partial}{\partial x}H & \frac{\partial}{\partial y}H - \frac{\partial}{\partial y}D \end{pmatrix}_{|_p} \tag{A.3.2}$$

By the chain rule, we have that

$$\frac{\partial}{\partial x}G = G_x + G_\beta \frac{\partial \beta}{\partial x}$$
$$\frac{\partial}{\partial x}H = H_x + H_\beta \frac{\partial \beta}{\partial x}.$$

Using equation (1.9) for C_M, we compute the derivatives of α with respect to x on C_M to be

$$\frac{\partial \beta}{\partial x} = -\frac{H_{x\beta}}{H_{\beta\beta} - D_{\beta\beta}} \tag{A.3.3}$$

For the equilibrium point q of the evolutionary fixed system (A.3.1) we have

$$\begin{aligned} \det(J_{NE}|_q) &= [F_x(\bar{x}) - G_y(\bar{x},\bar{y},\bar{\beta})][H_y(\bar{x},\bar{y},\bar{\beta}) - D_y(\bar{y},\bar{\beta})] \\ &\quad + G_y(\bar{x},\bar{y},\bar{\beta})H_x(\bar{x},\bar{y},\bar{\beta}) \\ &= (F_x - G_x)(H_y - D_y) + G_y H_x\Big|_p \end{aligned} \tag{A.3.4}$$

$$\begin{aligned} \operatorname{tr}(J_{NE}|_q) &= F_x(\bar{x}) - G_x(\bar{x},\bar{y},\bar{\beta}) + H_y(\bar{x},\bar{y},\bar{\beta}) - D_y(\bar{y},\bar{\beta}) \\ &= F_x - G_y + H_y - D_y\Big|_p . \end{aligned} \tag{A.3.5}$$

Evaluating the trace and determinant of $J|_p$ and substituting in equations (A.3.3) through (A.3.5) yields the result. □

THEOREM A.2. *Assume C_M, defined by equation (A.2.6), depends on x, y and β. Let $p = (\bar{x},\bar{y},\bar{\beta})$ be a coexistence equilibrium point of system (1.3) on C_M and assume equation (1.9) is satisfied at p. Let $q = (\bar{x},\bar{y})$ be the associated equilibrium point of the non-evolving system (A.3.1). Let $J|_p$ denote the Jacobian for system (1.3) restricted to C_M, evaluated at p and $J_{NE}|_q$ denote the Jacobian for system (A.3.1) evaluated at q. Then*

the following relations hold between the trace and determinant of $J|_p$ and $J_{NE}|_q$:

$$\det(J|_p) = \det(J_{NE}|_q) - \frac{G_\beta}{H_{\beta\beta} - D_{\beta\beta}} \begin{vmatrix} \frac{\partial \dot{y}}{\partial x} & \frac{\partial \dot{y}}{\partial y} \\ \frac{\partial \dot{\beta}}{\partial x} & \frac{\partial \dot{\beta}}{\partial y} \end{vmatrix}_{|_p}$$

$$\operatorname{tr}(J|_p) = \operatorname{tr}(J_{NE}|_q) + G_\beta \frac{H_{x\beta}}{H_{\beta\beta} - D_{\beta\beta}}\Big|_p$$

Proof. As in the proof of theorem 1, by the implicit function theorem, we can write β locally as a function of x and y, $\beta(x, y)$. Using equation (A.2.6) for C_M, we compute the derivatives of β with respect x and y on C_M to be

$$\frac{\partial \beta}{\partial x} = -\frac{H_{x\beta}}{H_{\beta\beta} - D_{\beta\beta}} \tag{A.3.6}$$

$$\frac{\partial \beta}{\partial y} = -\frac{H_{y\beta} - D_{y\beta}}{H_{\beta\beta} - D_{\beta\beta}} \tag{A.3.7}$$

The trace and determinant of J_{NE} are given in equations (A.3.4) and (A.3.5) in the proof of theorem A.1. Evaluating the trace and determinant of $J|_p$ and applying the chain rule as in the proof of theorem A.1 yields the result. □

A.4 Trade-Off Curves

In this section we will work with system (1.3) under the assumption that the functions H and D factor into two components, one that is a function of x and y, and another that is just a function of β. Our system then looks like

$$\begin{aligned} \frac{dx}{dt} &= F(x) - G(x, y, \beta) \\ \frac{dy}{dt} &= h(x, y)\eta(\beta) - d(y)\delta(\beta) \\ \epsilon\frac{d\beta}{dt} &= B(\beta)Vy^{-1}[h(x, y)\eta_\beta(\beta) - d(y)\delta_\beta(\beta)]. \end{aligned} \tag{A.4.1}$$

Our trade-off curve is given by $\delta(\eta)$. With an abuse in notation, this is $\delta(\eta) = \delta(\beta^{-1}(\eta))$, where $\beta^{-1}(\eta)$ is the inverse function of $\eta(\beta)$. Note that H and D are assumed to be strictly increasing functions of β. Thus, δ and η are also increasing functions of β, and β^{-1} is well defined. Since compositions of increasing functions are also increasing functions, $\delta(\eta)$ is an increasing function η. Throughout this section $\delta(\beta)$ will define the piece of the functional response D and $\delta(\eta)$ will denote the trade-off curve.

Recall (after substitution) that the trait dynamics are stable at a point (x, y, β) on C_M if

$$h(x, y)\eta_{\beta\beta}(\alpha) - d(y)\delta_{\beta\beta}(\beta) < 0$$

and unstable if

$$h(x, y)\eta_{\beta\beta}(\beta) - d(y)\delta_{\beta\beta}(\beta) > 0.$$

In the following two theorems we relate the stability of the trait dynamics on C_M to the curvature of the trade-off curve, $\delta(\eta)$.

THEOREM A.3. *Let $\rho = (x, y, \beta)$ be a point on C_M. The trade-off curve, $\delta(\eta)$, is concave up if and only if trait dynamics are stable at ρ. That is, $\delta_{\eta\eta}(\eta) > 0$ if and only if $h(x, y)\eta_{\beta\beta}(\beta) - d(y)\delta_{\beta\beta}(\beta) < 0$.*

Proof. Let $\rho = (x, y, \beta) \in C_M$. We first derive some useful equalities. By the chain rule we compute $\delta_\beta(\beta) = \frac{\partial}{\partial\beta}\delta(\eta) = \delta_\eta(\eta)\eta_\beta(\beta)$ or after rearrangement

$$\delta_\eta(\eta) = \delta_\beta(\beta)/\eta_\beta(\beta). \tag{A.4.2}$$

Since $\rho \in C_M$ and satisfies $h(x, y)\eta_\beta(\beta) - d(y)\delta_\beta(\beta) = 0$, using equation (A.4.2) we have that

$$\delta_\eta(\eta) = \frac{\delta_\beta(\beta)}{\eta_\beta(\beta)} = \frac{h(x, y)}{d(y)}. \tag{A.4.3}$$

Finally, using the chain rule twice we have $\delta_{\beta\beta}(\beta) = \frac{\partial^2 \delta(\eta)}{\partial \beta^2} = \delta_{\eta\eta}(\eta)(\eta_\beta(\beta))^2 + \delta_\eta(\eta)\eta_{\beta\beta}(\beta)$, which after rearrangement yields

$$\delta_{\eta\eta}(\eta) = \frac{\delta_{\beta\beta}(\beta) - \delta_\eta(\eta)\eta_{\beta\beta}(\beta)}{(\eta_\beta)^2}. \tag{A.4.4}$$

To prove our result, observe that by equation (A.4.4), $\delta_{\eta\eta}(\eta) > 0$ if and only if $\delta_{\beta\beta}(\beta) - \delta_\eta(\eta)\eta_{\beta\beta} > 0$. By equation (A.4.3) this holds if and only if $\delta_{\beta\beta}(\beta) - \frac{h(x,y)}{d(y)}\eta_{\beta\beta}(\beta) > 0$. Since $d(y) > 0$ is assumed, the desired result is obtained after rearrangement. □

THEOREM A.4. *Let $\rho = (x, y, \beta)$ be a point on C_M. The trade-off curve, $\delta(\eta)$, is concave down if and only if trait dynamics are unstable at ρ. That is, $\delta_{\eta\eta}(\eta(\beta)) = \delta_{\eta\eta}(\eta) < 0$ if and only if $h(x, y)\eta_{\beta\beta}(\beta) - d(y)\delta_{\beta\beta}(\beta) > 0$.*

Proof. Let $\rho = (x, y, \beta) \in C_M$. By equation (A.4.4), $\delta_{\eta\eta}(\eta) < 0$ if and only if $\delta_{\beta\beta}(\beta) - \delta_\eta(\eta)\eta_{\beta\beta}(\beta) < 0$. Since ρ is a point on the critical manifold, this holds if and only if $\delta_{\beta\beta}(\beta) - \frac{h(x,y)}{d(y)}\eta_{\beta\beta}(\beta) < 0$ by equation (A.4.3). Since $d(y) > 0$ is assumed, the desired result is obtained after rearrangement. □

A.5 Boundary Plane Projections

In this section we prove results presented in Section 1.4.3 about repelling traits. We will use the following notation throughout this section. Primes will denote the derivative of a variable with respect to time, i.e. $y' = dy/dt$. $p_{min} = (x_{min}, y_{min}, \beta_{min})$ and $p_{max} = (x_{max}, y_{max}, \beta_{max})$ will denote the stable coexistence equilibria of the β_{min}- and β_{max}-planes, respectively. (p_{min} and p_{max} are the equilibria of system (A.3.1) with $\beta = \beta min$ or β_{max}.) The sets $\Phi_{min} = \{(x, \phi_{min}(x))\}$ and $\Phi_{max} =$

$\{(x, \phi_{max}(x))\}$ define the predator nullclines (where $y^{-1}y' = 0$) on the β_{min}- and β_{max}-planes, respectively. We assume that ϕ_{min} and ϕ_{max} are single-valued functions of x (but see theorem A.6). Finally, as a short hand notation, we will denote differences of functions like the following, $H(x, y, \beta) - D(y, \beta) = (H - D)(x, y, \beta)$.

The organization of this section follows. The first theorem defines a necessary condition for a repelling trait to yield oscillation in the trait. That is, if the condition is not met, then all solutions converge to states where evolution no longer occurs. The rest of the theorems are concerned with defining conditions under which the set ups in figures 1.6 *B*,1.6 *C*, and 1.6 *D* can or cannot occur. Most of the conditions are defined in terms of the shapes and intersections of the predator nullclines, ϕ_{min} and ϕ_{max}. theorem A.8 relates some of those conditions to systems with the factorization given in system (A.4.1). Finally, theorem A.12 proves that only the set up in figure 1.6 *D* can occur when one of two equilibria is an extinction equilibrium.

The first theorem proves that $H_{x\beta} < 0$ necessarily implies that evolution will cease in the system. We expect that for most biological systems, $H_{x\beta}$ will have a constant sign. Biologically this means that increased investment in the trait is always more or less rewarding (depending on the sign of $H_{x\beta}$) when prey density increases, regardless of how many prey there are. Because of this result, throughout this section we will assume $H_{x\beta} > 0$.

THEOREM A.5. *If $H_{x\beta} < 0$ then a repelling trait guarantees that any solution will converge to a non-evolving solution.*

Proof. Let $H_{x\beta} < 0$. Since H describes the growth of the predator due to consuming the prey, $H(0, y, \beta) = 0$ for all y and β. Thus, $H_\beta(0, y, \beta) = 0$ for all y and β. Since D is an increasing function of β and $D(0, y, \beta) \geq 0$, $(H_\beta - D_\beta)(0, y, \beta) \leq 0$ for any

$y, \beta \geq 0$. $H_{x\beta} \leq 0$ implies that $(H_\beta - D_\beta)(x, y, \beta) \leq 0$ for any $x \geq 0$. Thus β_{min}-plane is normally hyperbolic and attracting while the β_{max}-plane is normally hyperbolic and repelling. Any solution with an initial condition on the β_{max}-plane will stay there for all time, but any other solutions with generic initial conditions will converge to some solution set on the β_{min}-plane. □

Note that generic initial conditions in our system are any initial conditions that do not start on a limiting set that is already on the critical manifold. In particular, they do no include equilibria or periodic orbits on C_M (which in the above case would be repelling in the β-direction).

The next two theorems define two cases where having an equilibrium in each boundary plane results in every solution converging to an evolutionary fixed solution. That is, if the hypotheses of either theorem hold, then at least one equilibrium is a sink in three dimensions and relaxation oscillation are not possible. The first theorem deals with systems where the predator nullclines of the β_{min}- and β_{max}- planes are vertical lines in the x, y-plane (e.g. a Rosenzweig-MacArthur model with evolution). The second theorem deals with systems where the predator nullclines, ϕ_{min} and ϕ_{max}, do not cross in the x, y-plane. Note that for the relaxation oscillations in figures (1.6) B, C, and D to arise, we need $(H_\beta - D_\beta)(x_{min}, y_{min}, \beta) > 0$ and $(H_\beta - D_\beta)(x_{max}, y_{max}, \beta) < 0$ for all $\beta \in [\beta_{min}, \beta_{max}]$.

THEOREM A.6. *Assume that the predator nullclines of the β_{min}- and β_{max}-planes are the vertical lines $x = x_{min}$ and $x = x_{max}$, respectively. Assume that each boundary plane has one globally stable coexistence equilibrium, p_{min} and p_{max} respectively. Then one of the equilibria is a sink in three dimensions.*

Proof. If the predator nullclines of the two planes are vertical lines in the x, y-

plane, then the predator equation of system (1.3) must factor as $y'(x,y,\beta) = k(y)(h(x,\beta) - d(\beta))$. Consequently, the sign of $y^{-1}(H_\beta - D_\beta)$ does not depend on y as well. Note that the sign of $y^{-1}(H_\beta - D_\beta)$ determines if a point on the β_{min}- or β_{max}-plane is repelling.

We will prove the theorem by considering two cases. In the first case assume $x_{min} < x_{max}$ and that p_{min} and p_{max} are repelling. Since $H_{x\beta} > 0$ and D does not depend on x, for $x_1 < x_2$ and any y and β, $(H_\beta - D_\beta)(x_1,y,\beta) < (H_\beta - D_\beta)(x_2,y,\beta)$. By definition, p_{max} being repelling implies that $(H_\beta - D_\beta)(p_{max}) < 0$. Since $x_{min} < x_{max}$, $(H_\beta - D_\beta)(p_{max}) < 0$ tells us $(H_\beta - D_\beta)(x_{min}, y_{max}, \beta_{max}) < 0$. This yields $(H_\beta - D_\beta)(x_{min}, y_{max}, \beta_{min}) < 0$ because the trait is repelling. Since the sign of $y^{-1}(H_\beta - D_\beta)$ does not depend on the value of y, $(H_\beta - D_\beta)(x_{min}, y_{max}, \beta_{min}) < 0$ implies that $y^{-1}(H_\beta - D_\beta)(p_{min}) < 0$. This means p_{min} is not repelling and we have reached a contradiction.

Now assume $x_{min} > x_{max}$. Then $y'(x_{min}, y_{max}, \beta_{min}) = 0$ implies that $y'(x_{max}, y_{max}, \beta_{min}) < 0$. In order to get $y'(x_{max}, y_{max}, \beta_{max}) = 0$ we must have some β^* such that $y'(x_{max}, y_{max}, \beta^*) > 0$. Since the trait is repelling, $y'(x_{max}, y_{max}, \beta^*) > 0$ implies that $y'(x_{max}, y_{max}, \beta) > 0$ for all $\beta > \beta^*$. Hence the β_{max} equilibrium is a sink in three dimensions. □

THEOREM A.7. *Assume for all $x \neq 0$ that $\phi_{min}(x) \neq \phi_{max}(x)$. Assume that each boundary plane has one globally (in the plane) stable coexistence equilibrium. Then one of the equilibria is a sink in three dimensions.*

Proof. Assume $\phi_{min}(x) > \phi_{max}(x)$ for all x. Choose an x^* such that $x^* > x_{min}$ and $y_{min} > \phi_{max}(x^*)$. Note that such an x^* must always exist since $\phi_{min}(x) > \phi_{max}(x)$ for all x. Since H is an increasing function of x, D does not depend on x, and $x_{min} < x^*$, we have that $0 = y'(x_{min}, y_{max}, \beta_{min}) < y'(x^*, y_{min}, \beta_{min})$. By construction the

point (x^*, y_{min}) is above the predator nullcline $\phi_{max}(x)$. Thus, $y'(x^*, y_{min}, \beta_{max}) < 0$. To have both $0 < y'(x^*, y_{min}, \beta_{min})$ and $0 = y'(x^*, y_{min}, \beta_{max})$ hold, there must exist some value $\bar{\beta} \in [\beta_{min}, \beta_{max}]$ such that $(H_\beta - D_\beta)(x^*, y_{min}, \bar{\beta}) < 0$. We know $D_{x\beta} = 0$ and from theorem A.5 we know that $H_{x\beta} > 0$. Thus, $(H_\beta - D_\beta)(x^*, y_{min}, \bar{\beta}) < 0$ and $x_{min} < x^*$ imply that $(H_\beta - D_\beta)(x_{min}, y_{min}, \bar{\beta}) < 0$. Since the trait is repelling and $\bar{\beta} \geq \beta_{min}$, we must have that $(H_\beta - D_\beta)(x_{min}, y_{min}, \beta_{min}) < 0$. Hence p_{min} is a sink in three dimensions.

For the second half of the proof we assume $\phi_{min}(x) < \phi_{max}(x)$ for all x. Choose an x^* such that $\phi_{min}(x^*) < y_{max}$ and $x^* > x_{max}$. Note that such an x^* always exists because $\phi_{min}(x) < \phi_{max}(x)$. By construction, (x^*, y_{max}) is above the β_{min}-plane predator nullcline, $\phi_{min}(x)$. Thus, $y'(x^*, y_{max}, \beta_{min}) < 0$. Since H is an increasing function of x, D does not depend on x, and $x^* > x_{max}$, we have that $0 > y'(x^*, y_{max}, \beta_{min}) > y'(x_{max}, y_{max}, \beta_{min})$. To have both $y'(p_{max}) = 0$ and $y'(x_{max}, y_{max}, \beta_{min}) < 0$, there must exist $\bar{\beta} \in [\beta_{min}, \beta_{max}]$ such that $(H_\beta - D_\beta)(x_{max}, y_{max}, \bar{\beta}) > 0$. Since the trait is repelling and $\beta_{max} > \bar{\beta}$, we must have that $(H_\beta - D_\beta)(x_{max}, y_{max}, \beta_{max}) > 0$. Hence, p_{max} is a sink in three dimensions. □

Theorem A.7 is of particular interest because the predator nullclines either do not cross or agree at every point when the functions H and D factor as in system (A.4.1). In either case, one of the equilibria must be a sink in three dimensions. That is, when the H and D factor, having an equilibrium in each boundary plane will not yield solutions where the trait oscillates. All solutions converge to the β_{min}- or β_{max}-plane.

THEOREM A.8. *Assume the predator response functions factor as* $H(x, y, \beta) = h(x, y)\eta(\beta)$ *and* $D(y, \beta) = d(y)\delta(\beta)$. *Assume that each boundary plane has one globally (in the plane) stable coexistence equilibrium. Then one of the equilibria is a sink in*

three dimensions.

Proof. When the functions H and D factor, the predator nullclines of the β_{min}- and β_{max}-planes can be equivalently defined as the set of points

$$\Phi_{min} = \left\{(x,y) : \frac{d(y)}{h(x,y)} = \frac{\eta(\beta_{min})}{\delta(\beta_{min})}\right\} \tag{A.5.1}$$

$$\Phi_{max} = \left\{(x,y) : \frac{d(y)}{h(x,y)} = \frac{\eta(\beta_{max})}{\delta(\beta_{max})}\right\}. \tag{A.5.2}$$

We define the sets of points where $H_\beta(x,y,\beta_{min}) - D_\beta(y,\beta_{min}) = 0$ as

$$\Psi_{min} = \left\{(x,y) : \frac{d(y)}{h(x,y)} = \frac{\eta'(\beta_{min})}{\delta'(\beta_{min})}\right\} = \{(x,\psi_{min}(x))\} \tag{A.5.3}$$

where the primes in η' and δ' denotes a derivative with respect to β. Similarly, the set of points where $H_\beta(x,y,\beta_{max}) - D_\beta(y,\beta_{max}) = 0$ is defined as

$$\Psi_{max} = \left\{(x,y) : \frac{d(y)}{h(x,y)} = \frac{\eta'(\beta_{max})}{\delta'(\beta_{max})}\right\} = \{(x,\psi_{max}(x))\}. \tag{A.5.4}$$

The following Lemma tells us that Φ_{min} and Φ_{max} either do not cross or they agree at every point. That is, the predator nullclines, ϕ_{min} and ϕ_{max}, either do not intersect or are the same.

LEMMA A.9. *Assume H and D factor as in the statement of the theorem. Given any two of the functions ϕ_{min}, ϕ_{max}, ψ_{min}, and ψ_{max}, the functions either do not cross at any point or agree at every point.*

Proof. As an example consider ϕ_{min} and ψ_{min}. Either $\eta(\beta_{min})/\delta(\beta_{min}) = \eta'(\beta_{min})/\delta'(\beta_{min})$ or $\eta(\beta_{min})/\delta(\beta_{min}) \neq \eta'(\beta_{min})/\delta'(\beta_{min})$. Thus, ϕ_{min} and ψ_{min} either do not cross or they agree at every point. The same argument holds for any other choice of functions. □

If the nullclines do not intersect, then theorem A.7 tells us that one equilibrium is a sink. Let us assume then that the two nullcline agree at every point. Since the trait is repelling and h is an increasing function of x, $\psi_{min}(x) < \psi_{max}$ for all nonzero values of x. In order for the β_{min}-plane equilibrium to be repelling we need $(h\eta' - d\delta')(p_{min}) > 0 = (h\eta - d\delta)(p_{min})$. Lemma A.9 tells us that this can only happen if $\phi_{min} < \psi_{min}$ for all x. Similarly, for the β_{max}-plane to be repelling we need $\phi_{max} > \phi_{max}$ for all x. Since $\psi_{min} < \psi_{max}$, these two conditions cannot be met at the same time. Hence, one of the equilibria must be attracting. □

Figure 1.6 *C* shows that predator evolution can yield cryptic dynamics where the prey population cycles but the predator population does not. The next theorem proves why predator evolution cannot yield the opposite case - cryptic dynamics where the predator oscillates and the prey does not.

THEOREM A.10. *Assume p_{min} is a stable equilibrium in the β_{min}-plane and repelling in the β-direction. Also assume p_{max} is a stable equilibrium in the β_{max}-plane and repelling in the β-direction. Then $x_{min} \neq x_{max}$.*

Proof. By way of contradiction, assume $x_{min} = x_{max}$. Let the sets $\Psi_{min} = \{(x, \psi_{min}(x))\}$ and $\Psi_{max} = \{(x, \psi_{max}(x))\}$ define the points where $(H_\beta - D_\beta)(y, \beta_{min}) = 0$ and $(H_\beta - D_\beta)(y, \beta_{max}) = 0$, respectively. Note that $H_{x\beta} > 0$ and $D_{x\beta} = 0$ implies that ψ_{min} and ψ_{max} are increasing functions of x.

By assumption,

$$H_\beta(x_{min}, y_{min}, \beta) - D_\beta(x_{min}, y_{min}, \beta) > 0 \tag{A.5.5}$$

$$H_\beta(x_{max}, y_{max}, \beta) - D_\beta(x_{max}, y_{max}, \beta) < 0 \tag{A.5.6}$$

for all $\beta \in [\beta_{min}, \beta_{max}]$. Since $(H - D)(x_{min}, y_{min}, \beta_{min}) = 0$ and ψ_{min} is an increasing function of x, equation (A.5.5) implies that (x_{min}, y_{min}) is above ψ_{min}. That

is, $\phi_{min}(x_{min}) < \psi_{min}(x_{min})$. Similarly, $(H - D)(x_{max}, y_{max}, \beta_{max}) = 0$ and equation (A.5.6) together imply that $\phi_{max}(x_{max}) > \psi_{max}(x_{max})$. Finally, since the trait is repelling, $\psi_{min}(x) < \psi_{max}(x)$ for all x. Combining these inequalities yields $\phi_{min}(x_{min}) < \psi_{min}(x_{min}) < \psi_{max}(x_{min}) < \phi_{max}(x_{min})$. Since $(H - D)(x_{max}, y_{max}, \beta_{max}) = 0$, equation (A.5.5) implies that $(H - D)(x_{max}, y_{max}, \beta_{min}) > 0$. For this to be the case, we would need $y_{max} < y_{min}$. This is equivalent to requiring $\phi_{max}(x_{min}) < \phi_{min}(x_{min})$, which contradicts $\phi_{min}(x_{min}) < \phi_{max}(x_{min})$ in the string of inequalities above. Hence, $x_{min} \neq x_{max}$ must be true. □

When each boundary plane has only a single coexistence equilibrium, if the prey does not interfere with the predator, then H will be an increasing function of x and only the set up in figure 1.6 *B* will be possible. The following theorem proves this result. This tells us that in order for predator evolution to yield oscillations given by figures 1.6 *B* and 1.6 *C*, the prey must interfere with the predator's ability to capture prey when the prey are at high densities.

THEOREM A.11. *Assume H is an increasing function of x. Assume that each boundary plane has one globally stable coexistence equilibrium, p_{min} and p_{max}, respectively. Then for the boundary equilibria p_{min} and p_{max}, either (1) $x_{min} < x_{max}$ and $y_{min} < y_{max}$ or (2) $x_{min} > x_{max}$ and $y_{min} > y_{max}$.*

Proof. Assume $x_{max} < x_{min}$. By theorem A.7 there must exist at least one value of x such that $\phi_{min}(x) = \phi_{max}(x)$. Furthermore, at least one of these values must fall between x_{max} and x_{min}. If not, then the argument presented in theorem A.10 can be extended to prove that one of the equilibria is not repelling in the β-direction. Let

$$\Omega = \{x : \phi_{min}(x) = \phi_{max}(x), x_{max} < x < x_{min}\} \tag{A.5.7}$$

denote the set of such values between x_{max} and x_{min}. Let ω_{min} and ω_{max} be the minimum and maximum values of Ω. Since H being an increasing function of x implies ϕ_{min} and ϕ_{max} are as well, we have the following inequalities

$$\begin{aligned} y_{min} = \phi_{min}(x_{min}) &> \phi_{min}(\omega_{max}) \\ &\geq \phi_{min}(\omega_{min}) \\ &= \phi_{max}(\omega_{min}) \\ &> \phi_{max}(x_{max}) = y_{max}. \end{aligned}$$

The proof for the case where $x_{max} > x_{min}$ is nearly identical. □

In our final theorem, we now assume that one of the stable equilibria is not a coexistence equilibria. That is, one of the stable equilibria in the boundary planes is one in which the predator goes extinct. The following theorem shows that the only dynamics that can result are like those in figure 1.6 *D*.

THEOREM A.12. *(1) Assume* $(x_{min}, 0, \beta_{min})$ *is the globally stable equilibria of the* β_{min}*-plane and* $p_{max} = (x_{max}, y_{max}, \beta_{max})$ *is the globally stable coexistence equilibria of the* β_{max}*-plane. Assume both equilibria are unstable in the* β*-direction. Then* $x_{max} < x_{min}$*.*
(2) Assume $(x_{min}, 0, \beta_{max})$ *is the globally stable equilibria of the* β_{max}*-plane and* $p_{min} = (x_{min}, y_{min}, \beta_{min})$ *is the globally stable coexistence equilibria of the* β_{min}*-plane. Assume both equilibria are unstable in the* β*-direction. Then* $x_{min} < x_{max}$*.*

Proof. We will only prove part (1) of the statement since the proof of part (2) is similar. Let the sets $\Upsilon_{min} = \{(x, \upsilon_{min}(x))\}$ and $\Upsilon_{max} = \{(x, \upsilon_{max}(x))\}$ define the prey nullclines (where $x^{-1}x' = 0$) on the β_{min}- and β_{max}-planes, respectively. Since $G(x, 0, \beta) = 0$ for all x and β, $\upsilon_{min}(x_{min}) = \upsilon_{max}(x_{min}) = 0$. In addition, $\upsilon_{min}(x), \upsilon_{max}(x) < 0$ for all $x > x_{min}$. Since p_{max} must be on the β_{max}-plane prey nullcline and $\upsilon(x_{max}) = y_{max} > 0$, we have $x_{max} < x_{min}$. □

A.6 Predator-Prey Model with Prey Evolution

Due to the time reversal property proved in appendix A.1, only slight modifications of the material presented above are needed to understand the effects of fast prey evolution. Here we present the results for that case. Most proofs are omitted since they differ from previous proofs only by changes in notation and slight differences in algebraic manipulation.

Our general model with prey evolution is

$$\begin{aligned} \frac{dx}{dt} &= F(x,\alpha) - G(x,y,\alpha) \\ \frac{dy}{dt} &= H(x,y,\alpha) - D(y) \\ \epsilon\frac{d\alpha}{dt} &= A(\alpha)V\frac{\partial}{\partial\alpha}\left[\frac{1}{x}\frac{dx}{dt}\right] \end{aligned} \tag{A.6.1}$$

where all terms are interpreted as in system (1.3) except that α is now the prey trait. We will assume throughout that G and H are strictly increasing functions of x, y, and α and have continuous mixed second derivatives. Similarly, we assume F is a strictly increasing function of α.

The critical manifold for system (A.6.1) is given by

$$C = \{(x,y,\alpha) : \ A(\alpha)[F_\alpha(x,\alpha) - G_\alpha(x,y,\alpha)] = 0, x > 0\}. \tag{A.6.2}$$

This two dimensional surface has three branches defined as

$$C_L = \{(x,y,\alpha) : \ x > 0, y > 0, \alpha = \alpha_{min}\} \tag{A.6.3}$$

$$C_M = \{(x,y,\alpha) : \ A(\alpha)[F_\alpha(x,\alpha) - G_\alpha(x,y,\alpha)] = 0, x > 0, \alpha \in (\alpha_{min}, \alpha_{max})\} \tag{A.6.4}$$

$$C_R = \{(x,y,\alpha) : \ x > 0, y > 0, \alpha = \alpha_{max}\}. \tag{A.6.5}$$

Following the work in appendix A.3, the trait dynamics of the prey are tracking (stable) at a point $\rho \in C_M$ if

$$F_{\alpha\alpha}(\rho) - G_{\alpha\alpha}(\rho) < 0 \tag{A.6.6}$$

and repelling (unstable) if

$$F_{\alpha\alpha}(\rho) - G_{\alpha\alpha}(\rho) > 0. \tag{A.6.7}$$

Similarly, with an abuse of notation, points ρ on C_L or C_R have stable trait dynamics if

$$A_\alpha(\rho)[F_\alpha(\rho) - G_\alpha(\rho)] < 0 \tag{A.6.8}$$

and have unstable trait dynamics if

$$A_\alpha(\rho)[F_\alpha(\rho) - G_\alpha(\rho)] > 0. \tag{A.6.9}$$

We define a tracking prey trait to be one that satisfies equation (A.6.6) for all points on C_M. Similarly, we define a repelling prey trait to be one that satisfies equation (A.6.7) for all points on C_M.

A.6.1 Local Stability Analysis

Let $p = (\bar{x}, \bar{y}, \bar{\alpha})$ be an equilibrium point of system (A.6.1) on the middle branch of the critical manifold, C_M. As in appendix A.3, we are interested in how evolution affects the stability of the corresponding equilibrium point $q = (\bar{x}, \bar{y})$ of the non-evolving system

$$\begin{aligned} \frac{dx}{dt} &= F(x, \bar{\alpha}) - G(x, y, \bar{\alpha}) \\ \frac{dy}{dt} &= H(x, y, \bar{\alpha}) - D(y). \end{aligned} \tag{A.6.10}$$

Recall that an equilibrium point of the full system must be a point on the critical manifold and that for small ϵ, the dynamics of the full system will locally look like the dynamics restricted to the critical manifold. As in appendix A.3, we will use this to express the stability conditions of p in terms of the stability conditions

of q. The following theorems are the prey evolution analogs of theorems A.1 and A.2, respectively. The proofs of the results are essentially the same as the proofs of theorems A.1 and A.2.

THEOREM A.13. *Assume C_M, defined by equation (A.6.4), depends only on y and α. That is, C_M is constant with respect to x. Let $p = (\bar{x}, \bar{y}, \bar{\alpha})$ be a coexistence equilibrium point of system (A.6.1) on C_M and assume equation (A.6.6) is satisfied at p. Let $q = (\bar{x}, \bar{y})$ be the associated equilibrium point of the non-evolving system (A.6.10). Let $J|_p$ denote the Jacobian for system (A.6.1) restricted to C_M, evaluated at p and $J_{NE}|_q$ denote the Jacobian for system (A.6.10) evaluated at q. Then the following relations hold between the trace and determinant of $J|_p$ and $J_{NE}|_q$:*

$$\det(J|_p) = \det(J_{NE}|_q) + \frac{G_{y\alpha}}{F_{\alpha\alpha} - G_{\alpha\alpha}}[H_\alpha(F_x - G_x) - H_x G_\alpha]|_p$$
$$\operatorname{tr}(J|_p) = \operatorname{tr}(J_{NE}|_q) + H_\alpha \frac{G_{y\alpha}}{F_{\alpha\alpha} - G_{\alpha\alpha}}\bigg|_p$$

THEOREM A.14. *Assume C_M, defined by equation (A.6.4), depends on x, y, and α. Let $p = (\bar{x}, \bar{y}, \bar{\alpha})$ be a coexistence equilibrium point of system (A.6.1) on C_M and assume equation (A.6.6) is satisfied at p. Let $q = (\bar{x}, \bar{y})$ be the associated equilibrium point of the non-evolving system (A.6.10). Let $J|_p$ denote the Jacobian for system (A.6.1) restricted to C, evaluated at p and $J_{NE}|_q$ denote the Jacobian for system (A.6.10) evaluated at q. Then the following relations hold between the trace and determinant of $J|_p$ and $J_{NE}|_q$:*

$$\det(J|_p) = \det(J_{NE}|_q) - \frac{H_\alpha}{F_{\alpha\alpha} - G_{\alpha\alpha}} \begin{vmatrix} \frac{\partial \dot{x}}{\partial x} & \frac{\partial \dot{x}}{\partial y} \\ \frac{\partial \dot{\alpha}}{\partial x} & \frac{\partial \dot{\alpha}}{\partial y} \end{vmatrix}_{|_p}$$
$$\operatorname{tr}(J|_p) = \operatorname{tr}(J_{NE}|_q) + H_\alpha \frac{G_{y\alpha}}{F_{\alpha\alpha} - G_{\alpha\alpha}}\bigg|_p$$

A.6.2 Trade-off Curves

Now assume that the proportional effect of the prey trait on the prey growth and death rates is density independent. This yields a trade-off curve between the proportional increase of the prey recruitment and proportional increase in vulnerability to predation. Mathematically, we assume the functions F and G factor into a population dependent component and a trait dependent component

$$\begin{aligned} F(y,\alpha) &= f(x)\zeta(\alpha) \\ G(x,y,\alpha) &= g(x,y)\gamma(\alpha). \end{aligned} \tag{A.6.11}$$

After substitution, system (A.6.1) simplifies to

$$\begin{aligned} \frac{dx}{dt} &= f(x)\zeta(\alpha) - g(x,y)\gamma(\alpha) \\ \frac{dy}{dt} &= H(x,y,\alpha) - D(y) \\ \epsilon\frac{d\alpha}{dt} &= A(\alpha)Vx^{-1}[f(x)\zeta_\alpha(\alpha) - g(x,y)\gamma_\alpha(\alpha)]. \end{aligned} \tag{A.6.12}$$

Note that ζ and γ are strictly decreasing functions of α. Hence, with an abuse of notation, we define our trade-off curve for the prey trait to be $\gamma(\zeta) = \gamma(\alpha^{-1}(\zeta))$, where $\alpha^{-1}(\zeta)$ is the inverse function of $\zeta(\alpha)$. Throughout this section, $\gamma(\alpha)$ will define the piece of the functional response and $\gamma(\zeta)$ will denote the trade-off curve. Note that the prey trade-off curve $\gamma(\zeta)$ and the predator trade-off curve $\delta(\eta)$ are both written such that the function associated with the death rate (G and γ for prey, D and δ for predator) is a function of the function associated with the growth rate (F and ζ for prey, H and η for predator).

As with the predator trait trade-off curve, the concavity of the trade-off curve determines the stability of the trait dynamics. To summarize the following theorem, for a value $\alpha \in (\alpha_{min}, \alpha_{max})$, if $\gamma(\zeta)$ is concave up, then the trait dynamics are

tracking at α and if $\gamma(\zeta)$ is concave down, then the trait dynamics are repelling at α. The proof of the theorem follows the proofs of theorems A.3 and A.4.

THEOREM A.15. *Let $\rho = (x, y, \alpha)$ be a point on C_M.*
(1) The trade-off curve, $\gamma(\zeta) = \gamma(\zeta(\alpha))$, is concave up if and only if trait dynamics are stable at ρ. That is, $\gamma_{\zeta\zeta}(\zeta) > 0$ if and only if $f(x)\zeta_{\alpha\alpha}(\alpha) - g(x, y)\gamma_{\alpha\alpha}(\alpha) < 0$.
(2) The trade-off curve, $\gamma(\zeta) = \gamma(\zeta(\alpha))$, is concave down if and only if trait dynamics are unstable at ρ. That is, $\gamma_{\zeta\zeta}(\zeta) < 0$ if and only if $f(x)\zeta_{\alpha\alpha}(\alpha) - g(x, y)\gamma_{\alpha\alpha}(\alpha) > 0$.

A.6.3 Boundary Plane Projections

In this section we present theorems similar to those in section A.5. Since the proofs are identical to those in section A.5 we will only give the statements of the theorems and an intuitive summary of the results. Throughout we will assume the prey trait is repelling. We will also use the following notation throughout this section. Primes will denote the derivative of a variable with respect to time, i.e. $x' = dx/dt = F - G$. $p_{min} = (x_{min}, y_{min}, \alpha_{min})$ and $p_{max} = (x_{max}, y_{max}, \alpha_{max})$ will denote the stable coexistence equilibria of the α_{min}- and α_{max}-planes, respectively. The sets $\Upsilon_{min} = \{(x, \upsilon_{min}(x))\}$ and $\Upsilon_{max} = \{(x, \upsilon_{max}(x))\}$ define the prey nullclines (where $x^{-1}x' = 0$) on the α_{min}- and α_{max}-planes, respectively. We assume that υ_{min} and υ_{max} are functions. Finally, we will use the following short hand, $F(x, \alpha) - G(x, y, \alpha) = (F - G)(x, y, \alpha)$.

The organization of this section mimics that of section A.5. The first theorem defines a necessary condition for a repelling trait to yield oscillation in the trait. That is, the if the condition is not met, then all solutions converge to states where evolution no longer occurs. The rest of the theorems are concerned with

defining conditions under which the set ups in figures 1.8 *B*,1.8 *C*, and 1.8 *D* can or cannot occur. Most of the conditions are defined in terms of the shapes and intersections of the prey nullclines, υ_{min} and υ_{max}. theorem A.18 relates some of those conditions to systems with the factorization given in system (A.6.12). Finally, theorem A.20 mathematically states that only the set up in figure 1.8 *D* can occur when one of two equilibria is an extinction equilibrium.

The first theorem proves that $G_{y\alpha} > 0$ is necessary in order to have relaxation oscillations (i.e. oscillations in the trait) when the trait is repelling. Because of this result, we will assume $G_{y\alpha} > 0$ throughout this section.

THEOREM A.16. *If $G_{y\alpha} < 0$ then a repelling trait guarantees that solutions with generic initial conditions will converge to a non-evolving solution.*

The next theorem defines a case where having an equilibrium point in each boundary plane guarantees that every solution will converge to an evolutionary fixed solution. In this case, the prey nullclines, υ_{min} and υ_{max}, do not cross in the x, y-plane. Note that for the relaxation oscillations we need $(F_\alpha - G_\alpha)(x_{min}, y_{min}, \alpha) > 0$ and $(F_\alpha - G_\alpha)(x_{max}, y_{max}, \alpha) < 0$ for all $\alpha \in [\alpha_{min}, \alpha_{max}]$.

THEOREM A.17. *Assume for all $x \neq 0$ that $\upsilon_{min}(x) \neq \upsilon_{max}(x)$. Assume that each boundary plane has one globally (in the two dimensional plane) stable coexistence equilibrium. Then one of the equilibria is a sink in three dimensions.*

Theorem A.17 is of particular interest because the prey nullclines do not cross when the functions F and G factor as in system (A.6.12).

THEOREM A.18. *If the prey response functions factor as $F(x, \alpha) = f(x)\zeta(\alpha)$ and $G(x, y, \alpha) = g(x, y)\gamma(\alpha)$ and the α_{min}-plane equilibrium is repelling in the α-direction, then the prey nullclines of the α_{min}- and α_{max}-planes do not cross.*

As with predator evolution, it is impossible to get cryptic cycles where the predator is cycling and the prey is constant when there is a coexistence equilibrium on each boundary plane. Note that both types of cryptic dynamics are present in figure 1.8 because one equilibrium is an extinction equilibrium in figure 1.8 *E*.

THEOREM A.19. *Assume p_{min} is a stable coexistence equilibrium in the α_{min}-plane and repelling in the α-direction. Also assume p_{max} is a stable coexistence equilibrium in the α_{max}-plane and repelling in the α-direction. Then $x_{min} \neq x_{max}$.*

If one of the equilibria is not a coexistence equilibrium, then in order to have relaxation oscillations that equilibria must be in the α_{min}-plane. The following theorem is the mathematical statement of that result.

THEOREM A.20. *For any x and α, $F_\alpha(x, \alpha) - G_\alpha(x, 0, \alpha) > 0$.*

A.7 Phase Relations with Tracking Traits

Ecological dynamics with a predator lag greater than a quarter of the period, like those seen in figure 1.1 *C*, are easily generated with a repelling trait. These dynamics arise not from local phenomena like periodic orbits generated through a Hopf bifurcation, but instead from global dynamics known as relaxation oscillations. As shown in Bulmer [1975], such dynamics cannot be generated by local bifurcation conditions in a predator-prey system without evolution. That is, a Hopf bifurcation in a predator-prey system cannot give rise to ecological oscillations where the predator lags behind the prey by more than a quarter of the period of the oscillations. In this section we derive under what conditions tracking traits can yield ecological oscillations with a lag greater than a quarter of the

period. This demonstrates that evolution can produce ecological dynamics impossible in non-evolving systems through both local and global mechanisms.

We first review some results from Bulmer [1975]. Consider the non-evolving predator-prey system (A.3.1). Let J be the linearization of the system about a coexistence equilibrium point, $p = (\bar{x}, \bar{y})$.

$$J|_p = \begin{pmatrix} F_x - G_x & -G_y \\ H_x & H_y - D_y \end{pmatrix}_{|_p} \tag{A.7.1}$$

Assume the prey population oscillations about p are given by

$$x - \bar{x} = A \sin(2\pi\omega t) \tag{A.7.2}$$

where A is amplitude and ω is the frequency of the oscillations. Then the linearized predator equation is

$$\frac{dy}{dt} = H_x A \sin(2\pi\omega t) + (H_y - D_y)(y - \bar{y}). \tag{A.7.3}$$

Since $F_x - G_x > 0$ is expected, the lag between the two species is given by

$$L = \frac{1}{2\pi\omega}\left[\frac{\pi}{2} + \arctan\left(\frac{H_y - D_y}{2\pi\omega}\right)\right]. \tag{A.7.4}$$

It is expected that $H_y - D_y \leq 0$, thus $L \in (0, 1/(4\omega)]$ [Bulmer, 1975]. That is, in a non-evolving predator-prey system, the predator will have a lag of a quarter of the period or less.

Now consider the predator-prey system with predator evolution (1.3). Let $p = (\bar{x}, \bar{y}, \bar{\beta})$ be a coexistence equilibrium of the system on C_M. As in appendix A.3 we will compare the non-evolving system (A.3.1) to the evolving system restricted to the critical manifold. The following theorem proves that the lag in the non-evolving model is the same as that in the model restricted to the critical manifold with a tracking predator trait.

THEOREM A.21. *Let $p = (\bar{x}, \bar{y}, \bar{\beta})$ be a coexistence equilibrium of system (1.3) on C_M. Assume $H_{\beta\beta}(p) - D_{\beta\beta}(p) < 0$. Let $q = (\bar{x}, \bar{y})$ be the associated equilibrium point of the non-evolving system (A.3.1). Then the lag, L_{pred}, between the predator and prey oscillations in system (1.3) restricted to C_M is given by equation (A.7.4).*

Proof. Let $J_{CM}|_p$ denote the Jacobian for system (1.3) restricted to C_M and evaluated at p. Let $J_{NE}|_q$ denote the Jacobian for system (A.3.1) evaluated at q. Following the proof in theorem A.2 of section A.3 and recalling that $H_\beta - D_\beta = 0$ on the critical manifold, $J_{CM}|_p$ is given by

$$J|_p = \begin{pmatrix} F_x - G_x + \frac{G_\beta H_{x\beta}}{H_{\beta\beta} - D_{\beta\beta}} & -G_y - G_\beta \frac{H_{y\beta} - D_{y\beta}}{H_{\beta\beta} - D_{\beta\beta}} \\ H_x & H_y - D_y \end{pmatrix}_{|_p}. \tag{A.7.5}$$

Following the derivation in Bulmer [1975], the lag between the predator and prey oscillations when the predator is evolving is given by

$$L_{pred} = \frac{1}{2\pi\omega}\left[\frac{\pi}{2} \pm \arctan\left(\frac{H_y - D_y}{2\pi\omega}\right)\right] \tag{A.7.6}$$

where ω is the frequency of the oscillations and the sign of $\pm$ is given by the sign of H_x.

Note that we need a complex pair of eigenvalues with positive real part in our linearization (A.7.5) in order to get cycling of the dynamics. A general matrix

$$M = \begin{pmatrix} M_1 & M_2 \\ M_3 & M_4 \end{pmatrix}, \tag{A.7.7}$$

has a complex pair of eigenvalues with nonnegative real part only if $M_1 + M_2 \geq 0$ and $M_2 M_3 < 0$. Since we assume $-G_y - G_\beta(H_{y\beta} - D_{y\beta})/(H_{\beta\beta} - D_{\beta\beta}) < 0$ (more predators are bad for the prey) and $H_y - D_y < 0$ [Bulmer, 1975], in order to generate cycles we must have $F_x - G_x + G_\beta H_{x\beta}/(H_{\beta\beta} - D_{\beta\beta}) > 0$ and $H_x > 0$. This implies that sign of $\pm$ in equation (A.7.6) is in fact positive and $L_{pred} = L$. □

We now focus our attention on a predator-prey system with prey evolution (A.6.1). Let $p = (\bar{x}, \bar{y}, \bar{\alpha})$ be a coexistence equilibrium on C_M. Following the same proof as above, we have the following theorem about the effects of prey evolution on the phase relations of the two species.

THEOREM A.22. *Let $p = (\bar{x}, \bar{y}, \bar{\alpha})$ be a coexistence equilibrium of system (A.6.1) on C_M. Assume $F_{\alpha\alpha}(p) - G_{\alpha\alpha}(p) < 0$. Then the lag, L_{prey}, between the predator and prey oscillations in system (A.6.1) restricted to C_M is given by*

$$L_{prey} = \frac{1}{2\pi\omega}\left[\frac{\pi}{2} + \arctan\left(\frac{H_y - D_y}{2\pi\omega} + \frac{1}{2\pi\omega}\frac{H_\alpha G_{y\alpha}}{F_{\alpha\alpha} - G_{\alpha\alpha}}\right)\right]. \tag{A.7.8}$$

A.8 Figure Equations and Parameters

In the following we present the models used to generate the figures presented in this study. When β is used for the trait, the model has the predator evolving and when α is used for the trait, the model has the prey evolving. Unless otherwise stated we set $B(\beta) = \beta(1-\beta)$, $A(\alpha) = \alpha(1-\alpha)$, $V = 1$, and $\epsilon = 0.1$. Also, all traits have been rescaled (non-dimensionalized) such that the minimum value corresponds to 0 and the maximum value corresponds to either 1 or 2.

figure 1.1

The model for figure 1.1 follows from Jones and Ellner [2007].

$$
\begin{aligned}
F &= m(1-x-y)\left[\frac{(1-\alpha)x}{k_1+1-x-y}+\frac{\alpha x}{k_2+1-x-y}\right]-x \\
G &= \frac{y(p_1x+y)g}{k_b+p_1x+y} \\
H &= \frac{y(p_1x+y)g}{k_b+p_1x+y} \\
D &= y
\end{aligned}
$$

where $k_1 = 0.108$, $k_2 = 0.054$, $\delta = 1.25$, $m = 3.3/\delta$, $g = 2.55/\delta$, $k_b = 0.25$, and $p_1 = 0.05$. ϵ is 1, 0.2 and 0.1 in subplots A, B and C, respectively.

figure 1.3

For figure 1.3 A

$$
\begin{aligned}
F &= x(r-kx) \\
G &= \frac{xy(b\beta+c)}{1+x} \\
H &= \frac{xy(b\beta+c)}{1+x} \\
D &= a\beta^4+d
\end{aligned}
$$

where $B(\beta) = \beta(2-\beta)$, $a = 0.1$, $b = 3$, $c = 0.5$, $d = 0.5$, $k = 0.1$, and $r = 1.6$.

For figure 1.3 *B*

$$
\begin{aligned}
F &= x(\alpha + r - kx) \\
G &= \frac{xy(a\alpha^2 + b\alpha + c)}{1 + x} \\
H &= \frac{xy(a\alpha^2 + b\alpha + c)}{1 + x} \\
D &= dy
\end{aligned}
$$

where $a = -0.1$, $b = 3$, $c = 1$, $d = 2.8$, $k = 1$ and $r = 10$.

figure 1.4

For figures 1.4 *A* and *B*

$$
\begin{aligned}
F &= x(r - kx) \\
G &= \frac{xyb}{1 + cx/\beta} \\
H &= \frac{xyb}{1 + cx/\beta} \\
D &= a\beta^2 + d
\end{aligned}
$$

where $a = 3$, $b = 1.86$, $c = 0.1$, $d = 1.3$, $k = 0.4$ and $r = 2.95$. For the evolutionarily fixed dynamics $\beta \approx 0.27$.

For figures 1.4 *C* and *D*

$$
\begin{aligned}
F &= x(r - kx) \\
G &= \frac{\beta bxy}{1 + x\beta} \\
H &= \frac{\beta bxy}{1 + x\beta} \\
D &= d + c\beta
\end{aligned}
$$

where $b = 3.82$, $c = 1$, $d = 1.21$, $k = 0.34$ and $r = 1.25$. For the evolutionarily fixed dynamics $\beta \approx 0.94$.

figure 1.5

For all figures the general form of the equations is given by

$$F = x(r - kx)$$
$$G = \frac{xy\eta(\beta)}{1 + x}$$
$$H = \frac{xy\eta(\beta)}{1 + x}$$
$$D = \delta(\beta).$$

In figure 1.5 *A* we have $\eta(\beta) = b\beta + c$ and $\delta(\beta) = a\beta^4 + d$, where $a = 16$, $b = 3$, $c = 0.5$, $d = 0.5$, $k = 0.07$, and $r = 1$. In figure 1.5 *B* we have $\eta(\beta) = b\beta + a$ and $\delta(\beta) = c\beta^2 + d\beta + g$, where $a = 3$, $b = 0.5$, $c = 0.0137$, $d = 0.0415$, and $g = 0.0313$. In figure 1.5 *C* we have $\eta(\beta) = a\beta + b$ and $\delta(\beta) = c\beta^2 + d\beta + g$, where $a = 10$, $b = 3$, $c = -0.2$, $d = 5.8$, $g = 1.5$, $k = 1.5$, and $r = 20$. In figure 1.5 *D* we have $\eta(\beta) = a_0\beta^3 + a\beta + b$ and $\delta(\beta) = c\beta^2 + d\beta + g$, where $a_0 = 1/3$, $a = 2.5$, $b = 4.8$, $c = 0.5$, $d = .9$, $g = 2$, $k = 2$ and $r = 8$.

figure 1.7

For figure 1.7 A

$$
\begin{aligned}
F &= rx \\
G &= xy(l\beta + m) + \frac{gxy(b\beta + a)^2}{p\beta + q + x(b\beta + a)} \\
H &= \frac{gxy(b\beta + a)^2}{p\beta + q + x(b\beta + a)} \\
D &= y^2(d\beta + c)
\end{aligned}
$$

where $a = 1$, $b = 2$, $c = 1$, $d = 1.3$, $g = 1$, $l = 1.5$, $m = 0.08$, $p = 8$, $q = 2$, $r = 1$ and $\epsilon = 0.001$.

For figures 1.7 B and C the systems is

$$
\begin{aligned}
F &= x(\alpha + r) - kx^2 \\
G &= \frac{xy(a\alpha^2 + b\alpha + c)}{1 + x} \\
H &= \frac{xy(a\alpha^2 + b\alpha + c)}{1 + x} \\
D &= dy.
\end{aligned}
$$

In figure 1.7 B we have $a = -0.1$, $b = 3$, $c = 1$, $d = 2.8$, $k = 1$, and $r = 10$. We also have $A(\alpha) = \alpha(0.8 - \alpha)$. In figure 1.7 C we have $a = -0.1$, $b = 3$, $c = 1$, $d = 2.8$, $k = 1$ and $r = 10$.

For figure 1.7 D

$$
\begin{aligned}
F &= rx - kx^2 \\
G &= \frac{xy(b\beta + a)}{1 + x} \\
H &= \frac{xy(b\beta + a)}{1 + x} \\
D &= y(c\beta^2 + d\beta + g)
\end{aligned}
$$

where $a = 3$, $b = 10$, $c = -0.2$, $d = 5.8$, $g = 1.5$, $k = 1.5$ and $r = 20$.

APPENDIX B

APPENDIX OF CHAPTER 2

B.1 Approximate Model of system (2.1)

In this section we present the transformation that takes system (2.1) to system (2.2) and discuss the error we introduce with our approximation. In addition, we present an alternative model to system (2.1) that has all new prey entering a single class.

We begin by deriving system (2.2). Our new state variables are $x = x_1 + x_2$ and $\alpha = (\alpha_1 x_1 + \alpha_2 x_2)/x$. Differentiating x and y yields the population dynamics of the system

$$\frac{dx}{dt} = F_1(x_1, x_2) + F_2(x_1, x_2) - G_1(x_1, x_2, y) - G_2(x_1, x_2, y)$$
$$\frac{dy}{dt} = H_1(x_1, x_2, y) + H_2(x_1, x_2, y) - D(y).$$

At this point there are two approximations we can make. In the first, the population dynamics are the dynamics of a monomorphic population with mean trait α. For example, if $F_i = x_i(\alpha_i^2 - x/K)$, then we would use $F = x(\alpha^2 - x/K)$. In the second, we use the definitions of x and α to get x_1 and x_2 in terms of x and α. This allows us to define F by $F(x, \alpha) = (F_1 + F_2)(\frac{\alpha_2 - \alpha}{\alpha_2 - \alpha_1}x, \frac{\alpha - \alpha_1}{\alpha_2 - \alpha_1}x)$ and similarly define G and H in terms of x and α. With this approximation, the previous example would yield

$$F = F_1 + F_2 = \frac{\alpha_2 - \alpha}{\alpha_2 - \alpha_1}x\left(\alpha_1^2 - \frac{x}{K}\right) + \frac{\alpha - \alpha_1}{\alpha_2 - \alpha_1}x\left(\alpha_2^2 - \frac{x}{K}\right)$$

In the following, we will use the second approximation for two reasons. First, the population dynamics in the second approximation are always exact,

while the population dynamics in the first are exact only for a small class of functions. Second, when we approximate the trait equation below, the class of functions for which the second approximation is exact is larger than and contains the class of functions for which the first approximation is exact. Thus, if using the first approximation, one could be introducing unnecessary errors into both the population and the trait dynamics. In conclusion, our equations for the population dynamics are

$$\begin{aligned}\frac{dx}{dt} &= (F-G)(x,y,\alpha) = (F_1+F_2-G_1-G_2)(\frac{\alpha_2-\alpha}{\alpha_2-\alpha_1}x, \frac{\alpha-\alpha_1}{\alpha_2-\alpha_1}x, y)\\ \frac{dy}{dt} &= (H-D)(x,y,\alpha) = (H_1+H_2-D)(\frac{\alpha_2-\alpha}{\alpha_2-\alpha_1}x, \frac{\alpha-\alpha_1}{\alpha_2-\alpha_1}x, y).\end{aligned} \tag{B.1.1}$$

For the trait equation, differentiate α to get

$$\begin{aligned}\frac{d\alpha}{dt} &= ([\alpha_1(F_1-G_1)+\alpha_2(F_2-G_2)]x - [\alpha_1x_1+\alpha_2x_2][F_1-G_1+F_2-G_2])\,x^{-2}\\ &\quad + \epsilon^{-1}(\alpha_1-\alpha_2)(x_2P_1-x_1P_2)x^{-1}\\ &= I_1+I_2\end{aligned}$$

where I_1 is the term on the first line and $I_2 = \epsilon(\alpha_1-\alpha_2)(x_2P_1-x_1P_2)x^{-1}$. Adding and subtracting α_1x_1 and α_2x_2 in the following respective terms of I_2 and using the definition of α above yields

$$\epsilon I_2 = (\alpha_1x_2-\alpha_2x_2)P_1x^{-1} + (\alpha_1x_1-\alpha_2x_1)P_2x^{-1} = (\alpha_2-\alpha)P_2 - (\alpha-\alpha_1)P_1.$$

Through algebraic manipulation it follows that

$$\begin{aligned}I_1 &= \frac{x_1x_2}{x^2}\left[\frac{\alpha_1}{x_1}(F_1-G_1)+\frac{\alpha_2}{x_2}(F_2-G_2)-\frac{\alpha_1}{x_x}(F_2-G_2)-\frac{\alpha_2}{x_1}(F_1-G_1)\right]\\ &= \left[\frac{x_1x_2(\alpha_1-\alpha_2)^2}{x^2}\right]\frac{1}{\alpha_1-\alpha_2}\left[\frac{F_1-G_1}{x_1}-\frac{F_2-G_2}{x_2}\right].\end{aligned} \tag{B.1.2}$$

The first term in square brackets of equation (B.1.2) is the population variance of the prey trait, $\bar{V}$. The remaining terms of equation (B.1.2) represent the fitness difference between individuals of the two classes. We will approximate the

fitness difference by the fitness gradient. Typically an individual's fitness and the fitness gradient will be frequency dependent, $\frac{\partial}{\partial \alpha^*}\left[\frac{1}{x}\frac{dx}{dt}(x, y, \alpha, \alpha^*)\right]$, where α^* represents the trait value of an invading individual and α is the mean trait of the prey population. To begin with a simpler case, we consider the frequency independent fitness gradient, $\frac{\partial}{\partial \alpha}\left[\frac{1}{x}\frac{dx}{dt}\right]$, in system (2.2). Note that the stability of the critical manifold (equation (B.2.6) of appendix B.2) is the same for both frequency dependent and independent fitness.

After simplification, $\bar{V} = (\alpha_2 - \alpha)(\alpha - \alpha_1)$. Thus, the genetic variance of the population goes to zero as α approaches α_1 or α_2. To account for this, we model the genetic variance $\bar{V}$ by $A(\alpha)V$, where $A(\alpha_1) = A(\alpha_2) = 0$. Adding I_1 and I_2, multiplying by ϵ, and combining the resulting equation with equation (B.1.1) yields system (2.2).

B.1.1 Error Analysis of Approximation

As mentioned above, the population dynamics of system (2.2) are exact. Here we determine the error we introduce into the trait equation and determine the class of functions for which the trait equation is exact. Our approximation is

$$\frac{1}{\alpha_1 - \alpha_2}\left[\frac{F_1 - G_1}{x_1} - \frac{F_2 - G_2}{x_2}\right] \approx \frac{\partial}{\partial \alpha}\left[\frac{F_1 + F_2 - G_1 - G_2}{x}\right]. \tag{B.1.3}$$

where we are approximating the fitness difference between individuals in each class (left side) with the fitness gradient (right side). In order to determine the error, we will evaluate the derivative on the right side of the equation and compare the result to the left side of the equation.

First consider, the F_i terms in equation (B.1.3). We write x_1 and x_2 in terms of α and x, differentiate with respect to α, and then rewrite the functions F_i in

terms of x_1 and x_2 again to get

$$\begin{aligned}\frac{\partial}{\partial\alpha}\left[\frac{F_1+F_2}{x}\right] &= \frac{1}{\alpha_1-\alpha_2}\left[\frac{F_1}{x_1}-\frac{F_2}{x_2}\right] \\ &+ \frac{x}{(\alpha_1-\alpha_2)^2}\left[(\alpha_2-\alpha)\left(\frac{\partial f_1}{\partial x_1}-\frac{\partial f_1}{\partial x_2}\right)+(\alpha-\alpha_1)\left(\frac{\partial f_2}{\partial x_2}-\frac{\partial f_2}{\partial x_1}\right)\right]\end{aligned} \tag{B.1.4}$$

where $f_i = F_i/x_i$ is the per capita growth rate of an individual in class i. Similarly, for the G_i terms we have

$$\begin{aligned}\frac{\partial}{\partial\alpha}\left[\frac{-G_1-G_2}{x}\right] &= -\frac{1}{\alpha_1-\alpha_2}\left[\frac{G_1}{x_1}-\frac{G_2}{x_2}\right] \\ &- \frac{x}{(\alpha_1-\alpha_2)^2}\left[(\alpha_2-\alpha)\left(\frac{\partial g_1}{\partial x_1}-\frac{\partial g_1}{\partial x_2}\right)+(\alpha-\alpha_1)\left(\frac{\partial g_2}{\partial x_2}-\frac{\partial g_2}{\partial x_1}\right)\right]\end{aligned} \tag{B.1.5}$$

where $g_i = G_i/x_i$ is the per capita predation rate of an individual in class i.

The sum of the first terms on the right sides of equations (B.1.4) and (B.1.5) is exactly equal to the fitness difference on the left side of equation (B.1.3). Thus, the sum of the terms on the second lines of equations (B.1.4) and (B.1.5) represents the error in our approximation.

$$\begin{aligned}Error = \frac{x}{(\alpha_1-\alpha_2)^2}\Bigg[&(\alpha_2-\alpha)\left(\frac{\partial(f_1-g_1)}{\partial x_1}-\frac{\partial(f_1-g_1)}{\partial x_2}\right) \\ &+(\alpha-\alpha_1)\left(\frac{\partial(f_2-g_2)}{\partial x_2}-\frac{\partial(f_2-g_2)}{\partial x_1}\right)\Bigg]\end{aligned} \tag{B.1.6}$$

When this error is zero, our approximate model is in fact exact. When fitness is frequency independent, this error is zero if F_i and G_i have the forms $F_i = x_i f(x_1, x_2, \alpha_i)$ and $G_i = x_i g(x_1, x_2, y, \alpha_i)$, where f and g are symmetric with respect to x_1 and x_2. That is, $f(x_1, x_2, \alpha_i) = f(x_2, x_1, \alpha_i)$ and $g(x_1, x_2, y, \alpha_i) = g(x_2, x_1, y, \alpha_i)$ for all values of α_i, x_1, and x_2. When fitness is frequency dependent, our approximation is exact if we can write $F_i = x_i\bar{f}(x_1, x_2, \alpha, \alpha_i)$ and $G_i = x_i\bar{g}(x_1, x_2, y, \alpha, \alpha_i)$, where $\bar{f}$ and $\bar{g}$ are symmetric with respect to x_1 and x_2.

We give a few examples to illustrate when our approximation is exact and when it is not. When fitness is frequency independent, our approximation is

exact for the following logistic growth and type 2 functional response,

$$\begin{aligned} F_i &= x_i(a\alpha_i^2 + b\alpha_i + r - x/K) \\ G_i &= \frac{(c\alpha_i^2 + d\alpha_i + e)x_i y}{1 + x}. \end{aligned} \tag{B.1.7}$$

A slight modification of the above yields a case where our approximation is exact when fitness is frequency dependent, but not exact in the frequency independent regime.

$$\begin{aligned} F_i &= x_i(a\alpha_i^2 + b\alpha_i + r - (\alpha_1 x_1 + \alpha_2 x_2)/K) = x_i(a\alpha_i^2 + b\alpha_i + r - \alpha x/K) \\ G_i &= \frac{(c\alpha_i^2 + d\alpha_i + e)x_i y}{1 + \alpha_1 x_1 + \alpha_2 x_2} = \frac{(c\alpha_i^2 + d\alpha_i + e)x_i y}{1 + \alpha x} \end{aligned} \tag{B.1.8}$$

Note that the second example is not exact in the frequency independent case because f and g cannot be functions of α and the term $(\alpha_1 x_1 + \alpha_2 x_2)$ is not symmetric in x_1 and x_2. Replacing F_i with $F_i = x_i(\alpha_i r - [k_1 x_1 + k_2 x_2]/K)$, where $k_1 \neq k_2$ and $k_1/\alpha_1 \neq k_2/\alpha_2$, yields an example where the approximation is not exact in either case.

B.1.2 Single class recruitment form of system (2.1)

We now revisit our assumption about prey recruitment. Assume all new prey enter the undefended class, x_2. The class explicit model is

$$\begin{aligned} \frac{dx_1}{dt} &= -G_1(x_1, x_2, y) + \epsilon^{-1} x_2 P_1(y) - \epsilon^{-1} x_2 P_2(y) \\ \frac{dx_2}{dt} &= F_1(x_1, x_2) + F_2(x_1, x_2) - G_2(x_1, x_2, y) - \epsilon^{-1} x_2 P_1(y) + \epsilon^{-1} x_2 P_2(y) \\ \frac{dy}{dt} &= H_1(x_1, x_2, y) + H_2(x_1, x_2, y) - D(y) \end{aligned} \tag{B.1.9}$$

where the terms F_1 and F_2 in the dx_2/dt equation specify that all new prey are born into the x_2 class. Define $x = x_1 + x_2$ and $\alpha = (\alpha_1 x_1 + \alpha_2 x_2)/x$. Following the

steps in the previous subsections, system (B.1.9) is approximated by

$$\begin{aligned}
\frac{dx}{dt} &= F(x,\alpha) - G(x,y,\alpha) \\
\frac{dy}{dt} &= H(x,y,\alpha) - D(y) \\
\epsilon\frac{d\alpha}{dt} &= -\epsilon A(\alpha) V \frac{\partial}{\partial\alpha}\left[\frac{1}{x}G\right] + \epsilon(\alpha_2 - \alpha)\frac{F}{x} + (\alpha_2 - \alpha)P_2(y) - (\alpha - \alpha_1)P_1(y).
\end{aligned} \tag{B.1.10}$$

Since the first two terms of the $d\alpha/dt$ equation are multiplied by ϵ, changes in the mean trait are dominated by phenotypic plasticity and the critical manifolds of systems (2.2) and (B.1.10) are the same. Thus, in the fast induction limit, all of the results presented in the main text hold for this model as well. Numerical differences will arise between systems (2.2) and (B.1.10), but in the fast induction limit, these differences will be small and the dynamics of system (B.1.10) will not be differ qualitatively from those presented in the main text. The same conclusions hold and similar equations can be derived if we assume all prey are born into the defended class, x_1.

The population dynamics of system (B.1.10) are exact. The error introduced by approximating system (B.1.9) by system (B.1.10) only arises in the $\frac{\partial}{\partial\alpha}\left(\frac{G}{x}\right)$ term of the trait equation. Our approximation is exact under the conditions for G_i presented in the previous section. That is, $g(x_1, x_2, y, \alpha_i) = g(x_2, x_1, y, \alpha_i)$ and $\bar{g}(x_1, x_2, y, \alpha, \alpha_i) = \bar{g}(x_2, x_1, y, \alpha, \alpha_i)$ must be symmetric in x_1 and x_2 when fitness is frequency independent and frequency dependent, respectfully. When the system is not exact, the error is given by the term on the second line of equation (B.1.5).

B.2 Fast-Slow Analysis of system (2.2)

For $\epsilon \ll 1$, system (2.2) is a fast-slow dynamical system. In the following we will consider two related dynamical systems were we have set $\epsilon = 0$. The first describes the slow dynamics of system (2.2) (the slow flow) and the second describes the fast dynamics (the fast flow). These two systems are called singular limits and their behavior tells us about the dynamics of system (2.2) when $\epsilon \ll 1$.

Setting $\epsilon = 0$ in system (2.2) yields the slow flow:

$$\begin{aligned} \frac{dx}{dt} &= F(x,\alpha) - G(x,y,\alpha) \\ \frac{dy}{dt} &= H(x,y,\alpha) - D(y) \\ 0 &= (\alpha_2 - \alpha)P_2(y) - (\alpha - \alpha_1)P_1(y). \end{aligned} \tag{B.2.1}$$

system (B.2.1) is a differential algebraic equation - a differential equation (dx/dt and dy/dt equations) with an algebraic constraint (third equation). It describes the population and trait dynamics of system (2.2) when the state variables are constrained by the algebraic equation and the trait responds instantaneously to the population dynamics. Note that the algebraic constraint of system (B.2.1) can be solved explicitly for α, $\alpha = \alpha_1 P_1(y) + \alpha_2 P_2(y)$. Consequently, system (B.2.1) is equivalent to the system

$$\begin{aligned} \frac{dx}{dt} &= F(x,\alpha_1 P_1(y) + \alpha_2 P_2(y)) - G(x,y,\alpha_1 P_1(y) + \alpha_2 P_2(y)) \\ \frac{dy}{dt} &= H(x,y,\alpha_1 P_1(y) + \alpha_2 P_2(y)) - D(y) \end{aligned} \tag{B.2.2}$$

where we have kept the first two lines of system (B.2.1) and substituted $\alpha = \alpha_1 P_1(y) + \alpha_2 P_2(y)$.

To see the fast flow, we first rescale time with $\tau = t/\epsilon$.

$$\begin{aligned}
\frac{dx}{d\tau} &= \epsilon[F(x,\alpha) - G(x,y,\alpha)] \\
\frac{dy}{d\tau} &= \epsilon[H(x,y,\alpha) - D(y)] \\
\frac{d\alpha}{d\tau} &= \epsilon A(\alpha) V \frac{\partial}{\partial \alpha}\left[\frac{1}{x}\frac{dx}{dt}\right] + (\alpha_2 - \alpha)P_2(y) - (\alpha - \alpha_1)P_1(y).
\end{aligned} \tag{B.2.3}$$

Setting $\epsilon = 0$ yields the fast flow

$$\begin{aligned}
\frac{dx}{d\tau} &= \frac{dy}{d\tau} = 0 \\
\frac{d\alpha}{d\tau} &= (\alpha_2 - \alpha)P_2(y) - (\alpha - \alpha_1)P_1(y).
\end{aligned} \tag{B.2.4}$$

system (B.2.4) describes the fast trait dynamics when the population densities are held constant.

The set of equilibrium points of the fast flow is called the critical manifold. It is given by

$$C = \{(x,y,\beta) :\ 0 = (\alpha_2 - \alpha)P_2(y) - (\alpha - \alpha_1)P_1(y)\}. \tag{B.2.5}$$

Note that the critical manifold is the set of points to which the slow flow (B.2.1) is constrained by its algebraic equation. Thus, we can write it explicitly in terms of α as above, $\alpha = \alpha_1 P_1(y) + \alpha_2 P_2(y)$.

As explained in the main text, the dynamics of the fast-slow system can be understood by knowing what solutions do on the critical manifold, where they jump away from it, and where they land on it. A point ρ on the critical manifold, C, is a jumping point if it is an unstable equilibrium point of the fast flow (B.2.4) and a landing point if it is a stable equilibrium point of the fast flow. The stability of ρ can be determined by computing the eigenvalues of the Jacobian at each point. Two eigenvalues are guaranteed to be zero. The third eigenvalue is

$$Q = \frac{\partial}{\partial \alpha}[(\alpha_2 - \alpha)P_2(y) - (\alpha - \alpha_1)P_1(y)] = -1. \tag{B.2.6}$$

Since this value is always negative, the critical manifold is composed of stable equilibria of the fast flow. This tells us that the solutions to system (2.2) will first run quickly towards the critical manifold and then behave as if they were on it. (To be more precise, this means that the slow manifold, the perturbation of the critical manifold when ϵ is small but nonzero, is attracting and solutions will converge to it and not run away from it. Since the dynamics on the slow manifold are approximated by the dynamics on the critical manifold, solutions to (2.2) will behave as if they were constrained to the critical manifold.)

B.3 Local Stability Analysis

Here we capture the effects phenotypic plasticity has on the local stability of the ecological dynamics. We do this by comparing the stability of an equilibrium point, p, of system (2.2) with an inducible defense to the stability of an equilibrium point, q, of a system with a fixed level of defense.

Let p be an equilibrium point of system (2.2) and assume ϵ is small. Then p lies close the critical manifold, but not on it. The stability of the trait dynamics at p are determined by the stability of p in the fast flow (B.2.4). Since $Q < 0$, p will always be stable in the fast flow and hence, the trait dynamics are stable at p. For small ϵ, the stability of the population dynamics near p is approximated by the stability of the population dynamics near an associated equilibrium, $\bar{p}$, of the slow flow (B.2.1). This equilibrium point of interest, $\bar{p} = (\bar{x}, \bar{y}, \bar{\alpha})$, is $O(\epsilon)$-close to p and lies on the critical manifold. We can understand the stability of the equilibrium p of system (2.2) by understanding the stability of $\bar{p}$. That is, we can understand the local stability of the population dynamics in the full system (2.2)

by understanding the local stability of the population dynamics restricted to the critical manifold (which are given by the slow flow (B.2.1)).

For the equilibrium $\bar{p}$ of system (B.2.1), let $q = (\bar{x}, \bar{y})$ be the associated equilibrium point of the system with a fixed level of defense $\bar{\alpha}$:

$$\begin{aligned} \frac{dx}{dt} &= F(x, \bar{\alpha}) - G(x, y, \bar{\alpha}) \\ \frac{dy}{dt} &= H(x, y, \bar{\alpha}) - D(y) \end{aligned} \tag{B.3.1}$$

system (B.3.1) represents the population dynamics of the full system (2.2) where the prey trait value is fixed at the equilibrium trait value $\bar{\alpha}$. The stability of q is completely determined by the trace and determinant of the Jacobian matrix at the equilibrium, respectively $\text{tr}(J_f|_q)$ and $\det(J_f|_q)$. If q is stable, then $\det(J_f|_q) > 0$ and $\text{tr}(J_f|_q) > 0$. If either inequality is reversed then q will be unstable.

We compare the stabilities of q and $\bar{p}$ via differences in the values of their traces and determinants. Since the stability of p is approximated by the stability of $\bar{p}$, this allows us to express the stability of the inducible defense system in terms of the stability of the fixed defense system plus a perturbation.

We make a note about the notation used throughout the proof. Let $G(x, y, z)$ be a function where y and z could be functions of x. We write $\partial G/\partial x$ to denote the partial derivative of G with respect to x. We contrast this with the notation G_x, where we are denoting the partial derivative of G with respect to its first argument. The following illustrates the difference,

$$\frac{\partial G}{\partial x} = G_x + G_y \frac{\partial y}{\partial x} + G_z \frac{\partial z}{\partial x}.$$

Often the arguments of G will be independent of each other and the notations will imply the same result, i.e., $\partial G/\partial x = G_x$. When this is not the case, we will stick to the above convention.

THEOREM B.1. *Assume $\epsilon \ll 1$. Let p be an equilibrium point of system (2.2) and let $\bar{p} = (\bar{x}, \bar{y}, \bar{\alpha})$ be the equilibrium point of system (B.2.1) that is $O(\epsilon)$-close. Let $q = (\bar{x}, \bar{y})$ be the associated equilibrium point of system (B.3.1) where we fix $\alpha = \bar{\alpha}$. Let $J_i|_{\bar{p}}$ denote the Jacobian for system (B.2.1), evaluated at $\bar{p}$ and $J_f|_q$ denote the Jacobian for fixed trait system (B.3.1) evaluated at q. Then,*

$$\det(J_i|_{\bar{p}}) = \det(J_f|_q) - (\alpha_2 - \alpha_1)P_1' \left| \begin{array}{cc} \frac{\partial \dot{x}}{\partial x} & \frac{\partial \dot{x}}{\partial \alpha} \\ \frac{\partial \dot{y}}{\partial x} & \frac{\partial \dot{y}}{\partial \alpha} \end{array} \right|_{|_p}$$

$$\operatorname{tr}(J_i|_{\bar{p}}) = \operatorname{tr}(J_f|_q) - (\alpha_2 - \alpha_1)H_\alpha P_1'\Big|_p$$

where $P_1' = dP_1/dy$. For ϵ small enough, the stability of p is determined by the sign of Q and the stability of $\bar{p}$.

Proof. Since $Q < 0$ (see equation section 2.4.1 of the main text), the implicit function theorem allows us to write α locally as a function of y. For notational ease in the following, we will not explicitly denote this dependence of α on y.

The Jacobian evaluated at $\bar{p}$ is

$$J_i|_{\bar{p}} = \left(\begin{array}{cc} F_x - G_x & \frac{\partial}{\partial y}F - \frac{\partial}{\partial y}G \\ H_x & \frac{\partial}{\partial y}H - D_y \end{array} \right)_{|_{\bar{p}}} \tag{B.3.2}$$

By the chain rule, we have that

$$\begin{aligned} \frac{\partial}{\partial y}F &= F_\alpha \frac{\partial \alpha}{\partial y} \\ \frac{\partial}{\partial y}G &= G_y + G_\alpha \frac{\partial \alpha}{\partial y} \\ \frac{\partial}{\partial y}H &= H_y + H_\alpha \frac{\partial \alpha}{\partial y}. \end{aligned} \tag{B.3.3}$$

Using the defining equation for the critical manifold, $\alpha = \alpha_1 P_1(y) + \alpha_2 P_2(y)$,we compute the derivatives of α with respect y on C to be $\frac{\partial \alpha}{\partial y} = -(\alpha_2 - \alpha_1)P_1'$, where we have recognized that $P_1 + P_2 = 1$ implies $P_1' = -P_2'$.

The trace and determinant of J_f evaluated at q are given by

$$\begin{aligned}
\det(J_f|_q) &= [F_x(\bar{x},\bar{\alpha}) - G_y(\bar{x},\bar{y},\bar{\alpha})][H_y(\bar{x},\bar{y},\bar{\alpha}) - D_y(\bar{y})] \\
&\quad + G_y(\bar{x},\bar{y},\bar{\alpha})H_x(\bar{x},\bar{y},\bar{\alpha}) \\
&= (F_x - G_x)(H_y - D_y) + G_y H_x\big|_{\bar{p}} \qquad \text{(B.3.4)} \\
\operatorname{tr}(J_f|_q) &= F_x(\bar{x},\bar{\alpha}) - G_x(\bar{x},\bar{y},\bar{\alpha}) + H_y(\bar{x},\bar{y},\bar{\alpha}) - D_y(\bar{y}) \\
&= [F_x - G_y + H_y - D_y]\big|_{\bar{p}}\,. \qquad \text{(B.3.5)}
\end{aligned}$$

Evaluating the trace and determinant of $J_i|_{\bar{p}}$ and substituting in equations (B.3.3) yields the equalities in the statement of the theorem. Recalling that for small enough ϵ the stability of p is approximated by the stability of $\bar{p}$ and the sign of Q, we have the final result. □

Perturbations to the trace of the Jacobian determine how rapidly induced defenses affect population oscillations in the system. Since $H_\alpha > 0$ and $P_1' \geq 0$, the previous result shows that the perturbation to the trace is is zero when $\alpha = \alpha_1$ or $\alpha = \alpha_2$ and negative otherwise. Negative perturbations to the trace result in the dampening or loss of oscillations. Thus, rapidly induced defenses stabilize population oscillations.

Perturbations to the determinant of the Jacobian determine how rapidly induced defenses affect the coexistence of two species. A positive determinant implies coexistence at steady state or while undergoing oscillations. A negative determinant implies that the predator can not coexist with the prey and goes extinct. Consequently, positive perturbations to the determinant promote coexistence and negative perturbations to the determinant promote predator extinction. We expect that the expressed phenotype at the equilibrium is nearly optimal, where optimal is defined by the fitness of an individual. Under this

expectation, $\frac{\partial \dot{x}}{\partial \alpha} \approx 0$ and the perturbation to the determinant is approximately $(\alpha_2 - \alpha_1)P_1' \frac{\partial \dot{x}}{\partial x}\frac{\partial \dot{y}}{\partial \alpha}$. Since $\frac{\partial \dot{y}}{\partial \alpha} > 0$, this perturbation is negative when the ecological dynamics cycle and positive most of the time when the ecological dynamics tend to equilibrium. Thus, inducible defenses tend to promote coexistence when the ecological dynamics are stable and promote predator extinction when the ecological dynamics are unstable.

B.4 Phase Relations with Phenotypic Plasticity

Before proving that inducible defenses always reduce the phase lag between predator and prey oscillations, we review results from Bulmer [1975]. Let $q = (\bar{x}, \bar{y})$ be a coexistence equilibrium (both predator and prey have positive density) of system (B.3.1) and J_f be the linearization of the system about q,

$$J_f|_q = \begin{pmatrix} F_x - G_x & -G_y \\ H_x & H_y - D_y \end{pmatrix}_{|_q} \tag{B.4.1}$$

Assume the populations oscillate about q and that the prey oscillations are given by

$$x - \bar{x} = A \sin(2\pi\omega t) \tag{B.4.2}$$

where A is amplitude and ω is the frequency of the oscillations. Then the linearized predator equation is

$$\frac{dy}{dt} = H_x A \sin(2\pi\omega t) + (H_y - D_y)(y - \bar{y}). \tag{B.4.3}$$

For oscillations to occur about the equilibrium q, the trace of the Jacobian in equation (B.4.1) needs to be positive. Typically $H_y - D_y \leq 0$. Thus, we expect $F_x - G_x > 0$. Together, these two inequalities imply [Bulmer, 1975] that the lag

between the two species is given by

$$L = \frac{1}{2\pi\omega}\left[\frac{\pi}{2} + \arctan\left(\frac{H_y - D_y}{2\pi\omega}\right)\right]. \tag{B.4.4}$$

Note that $L \in (0, 1/(4\omega)]$. This means that the predator will have a lag of a quarter of the period or less when the level of defense is fixed

Now we consider predator-prey oscillations in system (2.2). Let p be a coexistence equilibrium of system (2.2) and $\bar{p} = (\bar{x}, \bar{y}, \bar{\alpha})$ be the associated equilibrium of system (B.2.1). For small enough ϵ, the phase lags exhibited by the oscillations about p will be approximated by the phase lags exhibited by oscillations about $\bar{p}$. Thus, as in appendix B.2, we will make statements about the lags in system (B.2.1) and use those results to say something about the lags in system (2.2).

THEOREM B.2. *Assume $\epsilon << 1$. Let p be a coexistence equilibrium of system (2.2) and let $\bar{p} = (\bar{x}, \bar{y}, \bar{\alpha})$ be the associated equilibrium of system (B.2.1) that is $O(\epsilon)$-close. Then for ϵ small enough, the lag between the predator and prey oscillations in system (2.2) is approximately*

$$L_A = \frac{1}{2\pi\omega}\left[\frac{\pi}{2} + \arctan\left(\frac{H_y - D_y}{2\pi\omega} - \frac{(\alpha_2 + \alpha_1)H_\alpha P_1'}{2\pi\omega}\right)\right]. \tag{B.4.5}$$

Proof. Let $J_i|_{\bar{p}}$ denote the Jacobian for system (B.2.1) evaluated at $\bar{p}$. Following the work in the theorem of appendix B.3 we have

$$J_i|_{\bar{p}} = \begin{pmatrix} F_x - G_x & -G_y + (\alpha_2 - \alpha_1)G_\alpha P_1' \\ H_x & H_y - D_y - (\alpha_2 - \alpha_1)H_\alpha P_1' \end{pmatrix}_{|_p}. \tag{B.4.6}$$

Following the derivation in Bulmer (1975), the lag between small oscillations of the predator and prey in system (B.2.1) is given by

$$L_A = \frac{1}{2\pi\omega}\left[\frac{\pi}{2} \pm \arctan\left(\frac{H_y - D_y}{2\pi\omega} - \frac{(\alpha_2 + \alpha_1)H_\alpha P_1'}{2\pi\omega}\right)\right]. \tag{B.4.7}$$

where ω is the frequency of the oscillations and the sign of $\pm$ is given by the sign of H_x. Note that to have oscillations, H_x evaluated at the equilibrium point must be positive. Recalling that for small ϵ the dynamics on the critical manifold are a first order approximation to the dynamics on the slow manifold yields the result. □

Since $(\alpha_2 - \alpha_1)H_\alpha P_1' > 0$, the term within the arctan function in equation (B.4.5) is smaller than the value in the arctan of equation (B.4.4). Thus, phenotypic plasticity decreases the lag between the predator and prey oscillations.

B.5 An Alternative Inducible Defense Model

Here we present an alternative model where the phenotype of an individual is determined at birth by the current predator density. Let x_1 and x_2 be the defended and undefended classes of prey with expressed phenotypes α_1 and α_2, respectively. Our model with phenotype determined at birth is

$$\begin{aligned}
\frac{dx_1}{dt} &= [F_1(x_1, x_2) + F_2(x_1, x_2)]P_1(y) - G_1(x_1, x_2, y) \\
\frac{dx_2}{dt} &= [F_1(x_1, x_2) + F_2(x_1, x_2)]P_2(y) - G_2(x_1, x_2, y) \\
\frac{dy}{dt} &= H_1(x_1, x_2, y) + H_2(x_1, x_2, y) - D(y)
\end{aligned} \tag{B.5.1}$$

where $P_1 + P_2 = 1$.

Following the work in appendix B.1, this model is approximated by

$$\begin{aligned}
\frac{dx}{dt} &= F(x, \alpha) - G(x, y, \alpha) \\
\frac{dy}{dt} &= H(x, y, \alpha) - D(y) \\
\frac{d\alpha}{dt} &= x^{-1}F[(\alpha_2 - \alpha)P_2 - (\alpha - \alpha_1)P_1] - A(\alpha)V\frac{\partial}{\partial \alpha}\left[\frac{G}{x}\right]
\end{aligned} \tag{B.5.2}$$

where $\alpha = (\alpha_1 x_1 + \alpha_2 x_2)/x$ and $x = x_1 + x_2$. As with model (B.1.10), the population equations are exact. The error introduced by approximating system (B.5.1) by system (B.5.2) arises only through the $\frac{\partial}{\partial \alpha}\left(\frac{G}{x}\right)$ term of the trait equation. The approximation is exact under the conditions for G_i presented in appendix (B.1). That is, $g(x_1, x_2, y, \alpha_i) = g(x_2, x_1, y, \alpha_i)$ and $\bar{g}(x_1, x_2, y, \alpha, \alpha_i) = \bar{g}(x_2, x_1, y, \alpha, \alpha_i)$ must be symmetric in x_1 and x_2 when fitness is frequency independent and frequency dependent, respectively. The error introduced by the approximations is given by the term on the second line of equation (B.1.5).

To gain understanding about this model, we consider the limit where there is rapid turnover of individuals within the prey population but the total number of prey changes slowly. Under this assumption, our system is

$$\begin{aligned} \frac{dx}{dt} &= F(x, \alpha) - G(x, y, \alpha) \\ \frac{dy}{dt} &= H(x, y, \alpha) - D(y) \\ \epsilon \frac{d\alpha}{dt} &= x^{-1} F[(\alpha_2 - \alpha)P_2 - (\alpha - \alpha_1)P_1] - \epsilon A(\alpha) V \frac{\partial}{\partial \alpha}\left[\frac{G}{x}\right] \end{aligned} \tag{B.5.3}$$

where ϵ is a small positive number. In this fast turnover limit, we assume that changes in the size of each class (x_1 and x_2) due to predation are much slower than the turnover of individuals in each class. This assumption may not always hold, but we consider the fast turnover limit in order to gain understanding about systems where the assumption is no longer valid.

In the following we analyze system (B.5.3) and present results analogous to those presented in the main text for system (2.2). All results presented here are qualitatively the same as those presented in the main text for system (2.2).

The slow flow for system (B.5.3) is given by

$$\begin{aligned} \frac{dx}{dt} &= F(x,\alpha) - G(x,y,\alpha) \\ \frac{dy}{dt} &= H(x,y,\alpha) - D(y) \\ 0 &= x^{-1}F[(\alpha_2-\alpha)P_2 - (\alpha-\alpha_1)P_1]. \end{aligned} \tag{B.5.4}$$

After the transformation $\tau = t/\epsilon$, the fast flow is given by

$$\begin{aligned} \frac{dx}{d\tau} &= \frac{dy}{d\tau} = 0 \\ \frac{d\alpha}{d\tau} &= x^{-1}F[(\alpha_2-\alpha)P_2 - (\alpha-\alpha_1)P_1] \end{aligned} \tag{B.5.5}$$

The critical manifold of system (B.5.3) is the set of points

$$C = \{(x,y,\beta) :\ 0 = F[(\alpha_2-\alpha)P_2 - (\alpha-\alpha_1)P_1], x > 0\}. \tag{B.5.6}$$

and consists of two planes. The first is similar to the critical manifold of system (2.2) and the second is defined by $F = 0$,

$$C_1 = \{(x,y,\beta) :\ 0 = [(\alpha_2-\alpha)P_2 - (\alpha-\alpha_1)P_1]\}. \tag{B.5.7}$$

$$C_2 = \{(x,y,\beta) :\ 0 = F, x > 0\}. \tag{B.5.8}$$

Note that the flow on the attracting parts of C_2 is always towards its intersection with C_1. Thus, we will primarily concern ourselves with the dynamics on C_1.

Following the work in appendix B.2, let ρ be a point on C_1. The nonzero eigenvalue of the fast flow for system (B.5.3) at ρ is given by

$$Q = \frac{\partial}{\partial\alpha}[(\alpha_2-\alpha)FP_2 - (\alpha-\alpha_1)FP_1]|_\rho = -F. \tag{B.5.9}$$

Since this value is never positive and solutions cannot cross the $F = 0$ plane, trajectories will never jump off or away from C_1 once near it.

We now summarize the results presented in appendices B.3 and B.4 for system (B.5.3). We will not prove the results since the proofs are nearly identical.

The first theorem shows that phenotypic plasticity stabilizes population oscillations and the second shows that phenotypic plasticity decreases the lag between predator and prey oscillations. Note that the effects of phenotypic plasticity in system (B.5.3) are the same as those in system (2.2).

THEOREM B.3. *Assume $\epsilon \ll 1$. Let p be an equilibrium point of system (B.5.3) and let $\bar{p} = (\bar{x}, \bar{y}, \bar{\alpha})$ be the associated equilibrium point of system (B.5.4) that is $O(\epsilon)$-close. Let $q = (\bar{x}, \bar{y})$ be the equilibrium point of system (B.3.1) where we fix $\alpha = \bar{\alpha}$. Let $J_i|_{\bar{p}}$ denote the Jacobian for system (B.5.4), evaluated at $\bar{p}$ and let $J_f|_q$ denote the Jacobian for system (B.3.1) evaluated at q. Then*

$$\det(J_i|_p) = \det(J_f|_q) - P_1'(\alpha_2 - \alpha_1)\begin{vmatrix} \frac{\partial \dot{x}}{\partial x} & \frac{\partial \dot{x}}{\partial \alpha} \\ \frac{\partial \dot{y}}{\partial x} & \frac{\partial \dot{y}}{\partial \alpha} \end{vmatrix}_{|_p}$$

$$\operatorname{tr}(J_i|_p) = \operatorname{tr}(J_f|_q) - H_\alpha P_1'(\alpha_2 - \alpha_1)\Big|_p$$

where $P_1' = dP_1/dy$. For ϵ small enough, the stability of p is determined by the sign of Q and the stability of $\bar{p}$.

THEOREM B.4. *Assume $\epsilon \ll 1$. Let p be a coexistence equilibrium of system (B.5.3) and let $\bar{p} = (\bar{x}, \bar{y}, \bar{\alpha})$ be the associated equilibrium of system (B.5.4) that is $O(\epsilon)$ close. Then for ϵ small enough, the lag between the predator and prey oscillations in system (B.5.3) is approximately*

$$L_B = \frac{1}{2\pi\omega}\left[\frac{\pi}{2} + \arctan\left(\frac{H_y - D_y}{2\pi\omega} - \frac{H_\alpha P_1'(\alpha_2 + \alpha_1)}{2\pi\omega}\right)\right]. \tag{B.5.10}$$

B.6 Induced Predator Traits

As shown in Cortez and Ellner [2010], the effects of predator and prey evolution are nearly equivalent. While some dynamics are harder to generate with predator evolution, only a few dynamics can only be generated by prey evolution.

This similarity between the effects of predator and prey adaptation also holds when we consider a predator with an inducible trait that is determined by prey density. The main conclusions here are that rapidly induced predator traits stabilize population oscillations and they do not alter the lags between predator and prey oscillations.

We begin with a predator-prey model where there are two predator classes (y_1, y_2) with expressed phenotypes β_1 and β_2, respectively. Here we think of β as measuring the effort being put into foraging. As β increases, there is an increased growth rate (energy gain) at the cost of an increased death rate (energy expenditure). The amount of effort is determined by the current prey density and increases with prey density. Our model is

$$\begin{aligned}
\frac{dx_1}{dt} &= F(x) - G_1(x, y_1, y_2) - G_2(x, y_1, y_2) \\
\frac{dy}{dt} &= H_1(x, y_1, y_2) - D_1(y_1, y_2) + \epsilon^{-1} y_2 P_1(x) - \epsilon^{-1} y_1 P_2(x) \\
\frac{dy}{dt} &= H_2(x, y_1, y_2) - D_2(y_1, y_2) - \epsilon^{-1} y_2 P_1(x) + \epsilon^{-1} y_1 P_2(x).
\end{aligned} \tag{B.6.1}$$

where G_i is the predation rate of class i, H_i is the growth rate of class i due to predation, and D_i is the death rate of class i. G_i and H_i are assumed to be increasing in x and y_i and D_i is assumed be increasing in y_1 and y_2. The functions $\epsilon^{-1} P_i$ represent the rates at which adults switch to expressing phenotype i given the current prey density. Note that P_2 is an increasing function of x (greater effort as prey density increases). We have assumed that predators can switch their phenotype as adults and that all individuals are born with their parent's phenotype. As in appendices B.1 and B.5, we can instead assume all individuals are born into a particular class or that the phenotype is determined at birth. In the fast induction limit, the differences that result are small and the results are the same as the ones that follow.

system (B.6.1) is approximated by the following model where $y = y_1 + y_2$ is the total predator population size and $\beta = (\beta_1 y_1 + \beta_2 y_2)/y$ is the average predator trait.

$$\begin{aligned} \frac{dx_1}{dt} &= F(x) - G(x, y, \beta) \\ \frac{dy}{dt} &= H(x, y, \beta) - D(y, \beta) \\ \epsilon \frac{d\beta}{dt} &= \epsilon B(\beta) V \frac{\partial}{\partial \beta}\left[\frac{1}{y}\frac{dy}{dt}\right] + (\beta_2 - \beta)P_2(x) - (\beta - \beta_1)P_1(x). \end{aligned} \tag{B.6.2}$$

The approximation is analogous to the one in appendix B.1. We define $G = (G_1 + G_2)(x, \frac{\beta_2 - \beta}{\beta_2 - \beta_1} y, \frac{\beta - \beta_1}{\beta_2 - \beta_1} y)$ and similarly define H and D in terms of H_i and D_i, respectively.

The approximation is exact for the population dynamics. That is, no error is introduced into the population equations when using our approximation. The trait equation is exact when fitness is frequency independent if $H_i = y_i h(x, y_1, y_2, \beta_i)$ and $D_i = y_i d(x, y_1, y_2, \beta_i)$ are symmetric with respect to y_1 and y_2, and it is exact when fitness is frequency dependent if we can write $H_i = y_i \bar{h}(x, y_1, y_2, \beta, \beta_i)$ and $D_i = y_i \bar{d}(x, y_1, y_2, \beta, \beta_i)$ with $\bar{h}$ and $\bar{d}$ symmetric with respect to y_1 and y_2. When the trait equation is not exact, the introduced error is given by

$$\begin{aligned} Error = \frac{x}{(\beta_1 - \beta_2)^2} \Bigg[&(\beta_2 - \beta)\left(\frac{\partial(h_1 - d_1)}{\partial y_1} - \frac{\partial(h_1 - d_1)}{\partial y_2}\right) \\ &+ (\beta - \beta_1)\left(\frac{\partial(h_2 - d_2)}{\partial y_2} - \frac{\partial(h_2 - d_2)}{\partial y_1}\right)\Bigg] \end{aligned} \tag{B.6.3}$$

where $h_i = H_i/y_i$ is the per capita growth rate of class i and $d_i = D_i/y_i$ is the per capita death rate of class i.

The critical manifold of system (B.6.2) is

$$C = \{(x, y, \beta) : \ 0 = (\beta_2 - \beta)P_2(x) - (\beta - \beta_1)P_1(x)\}. \tag{B.6.4}$$

The stability of a point ρ on C is determined by the sign of

$$Q_y = \frac{\partial}{\partial \beta}[(\beta_2 - \beta)P_2(x) - (\beta - \beta_1)P_1(x)] = -1. \tag{B.6.5}$$

Thus, as with induced defenses, rapidly induced offenses cannot produce some kinds of dynamics observed in rapidly evolving systems.

Mimicking the work in appendix B.3, we have the following result about the effect of induced offenses on the stability of the population dynamics.

THEOREM B.5. *Assume $\epsilon \ll 1$. Let p be an equilibrium point of system (B.6.2) and let $\bar{p} = (\bar{x}, \bar{y}, \bar{\beta})$ be an equilibrium point of the slow flow of system (B.6.2) that is $O(\epsilon)$-close. Let $q = (\bar{x}, \bar{y})$ be the associated equilibrium point where we fix $\beta = \bar{\beta}$. Let $J_i|_{\bar{p}}$ denote the Jacobian for system (B.6.2) evaluated at $\bar{p}$ and let $J_f|_q$ denote the Jacobian for fixed trait system evaluated at q. Then,*

$$\det(J_i|_{\bar{p}}) = \det(J_f|_q) - (\beta_2 - \beta_1)P_2' \begin{vmatrix} \frac{\partial \dot{x}}{\partial y} & \frac{\partial \dot{x}}{\partial \beta} \\ \frac{\partial \dot{y}}{\partial y} & \frac{\partial \dot{y}}{\partial \beta} \end{vmatrix}_{|_p}$$

$$\operatorname{tr}(J_i|_{\bar{p}}) = \operatorname{tr}(J_f|_q) - (\beta_2 - \beta_1)G_\beta P_2'\big|_p$$

where $P_2' = dP_2/dx$. For ϵ small enough, the stability of p is determined by the sign of Q_y and the stability of $\bar{p}$.

The perturbation to the trace is always nonnegative. Thus, inducible offenses dampen population oscillations and have the potential to cause oscillating systems to tend to equilibrium. Now consider the perturbation to the determinant. We expect the level of the trait to be nearly optimal at equilibrium, i.e., $\frac{\partial \dot{y}}{\partial \beta} \approx 0$. This implies that the perturbation to the determinant is approximately $(\beta_2 - \beta_1)P_2' \frac{\partial \dot{x}}{\partial \beta}\frac{\partial \dot{y}}{\partial y}$. We assume $\frac{\partial \dot{x}}{\partial \beta} > 0$ and we expect $\frac{\partial \dot{y}}{\partial y} \leq 0$. Thus, when inducible offenses do affect the population dynamics, they tend to promote predator extinc-

tion. Note the contrast with inducible defenses that inhibit predator extinction when the ecological dynamics are at equilibrium.

Following the work in appendix (B.4), it can be shown that inducible offenses do not affect the lags between predator and prey oscillations. That is, the predator lag is the same whether the predator's offense is fixed or changes with prey abundance. A similar result has been observed for evolved predator traits [Cortez and Ellner, 2010].

APPENDIX C

APPENDIX OF CHAPTER 3

C.1 Transformations to get Canonical Form (3.3)

Under assumptions (C1) through (C4), we can rewrite system (3.2) as

$$\begin{aligned} \epsilon\dot{x} &= x\left[\alpha_1 x + \alpha_2 y + \alpha_3 z + f(x,y,z,\epsilon)\right] \\ \dot{y} &= \beta_0 + \beta_1 x + \beta_2 y + \beta_3 z + g(x,y,z,\epsilon) \\ \dot{z} &= \delta_0 + \delta_1 x + \delta_2 y + \delta_3 z + h(x,y,z,\epsilon) \end{aligned} \tag{C.1.1}$$

where $\alpha_1 \neq 0$, either $\alpha_2 \neq 0$ or $\alpha_3 \neq 0$, and $f, g, h = O(\epsilon, \epsilon u, u^2, uv)$ for $u, v \in \{x, y, z\}$. We will assume $\alpha_2 \neq 0$. If this is not the case, then reversing the roles of the y and z equations will suffice. system (C.1.1) can be reduced to system (3.3) with the following linear transformations,

$$\begin{aligned} \bar{x} &= \alpha_1 x \\ \bar{y} &= -\alpha_2 y - \alpha_3 z \\ \bar{z} &= \gamma_0 + \gamma_1 \bar{x} + \gamma_2 \bar{y} + \gamma_4 z \\ \lambda &= \gamma_3\delta_0 - \left(\delta_3 - \frac{\delta_2\alpha_3}{\alpha_2}\right)\gamma_0 \\ a &= \frac{\gamma_3\delta_1}{\alpha_1} - \left(\delta_3 - \frac{\delta_2\alpha_3}{\alpha_2}\right)\gamma_1 \\ b &= -\frac{\gamma_3\delta_2}{\alpha_2} - \left(\delta_3 - \frac{\delta_2\alpha_3}{\alpha_2}\right)\gamma_2 \\ c &= \gamma_2 + \delta_3 - \frac{\delta_2\alpha_3}{\alpha_2} \end{aligned} \tag{C.1.2}$$

where

$$\gamma_0 = -\alpha_2\beta_0 - \alpha_3\delta_0$$
$$\gamma_1 = -\alpha_1^{-1}(\alpha_2\beta_1 + \alpha_3\delta_1)$$
$$\gamma_2 = \left(\beta_2 + \frac{\alpha_3}{\alpha_2}\right)$$
$$\gamma_3 = -\left(\alpha_3\beta_2 + \alpha_3\alpha_2 + \frac{\alpha_3^2\delta_2}{\alpha_2} + \alpha_3\delta_3\right).$$

C.2 Krupa and Szmolyan model (2001)

Here we introduce a model analyzed in Krupa and Szmolyan [2001] with a slight change in notation.

$$\begin{aligned} \dot{x} &= x^2 - y^2 + \bar{\lambda}\epsilon + h_1(x, y, \epsilon) \\ \dot{y} &= \epsilon(1 + h_2(x, y, \epsilon)). \end{aligned} \tag{C.2.1}$$

Here $h_1(x, y, \epsilon) = O(u^3, u^2v, \epsilon u)$ and $h_2(x, y, \epsilon) = O(u, \epsilon)$ for $u, v \in \{x, y\}$. The critical set of system (C.2.1) is the union of the lines $y = x$ (C_1) and $y = -x$ (C_2). With respect to the fast flow, each line has an attracting (C_1^a,C_2^a) and repelling half (C_1^r,C_2^r). A non-normally hyperbolic point exists at the origin where C_1 and C_2 intersect transversally. We will refer to this point as the intersection point in the following.

We summarize some of the results presented in Krupa and Szmolyan [2001] about the behavior of solutions near the intersection point. For $\bar{\lambda} < 1$, solutions that approach the intersection point along C_1^a will leave along C_2^a. For $\bar{\lambda} > 1$, solutions that approach the intersection point along C_1^a will follow the fast flow after following C_2^r for a short amount of time. For $\bar{\lambda} = 1$, C_1 is invariant in the truncated system. In this case, solutions that approach the intersection point

along C_1^a have canard like behavior and follow C_2^r for an $O(1)$-distance before running off in the direction of the fast flow.

System (3.12) of the main text can be transformed into the form of system (C.2.1) with the following

$$\begin{aligned}
\bar{x} &= \alpha(x + \frac{\beta}{\alpha}y) \\
\bar{y} &= \sqrt{\beta^2 - \gamma\alpha}y \\
\bar{\epsilon} &= \sqrt{\beta^2 - \gamma\alpha}|g_0|\hat{\epsilon} \\
\bar{\lambda} &= \frac{1}{|g_0|\sqrt{\beta^2 - \gamma\alpha}}(\delta\alpha + g_0\beta)
\end{aligned}$$

where $\alpha = 1, \beta = -1/2, \gamma = 0$, and $|g_0| = 1$. After simplifying, this yields

$$\begin{aligned}
\frac{d\bar{x}}{dt} &= \bar{x}^2 - \bar{y}^2 + \bar{\lambda}\bar{\epsilon} \\
\frac{d\bar{y}}{dt} &= \bar{\epsilon}(1 + \bar{g}(\bar{y}, \bar{\epsilon})
\end{aligned} \tag{C.2.2}$$

where $g = O(\bar{y}, \bar{z})$, $h = O(\bar{x}, \bar{y}, \bar{z})$, and $\bar{\lambda} = 1$.

BIBLIOGRAPHY

P. A. Abrams. Adaptive foraging by predators as a cause of predator-prey cycles. *Evolutionary Ecology*, 6:56–72, 1992.

P. A. Abrams. Modelling the adaptive dynamics of traits involved in inter- and intraspecific interactions: An assessment of three models. *Ecology Letters*, 4: 166–175, 2001.

P. A. Abrams. 'adaptive dynamics' vs. 'adaptive dynamics'. *Journal of Evolutionary Biology*, 18:1162–1165, 2005.

P. A. Abrams and H. Matsuda. Fitness minimization and dynamic instability as a consequence of predator-prey coevolution. *Evolutionary Ecology*, 11:1–20, 1997a.

P. A. Abrams and H. Matsuda. Prey adaptation as a cause of predator-prey cycles. *Evolution*, 51(6):1742–1750, 1997b.

P. A. Abrams and H. Matsuda. Consequences of behavioral dynamics for the population dynamics of predator-prey systems with switching. *Popul. Ecol.*, 46:13–25, 2004.

P. A. Abrams, H. Matsuda, and Y. Harada. Evolutionarily unstable fitness maxima and stable fitness minima of continuous traits. *Evolutionary Ecology*, 7: 465–487, 1993.

A. A. Agrawal. Phenotypic plasticity in the interactions and evolution of species. *Science*, 294:321–362, 2001.

A. A. Agrawal, C. Laforsch, and R. Tollrian. Transgenerational induction of defences in animals and plants. *Nature*, 401:60–63, 1999.

A. A. Agrawal, D. D. Ackerly, F. Adler, A. E. Arnold, C. Cáceres, D. F. Doak, E. Post, P. J. Hudson, J. Maron, K. A. Mooney, M. Power, D. Schemske, J. Stachowicz, S. Strauss, M. G. Turner, and E. Werner. Filling key gaps in population and community ecology. *Frontiers in Ecology and the Environment*, 5(3): 145–152, 2007.

L. Arnold, C. K. R. T. Jones, K. Mischaikow, and G. Raugel. *Dynamical Systems*, volume 1609, chapter Geometric Singular Perturbation Theory, pages 44–118. Springer Berlin/Heidelberg, 1995.

J. K. Bailey, J. A. Schweitzer, F. Ubeda, J. Koricheva, C. J. LeRoy, M. D. Madritch, B. J. Rehill, R. K. Bangert, D. G. Fischer, G. J. Allan, and T. G. Whitham. From genes to ecosystems: a synthesis of the effects of plant genetic factors across levels of organization. *Phil. Trans. R. Soc. B*, 364:1607–1616, 2009.

M. P. Berg and J. Ellers. Trait plasticity in species interactions: a driving force of community dynamics. *Evolutionary Ecology*, 24:617–629, 2010.

B. J. M. Bohannan and R. E. Lenski. Linking genetic change to community evolution: insights from studies of bacteria and bacteriophage. *Ecology Letters*, 3: 362–377, 2000.

B. Bolker, M. Holyoak, V. Křivan, L. Rowe, and O. Schmitz. Connecting theoretical and empirical studies of trait-mediated interactions. *Ecology*, 84(5): 1101–1114, 2003.

H. Boudjellaba and T. Sari. Dynamic transcritical bifurcations in a class of slow-fast predator-prey models. *Nonlinearity*, 14:1473–1491, 2009.

M. G. Bulmer. Phase relations in the ten-year cycle. *Journal of Animal Ecology*, 44 (2):609–621, 1975.

L. Buric, A. Klic, and L. Purmova. Canard solutions and traveling waves in the spruce budworm population model. *Applied Mathematics and Computation*, 183:1039 – 1051, 2006.

J. Van Buskirk and M. Arioli. Dosage response of an induced defense: how sensitive are tadpoles to predation risk? *Ecology*, 83(6):1580–1585, 2002.

J. Van Buskirk and U. K. Steiner. The fitness costs of developmental canalization and plasticity. *Journal of Evolutionary Biology*, 22:852–860, 2009.

D. O. Conover and S. B. Munch. Sustaining fisheries yields over evolutionary time scales. *Science*, 297:94–96, 2002.

M. H. Cortez and S. P. Ellner. Understanding rapid evolution in predator-prey interactions using the theory of fast-slow dynamical systems. *To appear in The American Naturalist*, 2010.

F. Decole, R. Ferrière, A. Gragnani, and S. Rinaldi. Coevolution of slow-fast populations: evolutionary sliding, evolutionary pseudo-equilibria and complex red queen dynamics. *Proceedings of the Royal Society B*, 273:983–990, 2006.

B. Deng. Food chain chaos due to junction-fold point. *Chaos*, 11(3):514–525, 2001.

B. Deng and G. Hines. Food chain chaos due to shilnikov's orbit. *Chaos*, 12(3): 533–538, 2002.

B. Deng and G. Hines. Food chain chaos due to transcritical point. *Chaos*, 13(2): 578–585, 2003.

B. Deng and I. Loladze. Competitive coexistence in stoichiometric chaos. *Chaos*, 17, 2007.

D. J. D. Earn, J. Dushoff, and S. A. Levin. Ecology and evolution of the flu. *TRENDS in Ecology & Evolution*, 17:334–340, 2002.

T. H. G. Ezard, S. D. Cote, and F. Pelletier. Eco-evolutionary dynamics: disentangling phenotypic, environmental and population fluctuations. *Phil. Trans. R. Soc. B*, 364:1491–1498, 2009.

Z. Feng, R. Liu, D. L. DeAngelis, J. P. Bryant, K. Kielland, F. S. Chapin III, and R. K. Swihart. Plant toxicity, adaptive herbivory, and plant community dynamics. *Ecosystems*, 12:534–547, 2009.

N. Fenichel. Persistence and smoothness of invariant manifolds for flows. *Indiana University Mathematics Journal*, 21:193–225, 1971.

N. Fenichel. Geometric singular perturbation theory for ordinary differential equations. *Journal of Differential Equations*, 31:53–98, 1979.

O. De Feo and S. Rinaldi. Singular homoclinic bifurcations in tritrophic food chains. *Mathematical Biosciences*, 148:7–20, 1998.

G. F. Fussmann, S. P. Ellner, K. W. Shertzer, and N. G. Hairston, Jr. Crossing the hopf bifurcation in a live predator-prey system. *Science*, 290:1358–1360, 2000.

G. F. Fussmann, M. Loreau, and P. A. Abrams. Eco-evolutionary dynamics of communities and ecosystems. *Functional Ecology*, 21:465–477, 2007.

S. Gandon and T. Day. The evolutionary epidemiology of vaccination. *Journal of the Royal Society Interface*, 4:803–817, 2007.

J. J. Gilbert and J. K. Waage. Asplanchna, asplanchna-substance, and posterolateral spine length variation of the rotifer brachionus calyciflorus in a natural environment. *Ecology*, 48(6):1027–1031, 1967.

J. Ginoux, B. Rossetto, and J. Jamet. Chaos in a three-dimensional volterra-gause model of predator-prey type. *International Journal of Bifurcation and Chaos*, 15 (5):1689–1708, 2005.

E. E. Goldwyn and A. Hastings. When can dispersal synchronize populations? *Theoretical Population Biology*, 73:395–402, 2008.

P. R. Grant and B. R. Grant. Unpredictable evolution in a 30-year study of darwin's finches. *Science*, 296:707–711, 2002.

T. R. Green and C. A. Ryan. Wound-induced proteinase inhibitor in plant leaves: a possible defense mechanism against insects. *Science*, 175(4023):776–777, 1972.

B. T. Grenfell, O. G. Pybus, J. R. Gog, J. L. N. Wood, J. M. Daly, J. A. Mumford, and E. C. Holmes. Unifying the epidemiological and evolutionary dynamics of pathogens. *Science*, 303:327–332, 2004.

N. G. Hairston, Jr. and T. A. Dillon. Fluctuating selection and reponse in a population of freshwater copepods. *Evolution*, 44(7):1796–1805, 1990.

N. G. Hairston, Jr. and W. E. Walton. Rapid evolution of a life history trait. *Proc. Natl. Acad. Sci. USA*, 83:4831–4833, 1986.

N. G. Hairston, Jr., W. Lampert, C. E. Caceres, C. L. Holtmeier, L. J. Weider, U. Gaedke, J. M. Fischer, J. A. Fox, and D. M. Post. Rapid evolution revealed by dormant eggs. *Nature*, 401:446, 1999.

I. Hanski and I Saccheri. Molecular-level variation affects population growth in a butterfly metapopulation. *PLoS Biology*, 4(5):719–726, 2006.

E. Haukioja. On the role of plant defenses in the fluctuation of herbivore populations. *Oikos*, 35(2):202–213, 1980.

D. D. Heath, J. W. Heath, C. A. Bryden, R. M. Johnson, , and C. W. Fox. Rapid evolution of egg size in captive salmon. *Science*, 299:1738–1740, 2003.

Y. Jiang and J. Yang. Complex dynamics in a food chain with slow and fast processes. *Chaos, Solitons and Fractals*, 42:3160–3168, 2009.

M. T. J. Johnson, M. Vellend, and J. R. Stinchcombe. Evolution in plant populations as a drive of ecological changes in arthropod communities. *Proc. Trans. R. Soc. B*, 364:1593–1605, 2009.

L. E. Jones and S. P. Ellner. Effects of rapid prey evolution on predator-prey cycles. *Journal of Mathematical Biology*, 55:541–573, 2007.

L. E. Jones, L. Becks, S. P. Ellner, N. G. Hairston, Jr., T. Yoshida, and G. F. Fussmann. Rapid contemporary evolution and clonal food web dynamics. *Phil. Trans. R. Soc. B*, 364(1523):1579–1591, 2009.

A. I. Khibnik and A. S. Kondrashov. Three mechanisms of red queen dynamics. *Phil. Trans. R. Soc. B*, 264:1049–1056, 1997.

M. T. Kinnison and N. G. Hairston, Jr. Eco-evolutionary conservation biology: contemporary evolution and dynamics of persistence. *Functional Ecology*, 21: 444–454, 2007.

M. T. Kinnison, M. J. Unwin, and T. P. Quinn. Eco-evolutionary vs. habitat contributions to invasion in salmon: experimental evaluation in the wild. *Molecular Ecology*, 17:405–414, 2008.

O. Kishida, G. C. Trussell, and K. Nishimura. Top-down effects on antagonistic inducible defense and offense. *Ecology*, 90(5):1217–1226, 2009.

M. Kot. *Elements fo Mathematical Biology*. Cambridge University Press, Cambridge, New York, 2001.

M. Krupa and P. Szmolyan. Extending slow manifolds near transcritical and pitchfork singularities. *Nonlinearity*, 14:1473–1491, 2001.

H. Kuhlmann and K. Heckmann. Interspecific morphogens regulating prey-predator relationships in protozoa. *Science*, 227(4692):1347–1349, 1985.

V. Křivan. The lotka-volterra predator-prey model with foraging-predation risk trade-offs. *The American Naturalist*, 170(5):771–782, 2007.

J. Kusch. Behavioural and morphological changes in ciliates induced by the predator amoeba proteus. *Oecologia*, 96:354–459, 1993.

Y. A. Kuznetsov. *Elements of Applied Bifurcation Theory*. Springer-Verlag, New York, third edition, 2000.

R. Lande. A quantitative genetic theory of life history evolution. *Ecology*, 63(3): 607–615, 1982.

S. Lavergne and J. Molofsky. Increased genetic variation and evolutionary potential drive the success of an invasive grass. *Proceedings of the National Academy of Sciences*, 2007:3883–3888, 2007.

R. Law, P. Marrow, and U. Dieckmann. On evolution under asymmetric competition. *Evolutionary Ecology*, 11:485–501, 1997.

Y. Lenbur, S. Rattanamongkonkul, N. Tumrasvin, and S. Amornsamankul. Predator-prey interaction coupled by parasitic infection: limit cycle and chaotic behavior. *Mathematical and Computer Modelling*, 30:131–146, 1999.

Y. Lenbury and C. Likasiri. Low- and high-frequency oscillations in a food chain where one of the competing species feeds on the other. *Mathematical and Computer Modelling*, 20(7):71–89, 1994.

Y. Lenbury and N. Tumrasvin. Singular perturbation analysis of a model for the effect of toxicants in single-species systems. *Mathematical and Computer Modelling*, 31:125–134, 2000.

Y. Lenbury, R. Ouncharoen, and N. Tumrasvin. Higher-dimensional separation principle for the analysis of relaxation oscillations in nonlinear systems: application to a model of hiv infection. *IMA Journal of Mathematics Applied in Medicine and Biology*, 17:243–261, 2000.

T. Li and J. A. Yorke. Period three implies chaos. *The American Mathematical Monthly*, 82:985–992, 1975.

S. L. Lima. Nonlethal effects in the ecology of predator-prey interactions. *Bioscience*, 48(1):25–34, 1998.

W. Liu, D. Xiao, and Y. Yi. Relaxation oscillations in a class of predator-prey systems. *Journal of Differential Equations*, 188:306–331, 2003.

P. Marrow, R. Law, and C. Cannings. The coevoltuion of predator-prey interactions: Esss and red queen dynamics. *Proceedings of the Royal Society of London Series B: Biological Sciences*, 250:133–141, 1992.

P. Marrow, U. Dieckmann, and R. Law. Evolutionary dynamics of predator-prey

systems: an ecological perspective. *Journal of Mathematical Biology*, 34:556–578, 1996.

N. Mehidi. A prey-predator-superpredator system. *Journal of Biological Systems*, 9(3):187–199, 2001.

J. R. Meyer, S. P. Ellner, N. G. Hairston, Jr., L. E. Jones, and T. Yoshida. Prey evolution on the time scale of predator-prey dynamics revealed by allele-specific quantitative pcr. *Proceedings of the National Academy of Sciences*, 28: 10690–10695, 2006.

B. G. Miner, S. E. Sultan, S. G. Morgan, D. K. Padilla, and R. A. Relyea. Ecological consequences of phenotypic plasticity. *TRENDS in Ecology and Evolution*, 20 (12):685–692, 2005.

S. Muratori. An application of the separation principle for detecting slow-fast limit cycles in a three-dimensional system. *Applied Mathematics and Computation*, 43:1–18, 1991.

S. Muratori and S. Rinaldi. Low- and high-frequency oscillation in three-dimensional food chain systems. *SIAM Journal of Applied Mathematics*, 52(6): 1688–1706, 1992.

T. Okuyama and R. L. Ruyle. Analysis of adaptive foraging in an intraguild predation system. *Web Ecology*, 4:1–6, 2003.

E. P. Palkovacs, M. C. Marshall, B. A. Lamphere, B. R. Lynch, D. J. Weese, D. F. Fraser, D. N. Reznick, C. M. Pringle, , and M. T. Kinnison. Experimental evaluation of evolution and coevolution as agents of ecosystem change in trinidadian streams. *Phil. Trans. R. Soc. B*, 364:1617–1628, 2009.

S. R. Palumbi. Humans as the world's greatest evolutionary force. *Science*, 293: 1786–1790, 2001.

K. Parvinen. Evolutionary suicide. *Acta Biotheoretica*, 53:241–264, 2005.

F. Pelletier, T. Clutton-Brock, J. Pemberton, S. Tuljapurkar, , and T. Coulson. The evolutionary demography of ecological change: linking trait variation and population growth. *Science*, 315:1571–1574, 2007.

J.-C. Poggiale, P. Auger, F. Cordoleani, and T. Nguyen-Huu. Study of a virus-bacteria interaction model in a chemostat: application of geometrical singular perturbation theory. *Nonlinearity*, 14:1473–1491, 2001.

D. M. Post and E. P. Palkovacs. Eco-evolutionary feedbacks in community and ecosystems ecology: interactions between the ecological theatre and the evolutionary play. *Philosophical Transactions of the Royal Society B*, 364:1629–1640, 2009.

E. L. Preisser, D. I. Bolnick, and M. F. Benard. Scared to death? the effects of intimidation and consumption in predator-prey interactions. *Ecology*, 86(2): 501–509, 2005.

R. Ramos-Jiliberto. Population dynamics of prey exhibiting inducible defenses: the role of associated costs and density-dependence. *Theoretical Population Biology*, 64:221–231, 2003.

R. Ramos-Jiliberto and L. Garay-Narváez. Qualitative effects of inducible defenses in tropic chains. *Ecological Complexity*, 4:58–70, 2007.

R. Ramos-Jiliberto, E. Frodden, and A. Aránguiz-Acu na. Pre-encounter versus post-encounter inducible defenses in predator-prey model systems. *Ecological Modelling*, 200:99–108, 2007.

R. Ramos-Jiliberto, J. Mena-Lorca, J. D. Flores, and W. Morales-Álvarez. Role of inducible defenses in the stability of a tritrophic system. *Ecological Complexity*, 5:183–192, 2008.

R. A. Relyea and J. R. Auld. Having the guts to compete: how intestinal plasticity explains costs of inducible defenses. *Ecology Letters*, 7:869–875, 2004.

D. N. Reznick, F. H. Shaw, F. H. Rodd, , and R. G. Shaw. Evaluation of the rate of evolution in natural populations of guppies (poecilia reticulata). *Science*, 275: 1934–1937, 1997.

D. N. Reznick, C. K. Ghalambor, and K. Crooks. Experimental studies of evolution in guppies: a model for understanding the evolutionary consequences of predator removal in natural communities. *Molecular Ecology*, 17:97–107, 2008.

S. Rinaldi. Synchrony in slow-fast metacommunities. *International Journal of Bifurcation and Chaos*, 19(7):2447–2453, 2009.

S. Rinaldi and A. Gragnani. Destabilizing factors in slow-fast systems. *Ecological Modelling*, 180:445–460, 2004.

S. Rinaldi and S. Muratori. Limit cycles in slow-fast forest-pest models. *Theoretical Population Biology*, 41:26–43, 1992a.

S. Rinaldi and S. Muratori. Slow-fast limit cycles in predator-prey models. *Ecological Modelling*, 61:287–308, 1992b.

M. L. Rosenzweig and R. H. MacArthur. Graphical representation and stability conditions of predator-prey interactions. *The American Naturalist*, 47(895):209–223, 1963.

I. Saccheri and I. Hanski. Natural selection and population dynamics. *Trends in Ecology and Evolution*, 21(6):341–347, 2006.

S. Schecter. Persistent unstable equilibria and closed orbits of a singularly perturbed equation. *Journal of Differential Equations*, 60:131–141, 1985.

H. Serizawa, T. Amemiya, T. Enomoto, A. G. Rossberg, and K. Itoh. Mathematical modeling of colony formation in algal blooms: phenotypic plasticity in cyanobacteria. *Ecological Research*, 23:841–850, 2008.

K. W. Shertzer, S. P. Ellner, G. F. Fussmann, and N. G. Hairston, Jr. Predator-prey cycles in an aquatic microcosm: testing hypotheses of mechanism. *Journal of Animal Ecology*, 71:802–815, 2002.

E. Siemann and W. E. Rogers. Genetic differences in growth of an invasive tree species. *Ecology Letters*, 4:514–518, 2001.

B. Sinervo, E. Svensson, and T. Comendant. Density cycles and an offspring quantity and quality game driven by natural selection. *Nature*, 406:985–988, 2000.

S. H. Strogatz. *Nonlinear Dynamics and Chaos with Applications to Physics, Biology, Chemistry, and Engineering*. Perseus Books, Cambridge, MA, 1994.

D. P. Swain, A. F. Sinclair, and J. Mark Hanson. Evolutionary response to size-selective mortality in an exploited fish population. *Proceedings of the Royal Society of London Series B: Biological Sciences*, 274:1015–1022, 2007.

R. Tollrian and C. D. Harvell. *The Ecology and Evolution of Inducible Defenses*. Princeton University Press, Princeton, NJ, 1999.

M. Tuda. Evolutionary character changes and population responses in an insect host-parasitoid experimental system. *Researches on Population Ecology*, 40(3): 293–299, 1998.

S. Uchida, B. Drossel, and U. Brose. The structure of food webs with adaptive behaviour. *Ecological Modelling*, 206:236–276, 2007.

N. Underwood. The influence of plant and herbivore characteristics on the interaction between induced resistance and herbivore population dynamics. *The American Naturalist*, 153(3):292–294, 1999.

A. Vidal. Stable periodic orbits associated with bursting oscillations in population dynamics. In *Positive Systems, Proceedings*, volume 341 of *Lecture Notes in Control and Information Sciences*, pages 493–446, 2006.

M. Vos, B. W. Kooi, D. L. DeAngelis, and W. M. Mooij. Inducible defences and the paradox of enrichment. *Oikos*, 105:471–480, 2004a.

M. Vos, A. M. Verschoor, B. W. Kooi, F. L. Wäckers, D. L. DeAngelis, and W. M. Mooij. Inducible defenses and trophic structure. *Ecology*, 85(10):2783–2794, 2004b.

C. Webb. A complete classification of darwinian extinction in ecological interactions. *American Naturalist*, 161:181–205, 2003.

E. E. Werner and S. D. Peacor. A review of trait-mediated indirect interactions in ecological communities. *Ecology*, 84(5):1083–1100, 2003.

A. Yamauchi and N. Yamamura. Effects of defense evolution and diet choice on population dynamics in a one-predator-two-prey system. *Ecology*, 86(9): 2513–2524, 2005.

T. Yoshida, L. E. Jones, S. P. Ellner, G. F. Fussmann, and N. G. Hairston, Jr. Rapid evolution drives ecological dynamics in a predator-prey system. *Nature*, 424: 303–306, 2003.

T. Yoshida, N. G. Hairston, Jr., and S. P. Ellner. Evolutionary trade-off between defence against grazing and competitive ability in a simple unicellular alga. *Proceedings of the Royal Society of London Series B: Biological Sciences*, 271:1947–1953, 2004.

T. Yoshida, S. P. Ellner, L. E. Jones, B. J. M. Bohannan, R. E. Lenski, and N. G. Hairston, Jr. Cryptic population dynamics: rapid evolution masks trophic interactions. *PLoS Biology*, 5(9):1–12, 2007.